2018

Performance of segmental post-tensioned concrete girders with minimum flexural reinforcement

Jacob Nolan Eull
Iowa State University

Performance of segmental post-tensioned concrete girders with minimum flexural reinforcement

by

Jacob Nolan Eull

A thesis submitted to the graduate faculty

in partial fulfillment of the requirements for the degree of

MASTER OF SCIENCE

Major: Civil Engineering (Structural Engineering)

Program of Study Committee:
Sri Sritharan, Major Professor
An Chen
Igor Beresnev

The student author, whose presentation of the scholarship herein was approved by the program of study committee, is solely responsible for the content of this thesis. The Graduate College will ensure this thesis is globally accessible and will not permit alterations after a degree is conferred

Iowa State University

Ames, Iowa

2018

TABLE OF CONTENTS

LIST OF TABLES

LIST OF FIGURES

LIST OF NOTATIONS

A = Area of concrete section

A_{ps} = Area of prestressing strand

A_s = Area of nonprestressed steel

c = Neutral axis depth

d = Flexural depth

Δ_u= Displacement at failure

Δ_{cr}= Displacement at first cracking

$\frac{\Delta_u}{\Delta_{cr}}$ = Displacement ductility beyond cracking limit state

e = Eccentricity

ε_s = Strain in prestress strand

ε_{su} = Ultimate strain in prestess strand

ε_t = Net tensile strain in the extreme tension steel at nominal resistance

ε_u = Ultimate strain

E_c = Young's modulus of concrete

E_{ps} = Young's modulus of prestressing strand

f'_c = Concrete compressive strength

f_{cpe} = Compressive stress in concrete due to effective prestess forces at extreme fiber

f_r = Modulus of rupture of concrete

f_{pe} = Effective stress in prestress strand

f_{pi} = Initial stress in prestress strand

f_{ps} = Stress is prestress strand at ultimate flexure

f_{py} = Yielding stress in prestress strand

f_{pu} = Ultimate stress in prestress strand (just before rupture)

f_{sp} = Concrete spliting strength (from split cylinder test)

f_y = Stress in mild reinforcement at specified yield strain

f_u = Ultimate stress in mild reinforcement (just before rupture)

γ_1 = Flexural cracking variability factor

γ_2 = Prestress variablility factor

γ_3 = Ratio of yield to ultimate reinforcement for non − prestressed steel

h = Height

θ_1, θ_2 = Rotations of the girder on each side of the concentrated crack

I = Moment of inertia

L = Span length

M_{cr} = Cracking moment

m_{cr} = Theoretical cracking moment $\left(\frac{f_r y}{I}\right)$

M_{dnc} = Total unfactored dead load moment acting on the section

M_n = Nominal flexural strength

M_u = Maximum moment capacity

$\frac{M_u}{M_{cr}}$ = Overstrength moment ratio

M_r = Factored moment resistance

M_u = Factored ultimate moment

ρ = Reinforcement ratio $\left(\frac{A_s}{bd}\right)$

ϕ = Resistance factor

S = Section Modulus

T_{pt} = Tensile force from prestressing strand

W_{cr} = Crack width

y_b = Centroid location from extreme bottom fiber

y_t = Centroid location from extreme top fiber

$Y - hinge$ = Distance from the centroid of the compression zone to the bottom of the girder

ABSTRACT

The main purpose of the minimum flexural reinforcement requirement is to ensure that a structural member possesses sufficient strength and ductility. If the minimum requirement is not met, the structure is subject to fail in a brittle manner, without adequate warning or redistribution of load, when it reaches the flexural cracking limit state. The current AASHTO LRFD Bridge Design Specifications minimum reinforcement requirement addresses this by ensuring a minimum ratio between the flexural nominal moment capacity and flexural cracking moment at the section level. This is an iterative process, which in some cases is never satisfied regardless of the amount of reinforcement provided within the structure. Additional methods for determining minimum reinforcement, such as Leonhardt's method, are commonly utilized in practice. However, these processes make assumptions that are not relevant in many current girder section designs.

To address these concerns, an experimental research project (NCHRP 12-94) was conducted to examine the current AASHTO LRFD Bridge Design Specifications on the minimum flexural reinforcement and improve the effectiveness of the requirement. This thesis will focus on the segmental post-tensioned concrete girder experimental study conducted as part of NCHRP 12-94. These test girders were designed at various reinforcement amounts, both above and below the minimum reinforcement requirement. The objective of this thesis is to establish better understanding of the overall performance of the girders, as well as provide complimentary analysis to ensure sufficient strength and ductility. From the experimental study, all test girders showed adequate strength and ductility beyond the cracking limit state. Additionally, it was consistently observed that the segmental post-tensioned girders with unbonded tendon experienced an overall behavior shift from flexural theory response to a

hinging mechanism response amidst the formation of a concentrated crack adjacent to the midspan section's joint. Based upon this observed behavior, an analytical method is proposed and validated with the experimental results to ensure adequate strength and ductility of a designed segmental post-tensioned girder.

CHAPTER 1 - INTRODUCTION

1.1 Overview

The use of minimum flexural reinforcement has traditionally been applied to ensure that a structural member possesses a desired level of strength and ductility. The girder should have sufficient strength to prohibit collapsing upon the development of flexural cracking, as well as adequate ductility to prevent undesirable sudden, brittle failure of the structure.

The current minimum flexural reinforcement requirement for segmental post-tensioned concrete girders from AASHTO LRFD Bridge Design Specifications (AASHTO, 2017) is experimentally based on research conducted prior to 1960 at the University of Illinois, Urbana by Joseph Warwaruk. However, no segmental girders were included within the experimental program due to lack of prevalence at the time. This raises concern to the application of such standards to current segmental structures. Additionally, an overall lack of research into the geometry and design controls of segmental post-tensioned concrete girders has led to decreased utilization in practice, specifically in seismic zones.

1.2 Code Development

The 1989 AASHTO Guide Specification for Design and Construction of Segmental Bridges did not require any amount of minimum flexural reinforcement. However, Art. 9.2.1.4 states that the allowable tension in areas without bonded non-prestressed reinforcement is zero. This requirement will provide sufficient amount of reinforcement, however does not guarantee adequate ductility in the girder. Furthermore, the 2nd version of the guide (1999) refers to AASHTO standards.

The current AASHTO LRFD Specifications standards (AASHTO, 2017) focus on ensuring the nominal moment capacity (M_n) of the section exceeds the larger of 1.33 times the ultimate moment (M_u) or the cracking moment (M_{cr}). This approach will allow the girder to possess adequate post-cracking strength, however, it does not explicitly ensure ductility in the girder. In previous AASHTO standards, a maximum reinforcement ratio provision was utilized to enforce ductility in the section. This provision has since been removed, stating that the reduction in the capacity of the section from the resistance factor (ϕ) compensates for the lack of ductility. This philosophy creates opportunity for a structure to collapse with little to no warning.

The design processes for determining the minimum amount of prestressed reinforcement in a section is an additional area of concern. When attempting to increase the nominal moment capacity by increasing the area of prestressed steel (A_{ps}), the cracking moment is also increased. This causes a “chasing-your-tail” effect that can lead to sections with large areas of prestressed steel to not meet the strength requirement. Experimental validation of this effect was presented by Aparacio (Aparacio et al., 2001). Aparacio tested girders with a box-shaped cross section. Results of the study showed the ratio of the design moment to the cracking moment never

reaches 1, as seen in Figure 1.1, even with a drastic increase in the area of prestressed steel provided. In contrast, a decrease in the ratio is present as the area of prestressed steel increases.

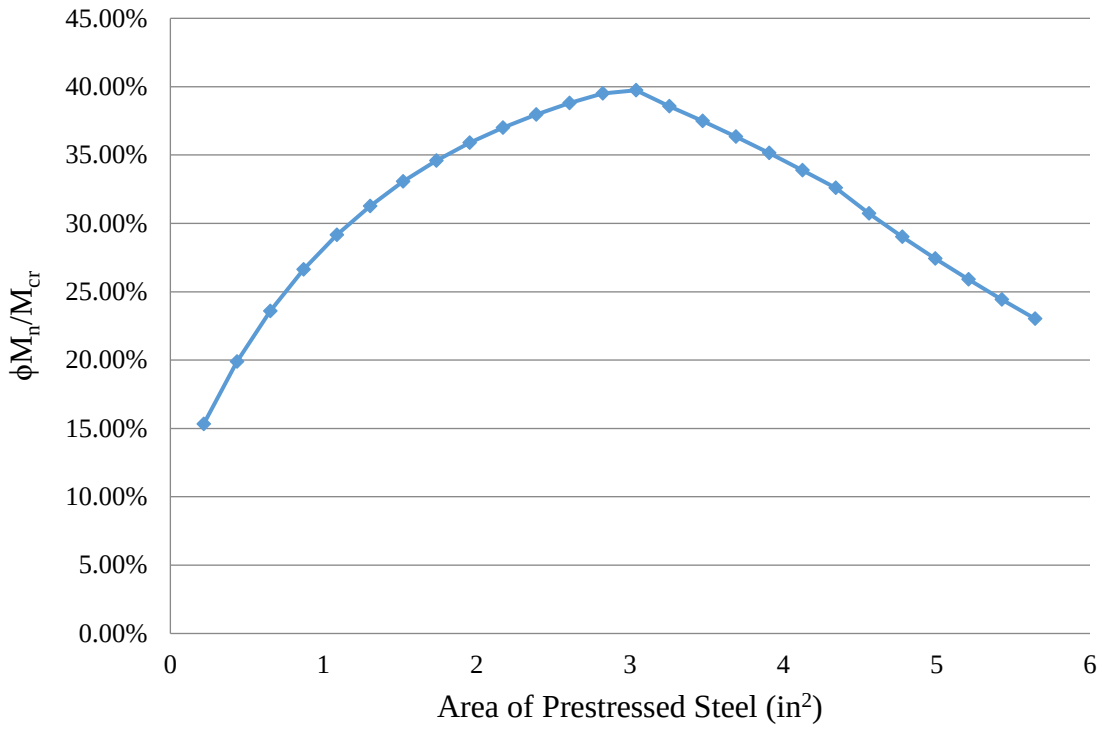

Figure 1.1 – $\frac{\phi M_n}{M_{cr}}$ Ratio as (A_{ps}) Increases from Aparacio (2001)

To avoid the "chasing-your-tail" effect, Leonhardt (1964) developed a method which is still utilized by bridge designers for solving the minimum reinforcement by equating the tensile forces to the change in steel stresses. This method is advantageous due to its simplistic nature and removes the iterative process of the calculation. However, if a non-rectangular section is used, as in most segmental-post tensioned girders, computing the tensile force becomes complex. Additionally, to create the simplistic design method Leonhardt neglected the depth of the steel in the section, as well as the concrete's capacity.

In general, there is a significant absence of experimental research regarding prestressed segmental concrete girders. To this point research has developed different parameters for

ductility, deflection, and other behavioral factors. However, there is no consensus on the behavior of these girders under flexural loading, as well as which of the section parameters are the best for ensuring adequate safety of flexural members after cracking occurs.

1.3 Scope of Research

This thesis will focus on the research conducted to evaluate the performance of large-scale segmental post-tensioned test girders in order to better understand the overall behavior of these girders. The test girder's flexural reinforcement was designed at varying amounts, both above and below that of the current AASHTO LRFD Specifications (AASHTO, 2017) requirement. The experimental study will include test girders, at varying spans and depths, with either unbonded or bonded high-strength steel tendons. Based upon the performance, an analytical method to ensure sufficient design strength and ductility of segmental post-tensioned girders was developed to provide an alternative to the aforementioned design methods. Additional analysis was conducted to validate the current methods of determining the stress of unbonded steel tendons at nominal strength.

1.4 Thesis Organization

This thesis consists of four chapters. Chapter one is the introduction, which has been detailed above. The introduction provides the overarching concerns, code development, and objectives of the research. Chapter two present the literature review of pertinent research that has been conducted in this area of study, U.S. and international code requirements, and prominent design approaches for prestressed concrete structures. Chapter three details the procedures utilized in construction, instrumentation, testing, as well as analysis of four segmental post-tensioned concrete girders. Chapter four provides conclusions from the literature review and experimental study, as well as recommendations for future research.

CHAPTER 2 – STATE-OF-KNOWLEDGE OF SEGMENTAL POST-TENSIONED CONCRETE GIRDERS

2.1 Introduction

This section presents the state-of-the-knowledge of segmental post-tensioned concrete structures, including its philosophical background, segmental concrete girder behavioral research history, U.S. and international code minimum reinforcement requirements, and suitable design approaches. Sections of this chapter were jointly developed with Michael Rosenthal (Rosenthal, 2018) and are additionally presented in the NCHRP 12-94 Project Report (Sritharan et. al., 2018).

2.2 Philosophical background of flexural reinforcement

The main purpose of the flexural reinforcement requirement in either a reinforced or prestressed concrete member is to ensure an adequate level of member strength and ductility is provided. This will prevent the member from failing suddenly in a brittle manner following the formation of flexural cracking under loading. The cracks begin to develop when flexural tensile stress within the extreme concrete tensile fiber exceeds the modulus of rupture of concrete (f_r). If a sufficient amount of reinforcement is provided, additional flexural cracks will develop along the length of the member; thus increasing the overall deflection and ductility. An insufficient amount of flexural reinforcement will result in the steels inability to take the tensile stress carried by the concrete, causing the reinforcement to yield/rupture at initial cracking. Resulting in a large localized crack development, leading to sudden failure.

2.3 Performance of segmental post-tensioned concrete structures research history

As mentioned in Section 1.1, The AASHTO LRFD Bridge Design Specifications (AASHTO, 2017) notes research completed at the University of Illinois at Urbana Champaign by J. Warwaruk as the experimental foundation for the minimum flexural reinforcement requirement (Warwaruk et al., 1960). The research study consisted of 82 prestressed concrete beams, all of which were simply supported during testing. Of these beams, 74 were post-tensioned and 8 were pretensioned. However, no segmental girders were included in the experimental program due to a lack of prevalence at the time of testing. Even with the exclusion of segmental girders in the study, the results and observations of the research study provides valuable insight into prestressed structures. Of the 74 post-tensioned beams, 26 utilized unbonded strands, 33 utilized bonded strands through grouting, and 15 had supplementary bonded mild steel reinforcement. A typical cross-section for a post-tensioned test specimen is show in Figure 2.1.

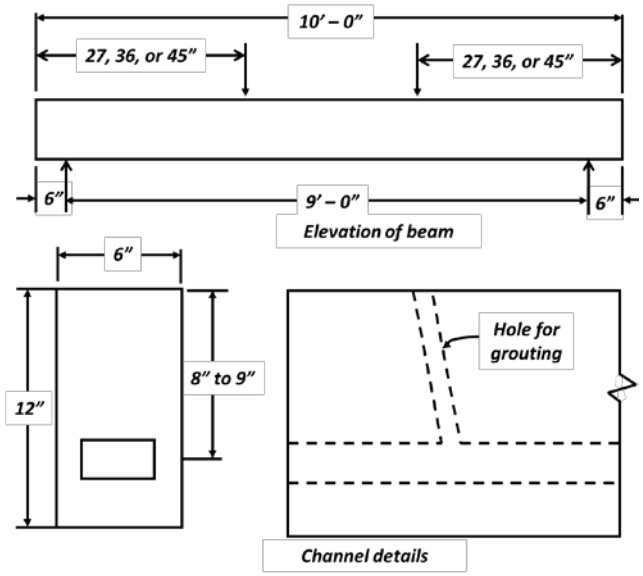

Figure 2.1 – Typical Detail for Test Specimen by Warwaruk (1960)

Note, only straight reinforcement was used for both the strand and mild reinforcing bars. The 28-day compressive concrete strength varied from 1,060 to 8,320 psi. Table 2.1 provides an overview of the material properties of the test specimen.

Table 2.1 – Beam Properties for Tested Specimen by Warwaruk (1960)

Beam Type	Quantity		f'c (ksi)	fse (ksi)	fpu (ksi)	fpy (ksi)	ds/H
Post-Tensioned Bonded	33	Max	8.32	151.3	257	245	80%
		Avg	4.75	101.8	241.8	209.2	72%
		Min	1.27	19	186	148	66%
Post-Tensioned Unbonded	26	Max	7.6	127.5	255	214	70%
		Avg	3.95	120.1	251.5	210.5	63%
		Min	1.53	111	250	199	58%
Post-Tensioned Unbonded with Supplementary Bondeded Reinforcement	15	Max	5.43	124.4	255	214	65%
		Avg	4.03	120.3	252.9	206	62%
		Min	1.06	117	251	199	59%
Pretensioned	8	Max	5.28	118.2	267	220	76%
		Avg	4.83	114.4	267	220	75%
		Min	3.97	112.1	267	220	74%

Based on the results of the research study, Warwaruk stated that prestressed beams can experience three phases in their load-deflection behavior. The first phase is the linear elastic phase with no flexural cracking. The second phase commences when flexural cracking occurs and results in a constantly changing slope while the steel reinforcement stress gradually increases. In the third, and final, phase, inelastic steel strain dominates the response resulting in very slow, almost linear, increase in load as deflection increases.

A major objective of this research study was to observe the effect of ρ/f'_c ratio. The reinforcement ratio (ρ) is determined by dividing the total reinforcement area (A_s) by the beam's width (b) and effective depth (d) (i.e. $\frac{A_s}{bd}$). $f'c$ is the 28-day concrete compressive strength of the

test specimen. For beams with a low value of ρ/f_c', an increase in the effective prestressing decreased the second phase behavior due to the steel reaching its inelastic range quicker. For beams with a high value of ρ/f_c', the increasing in prestressing led to a quicker progression for the second phase into the third phase and a slightly higher moment capacity. Bonded beams with a high value of ρ/f_c' and all unbonded beams did not undergo the third phase of the load-deflection behavior, this therefore resulted in a more brittle response. In order to maintain an adequate level of ductility, Warwaruk suggested an upper limit of $\frac{\rho f_{su}}{f_c'} = 0.25$, where f_{su} is the stress in the prestressed steel at failure. This was defined as the limit for the degree to which a section was compression-controlled. Additionally, to avoid collapse upon initial flexural cracking, a lower limit of $M_u > M_{cr}$ was suggested. Where M_u is the moment capacity of the beam.

Richard McClure and Harry West conducted one of the first large-scale experimental study on segmental post-tensioned concrete bridge girders (McClure and West, 1983). A short-term static test and overload test were performed on full scale girders, titled girder A and B respectfully, consisting of 17 segments, which were tied together with longitudinal and diagonal post-tensioning. Shear keys and epoxy were not provided between segments. Figure 2.2 shows the plan, elevation, and cross-section view of both girders. The design specifications for the experimental bridges were the Standard specifications for highway bridges of AASHTO (AASHTO, 1973).

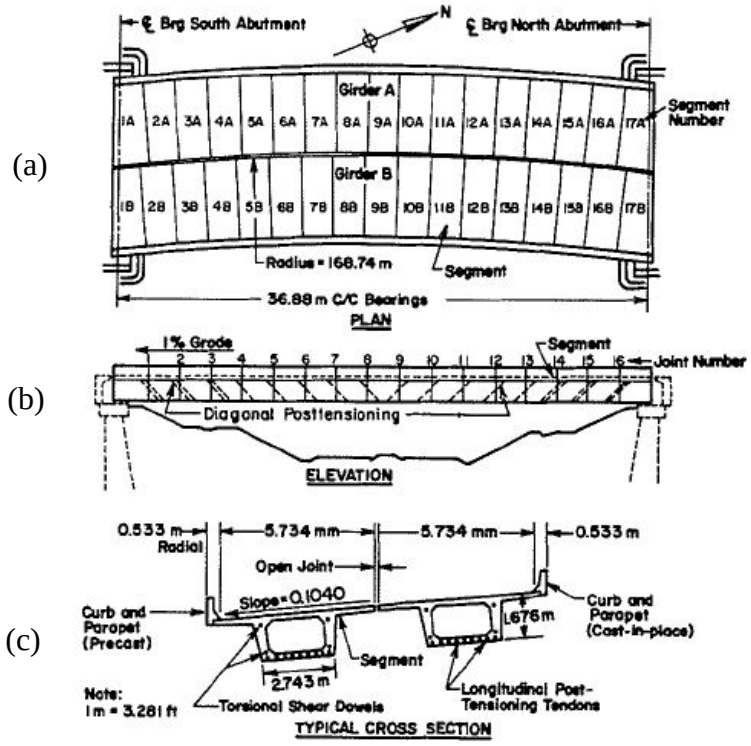

Figure 2.2 – (a) Plan View (b) Elevation View (c) Typical Cross-Section of Test Structure by McClure and West (1983)

Static service load tests were performed to determine the overall behavior of test girder A under live-load conditions. In these tests, the vehicle traveled from north to south on the girder. Measurements were made to determine live-load deflections and rotations using dial gages, and live-load strains were measured using strain gages. Test girder B was subjected to an overload test with static loading. The load schedule consisted of an initial load of 186 kip with daily increments of 100 kip until failure occurs. The bridge was instrumented to monitor deflections, rotations, change in alignment, surface strains in concrete, and forces in diagonal and anchor tendons.

Finite element analysis was conducted to accompany and compare against the experimental data. The research indicated that concrete behavior and fracture characteristics may

be explained by the development and propagation of microcracks within the concrete. Under applied loading, four stages of concrete behavior were described:

Stage I: The region up to 30-60% of the ultimate strength were microcracks are initiated at isolated points, however the cracks are completely stable without propagation. In this stage the concrete stress-strain relationship is linear and can be described by the two elastic constants, Poisson's ratio (ν) and Young's Modulus (E). All service-load calculations were treated as stage I.

Stage II: The region up to 70-90% of ultimate strength. As the applied load increases, cracking multiplies and propagates. Deviation of the linear elastic behavior causes irrecoverable deformation upon unloading. The start of such deformation behavior has been termed "onset of stable fracture propagation" (OSFP). In this zone deformation is effected by the following components: (1) a component dictated by the material characteristics and unaffected by the fracture processes. (2) A component expressing the effect of internal stresses caused by the fracture processes.

Stage III: The region up to the ultimate strength. Interface microcracks are linked to each other by mortar cracks, and void formation begins to have an effect on deformation. The start of this stage has been termed "onset of unstable fracture propagation" (OUFP). Deformation within this stage is effected by the two components detailed in stage II and a third component which expresses the effect of void formation.

Stage IV: The region beyond the ultimate strength. In this region, the energy released by the propagation of a crack is greater than the energy needed for propagation. Thus, the cracks become unstable and self-propagation occurs until failure.

Comparison of the experimental results to the finite element analysis revealed the tendency for the actual bridge to be stiffer than the finite element model throughout the study. This difference was attributed to some partial fixity at the supports of the actual structure. From the static load tests, the experimentally determined mid-span vertical deflections were about 15% less than the corresponding finite element values. However, both experimental and finite element methods led to inconclusive results for transverse bending stresses.

From the overload test, nothing usual was noticed until the eight day of testing, when two loud sounds were heard at different times, accompanied with the pressure gage readings dropping down slightly. The sound was described as if a strand or bar tendon had ruptured each time. Cracking at the joints accompanied the sound and opened widely and extended toward the top slab of the girder. At failure, the joint crack opened widely and concrete in the compression zone crushed and spalled on the surface. Upon inspection of the joint, it was found that all the strands were broken and only the bars were holding the bridge in place. Overall, the results of the three-dimensional finite element analysis compared reasonably well with the experimental results in the elastic and post-cracking range up to failure, as seen in Figure 2.3.

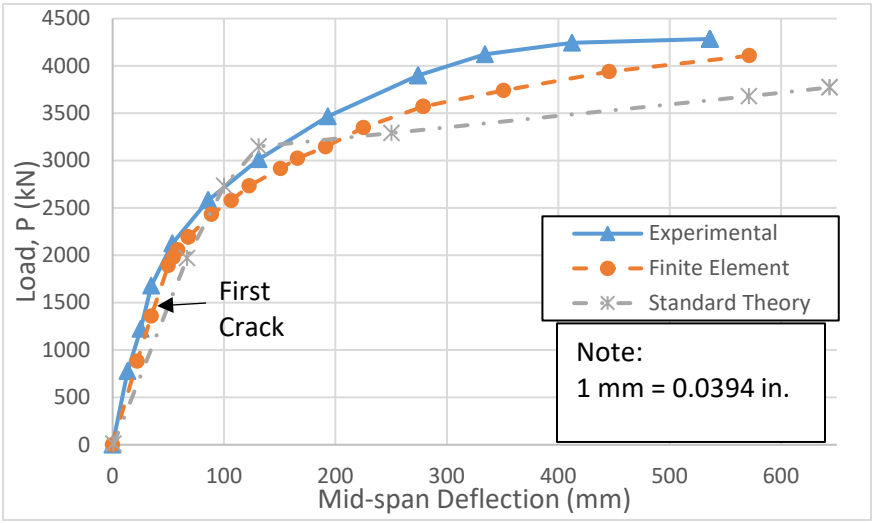

Figure 2.3 – Load–Deflection Curve under Overload Test Conditions by McClure and West (1983)

Rabbat and Sowlat tested three segmental girders to evaluate the differences in behavior of girders with external vs. internal tendons (Rabbet and Sowlat, 1987). The three test units were comprised of one unit with completely bonded internal tendons, another unit with external unbonded tendons, and final unit that was a modified combination. The modified test unit had external tendons covered with concrete in a second stage cast to produce a bonded-like condition. Figure 2.4 illustrates the different bonding conditions by showing each girder's cross section and reinforcement. There was no mild reinforcement crossing the joints in the test units. The joints between segments were free of grout or adhesives, similar to the joints of the test units in McClure and West's study.

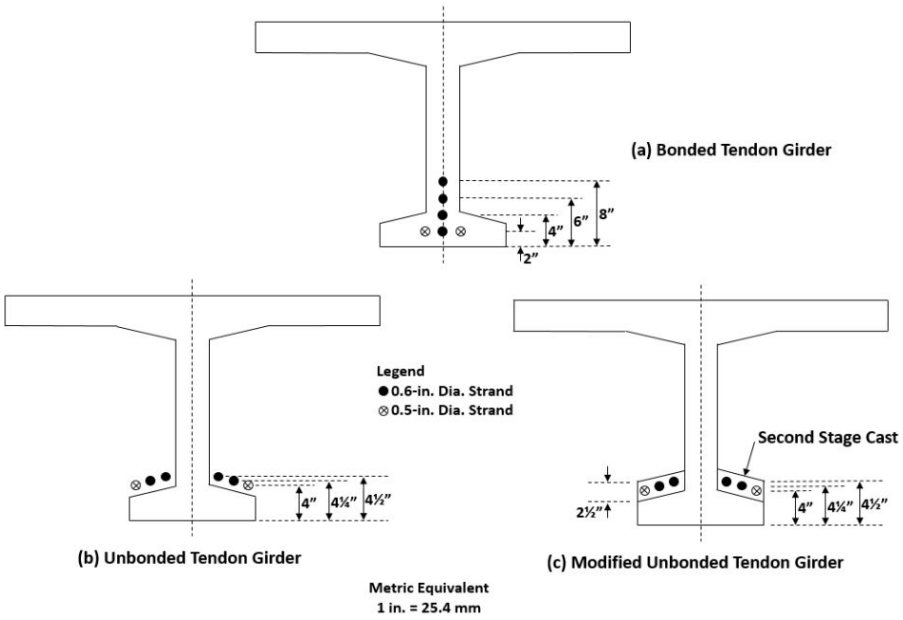

Figure 2.4 – Typical Cross-section of Girders tested by Rabbat and Sowlat (1987)

The simply supported spans were loaded in four-point bending. Measurements recorded during each test included the applied loads, deflections, joint openings, concrete surface strains, and strand strains. Table 2.2 summarizes the test results. In the first cycle, the beams were loaded to a displacement of approximately 3 inches, where significant nonlinear deformation was

observed. In the second cycle, the beams were forced to fail after torching the end anchorages of the top strand on each side of the web. The anchors were torched to represent a seismic-induced failure. Figure 2.5 shows the applied moment and deflection at the midspan of the beams. For a given moment, the external tendons had a higher deflection, but the internal tendons reached a larger displacement. The torching of the tendons did not affect the bonded tendon in the second cycle, whereas the two unbonded specimens' behavior were clearly influenced. Despite this loss of bond, the unbonded tendon and modified unbonded tendon girders exceeded the flexural strength predicated by the AASHTO specifications for members with unbonded tendons (AASHTO, 1983). The bonded test specimen had an initiation of failure with concrete crushing and then the strands ruptured whereas the unbonded and modified unbonded specimens failed in shear with the shear keys progressively breaking off, leading to loss of shear-carrying capacity. Ultimately, shear compression failure occurred in the top flange at a joint. This failure mode differs from that observed by McClure (McClure and West,1983).

Table 2.2– Summary of Test Results from Rabbat and Sowlat (1987)

Beam Type	ρ_l (%)	Δ/L	μ_Δ	M_o/M_{cre}*
Bonded	0.103	2.13%	28.4	2.08
Unbonded	0.103	1.20%	18.8	1.90
Modified Unbonded	0.103	1.21%	16.5	2.18

* M_o is from first cycle loading and M_{cre} is first joint opening

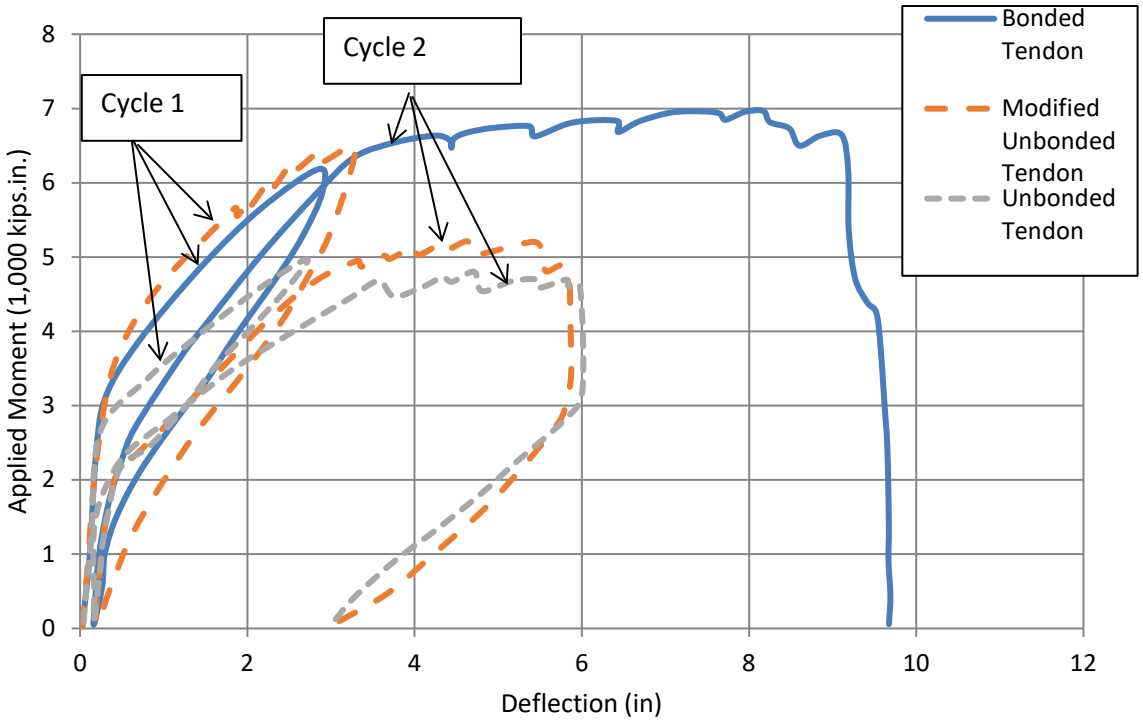

Figure 2.5 – Applied Moment-Deflection Curve of Girder under Downward Loading from Rabbat and Sowlat (1987)

Table 2.3 compares the experimental results to the current AASHTO standards, as well as a computer analysis of the test girders. Based on the observed test results of the unbonded tendon girders, it was concluded that the AASHTO provisions at the time for unbonded tendons significantly underestimated the flexural strength.

Table 2.3 – Comparison of Experimental Moment to Calculated Moments by Rabbat and Sowlat (1987)

Case Number	Number of Effective Strands	Girder Cross Section	Concrete compressive strength (psi)	Experimental Moment (kip-in)	Calculated Moment (kip-in)	
					Computer Analysis	AASHTO
1	All Six Strands	Bonded Tendon Girder	5810	6910	7260	7320
2		Unbonded Tendon Girder	5810	4980	7210	4380
3		Modified Unbonded Tendon Girder	6400	6530	7220	4390
4	Four bottom Strands only	Unbonded Tendon Girder	5810	4670	4600	2850
5		Modified Unbonded Tendon Girder	6400	5080	4600	2850

At the University of Texas at Austin, R. J. MacGregor examined the strength and ductility of externally unbonded post-tensioned segmental box girders (MacGregor et. al., 1989). A key difference in the determining the nominal strength of a girder with external tendons compared to internal tendons is that external tendons are considered unbonded. This is due to the majority of the tendon is not bonded to the concrete section and the strains in the tendon are independent of the strains in the adjacent concrete sections. In a fully bonded system, where the tendon is completely encased in the concrete section and effectively grouted, the tendon strains are assumed to be the same as the concrete section at the level of the tendon. In an unbonded system (as typical of external tendons), the tendon strains are not compatible with the adjacent concrete strains. Assuming no friction with the surrounding duct, the tendon strain is constant for the full length between the anchorages. The change in tendon strain due to the applied loads is calculated from the total change in length (ΔL) of the tendon over its entire length (L) (i. e. $\frac{\Delta L}{L}$).

This difference in design stresses had yet to be addressed in the AASHTO guidelines, as previously exemplified by Rabbet (Rabbet and Sowlat, 1987).

The ¼ scale test girder consisted of three-spans, where each span consisted of 10 segments. A primary interest of this study was to investigate the effect epoxy jointing material had on the ultimate load behavior. Thus, one exterior span was constructed with dry joints and the others with epoxy joints. The spans were separated by cast-in-place closure strips, as detailed in Figure 2.6. Pier segments, which contained the anchorages for all post-tensioning tendons, were present over each support.

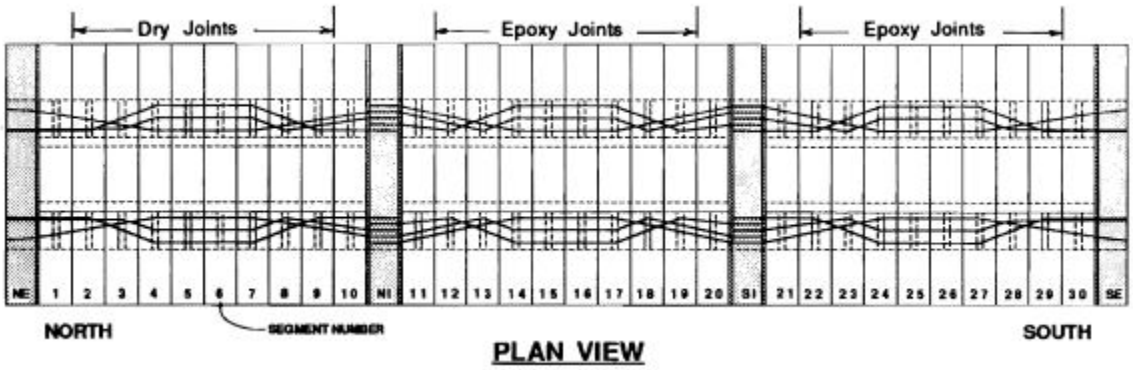

Figure 2.6 – Plan View of Girders Tested by MacGregor (1989)

The model structure was tested to investigate the complete range of flexural behavior and to conduct preliminary tests of shear and torsional behavior. The complete test program can be seen in Table 2.4. The first phase of testing involved loading the structure to the design service-level live loads and then increasing loads to higher levels to establish the decompression loads at critical joints along the structure. In the second phase, the structure was loaded with increases factored loads used for strength design. In the final phase, the structure was loaded until the ultimate strength was reached.

Table 2.4 – Test Program Completed by MacGregor (1989)

Phase 1 - Structural Characterization	# of Cycles
Design Service Load	4
Cracking	1
Decompression Load	3
Torsional Load	1
Phase 2 - Factored Load Tests	
Design Factored Load	3
Phase 3 - Ultimate Strength Tests	
Flexural Strength Test - Joint Opening	3
Flexural Strength Test - Ultimate	1
Shear Strength	1

The deflection of the dry jointed exterior span was roughly 10% greater than the epoxy-jointed exterior span, as seen in Figure 2.7. The reduced stiffness in the dry-jointed span was perhaps caused by differential shrinkage in the segments, which resulted in less than full contact between match-casted segments. Failure of the exterior spans with dry joints occurred after development of a failure mechanism involving concentrated rotations in a joint or crack near midspan of the exterior span and subsequent opening at a joint at the interior face of the first interior pier. This failure mode is consistent with that observed by McClure (McClure and West, 1983). It was also observed that cracking occurred through concrete adjacent to an epoxied joint, rather than at the joint, as observed within the dry-jointed spans.

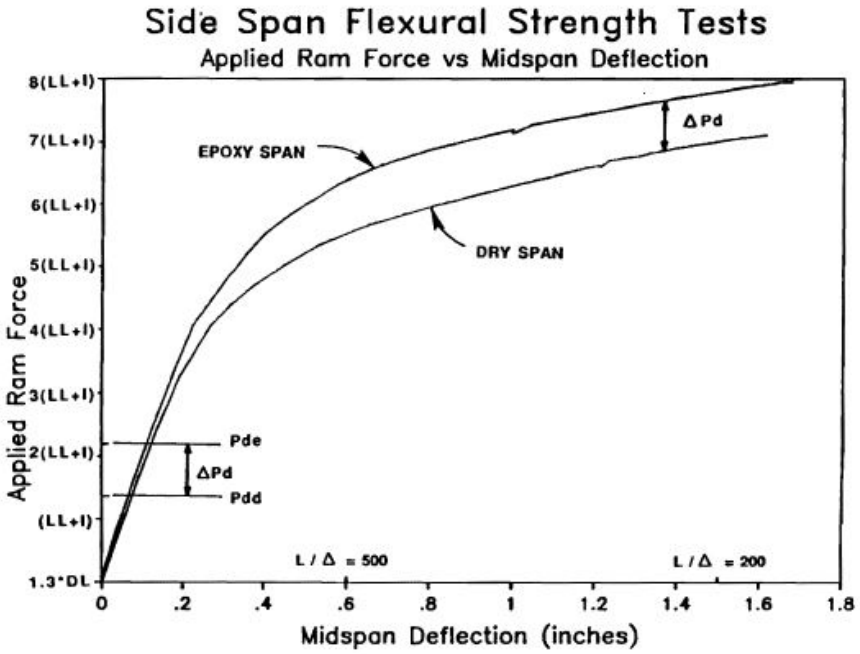

Figure 2.7 – Applied Load-Deflection Curves for Epoxy and Dry Spans from MacGregor (1989)

As a result of the experimental study, the following method to approximate prestressed tendon stress at nominal strength was recommended, and later accepted by AASHTO LRFD Specifications (AASHTO, 2017), for design of post-tensioned girders with unbonded external tendons:

$$f_{ps} = f_{pe} + 900\left(\frac{d_p - c_y}{l_e}\right) < f_{py} \text{ [ksi]} \qquad (2.1)$$

Where:

f_{ps} = the tendon stress corresponding to nominal strength (ksi)

f_{pe} = effective stress in the prestressed reinforcement after all prestress losses (ksi)

f_{py} = yielding stress in the prestressed reinforcement (ksi)

d_p = distance from the extreme copmression fiber to center

of prestressed reinforcement (in)

c_y = distance from the extreme conpression fiber to the neutral axis calculated using factored material strengths and assuming tension reinforcement has yielded (in)

l_e = effective length of the tendon for calculation on nominal strength

$$l_e = \left(\frac{l_i}{1+\frac{N_s}{2}}\right) \text{ [in]} \qquad (2.2)$$

Where:

l_i = the length of the tendond between anchorages (in)

N_s = the number of support hinges crossed by the tendon (draped tendons only)

A. Hindi studied the performance of a ¼ scaled model three-span segmental structure (Hindi et. al., 1995). The cross section of the structure is identical to that tested in MacGregor's study. Primary objectives of this study were to evaluate the influence that the number of deviators to which external tendons were bonded has on the strength and ductility of the member, as well as the evaluating the influence different joint types, dry or epoxied, has on the overall performance of the girder.

The same testing program as shown in Table 2.4 was utilized. At the conclusion of the first phase of the project, the structure was highly cracked and locally severely damaged but appeared to be structurally intact. Epoxy inject was used to repair the cracked segment of the model to good condition before continuing to the second phase.

The researchers found that the ductility increased with increase in the amount of grouted internal tendons and/or bonding points for external tendons. Bonding or grouting tendons increased the total amount of joint openings. Higher total joint openings resulted in larger deflection, as seen in Figure 2.8. Additionally, improved external tendon bonding raised the moment capacity for epoxy and dry-joint spans to 95 and 89 percent, respectfully, compared to that expected for a fully grouted internal tendon.

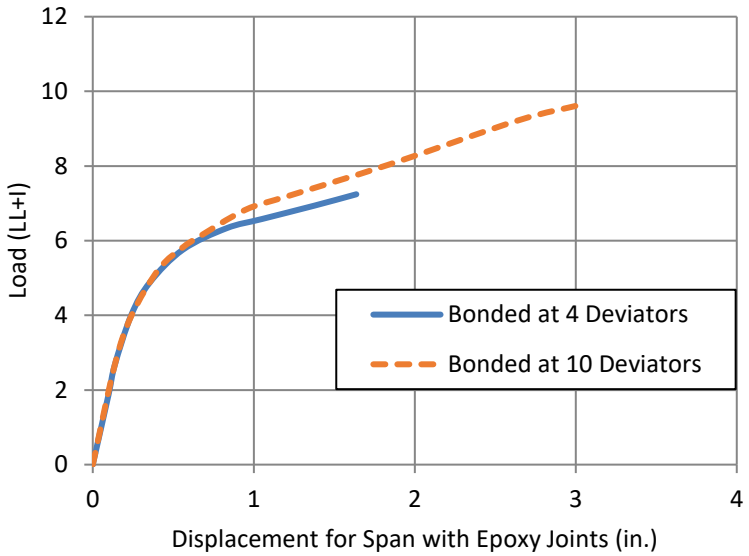

Figure 2.8 – Load-Deflection Curve of Testing Conducted by Hindi (1995)

The maximum joint openings was larger for epoxy joints, compared to dry joints, due to a more favorable crack pattern in the compressive zone of the critical section. The crack pattern in the epoxy joints, as illustrated in Figure 2.9, increased the volume of the highly compressed region and reduces concentration of the compressive strain in that region. Higher total joint opening in the epoxy-joints span leads to higher strength, deflection, and ductility compared to that for the dry-jointed spans. These crack patterns are consistent with those observed within dry and epoxied joints of the previously detailed research.

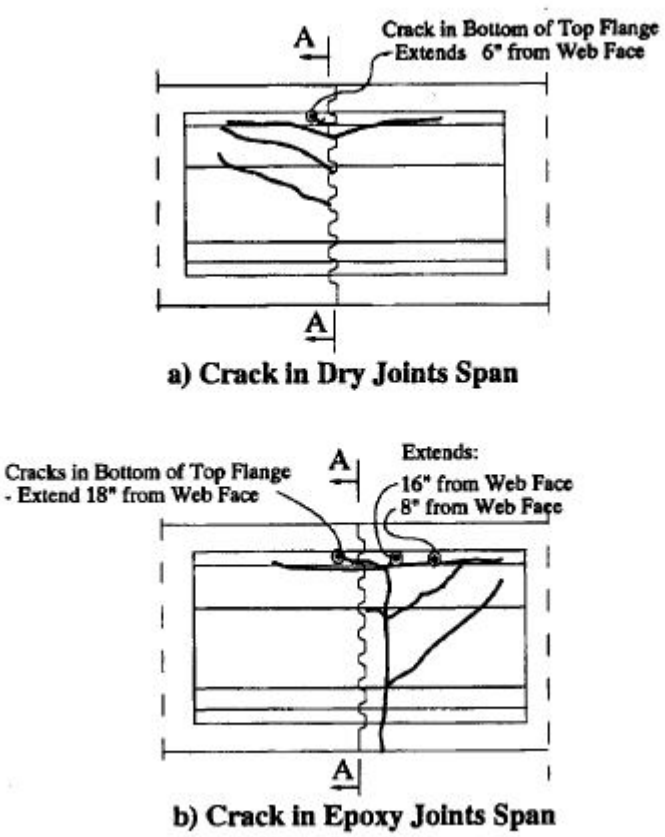

Figure 2.9 – Cracking Patterns Observed at Joints by Hindi (1995)

A. Aparicio tested five monolithic and three segmental beams in bending, as well as in combined bending and shear (Aparicio et. al., 2001). The main objective of this study was to evaluate the influence the prestressed tendon length has on the ultimate load capacity. The segmental beams were all simply supported and formed by seven segments with dry joints consisting of multiple shear keys and no mild reinforcement or bonding prestressed steel crossing the joints, as seen in Figure 2.10.

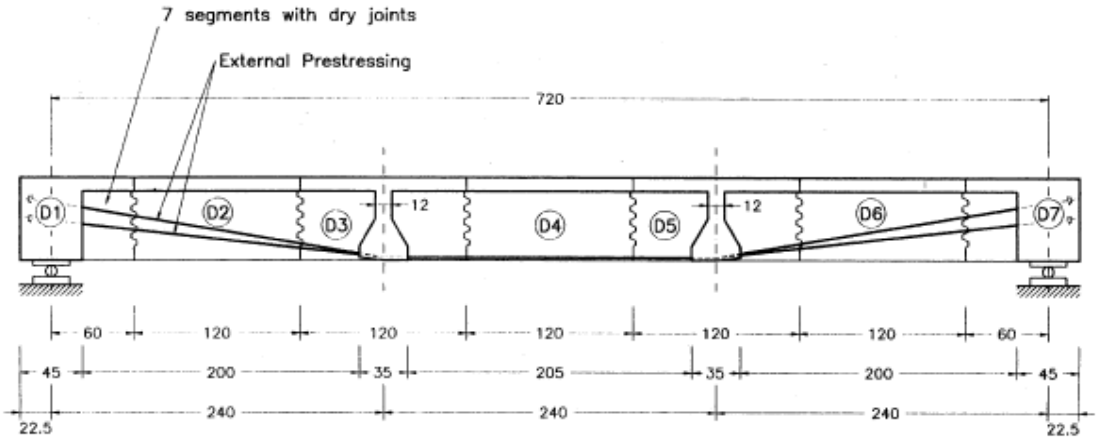

Figure 2.10 – Elevation View of Segmental Girder Tested by Aparicio (2001)

Of the three segmental beams, one was subjected to only flexural loading, while the other two beams were subjected to flexural-shear loading. The segmental beam under flexural loading reached a high ultimate load with a deflection of 100 mm (3.94 in). The failure was by spalling of the concrete upper slab, similar to that observed by McClure (McClure and West, 1983).

Based on the results, Aparicio determined that as the external tendon length decreased, the change in stress increased. A higher stress corresponds to an increase in moment capacity and ductility of the girder. This was due to the elongation in the strands. Furthermore, it was observed when the joints opened widely, a condition in which some codes consider that the beam has failed, the concrete remained elastic and deflection can be completely recovered when the beam is unloaded.

A three-phase research project was conducted at the University of California at San Diego to investigate the seismic performance of precast segmental bridges by S. Megally (Megally et al. 2003). This large-scale experimental program and finite element study was conducted to evaluate the seismic performance of segment-to-segment joints subjected to high

flexural moments and low shears (Phase I). The major objectives of Phase I were to investigate joint behavior in terms of opening and closure under cyclical loads, development of cracks patterns, and mode of failure.

Phase I, consisted of four 2/3 scale test units, in which each test unit was comprised of 6 segments. Unit 100-EXT has 100% of post-tensioning being external (unbonded) tendons. Unit 100-INT had an identical cross-section to Unit 100-EXT, however 100% of post-tensioning was internal (bonded) tendons. Test Unit 100-INT-CIP is identical to unit 100-INT with the addition of a cast-in-place concrete deck. Test Unit 50-INT/50-EXT consisted of 50% of post-tensioning for both internal and external tendons, with an identical cross-section to the other two test units. Figure 2.11 details the cross section of each unit. All test unit joints were epoxied.

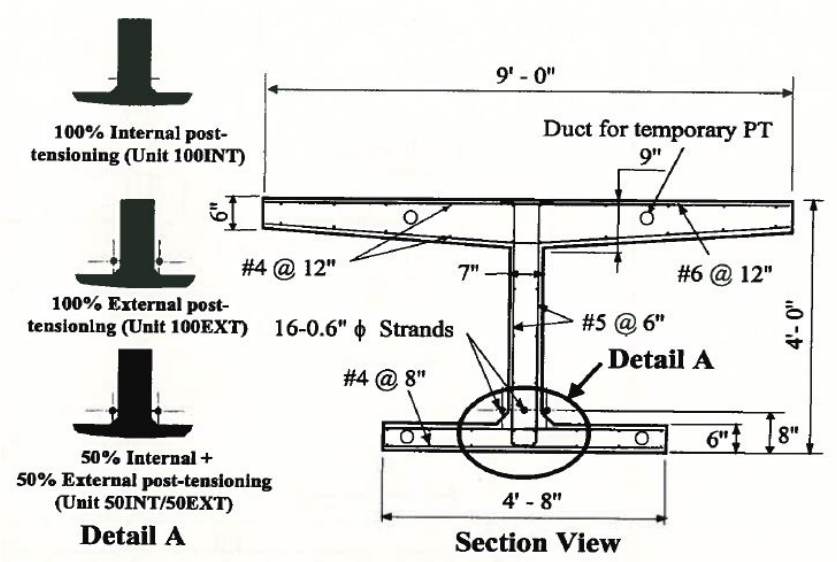

Figure 2.11 – Cross-Section of Girders Tested by Megally (2003)

The testing of each unit was conducted in two stages. Stage I was introduced to simulate the service load condition. The test units were loaded to a reference load level of 74.5 kip then loaded/unloaded cyclically between 112 and 65 kip 100,000 times. Stage II of testing was preformed to simulate a seismic test to evaluate each unit's response. Each test unit was loaded

to a reference load level of 162 kip. The test units were then subjected to fully reverse cyclical vertical displacements at midspan with increasing amplitude to failure.

Testing of units 100-INT, 100-INT-CIP and 50-INT/50-EXT was stopped due to rupture in prestressing strands at the midspan joint. The load carrying capacity was completely lost upon failure of unit 100-INT and 100-INT-CIP. However, Unit 50-INT/50-EXT had a residual load carrying capacity following rupture due to the external tendons still being intact. Testing of unit 100-EXT was terminated at a midspan downward displacement of around 6.6 in., when the displacement capacity of the hydraulic actuators was reached. The load-displacement response of each unit under downward loading direction is shown in Figure 2.12.

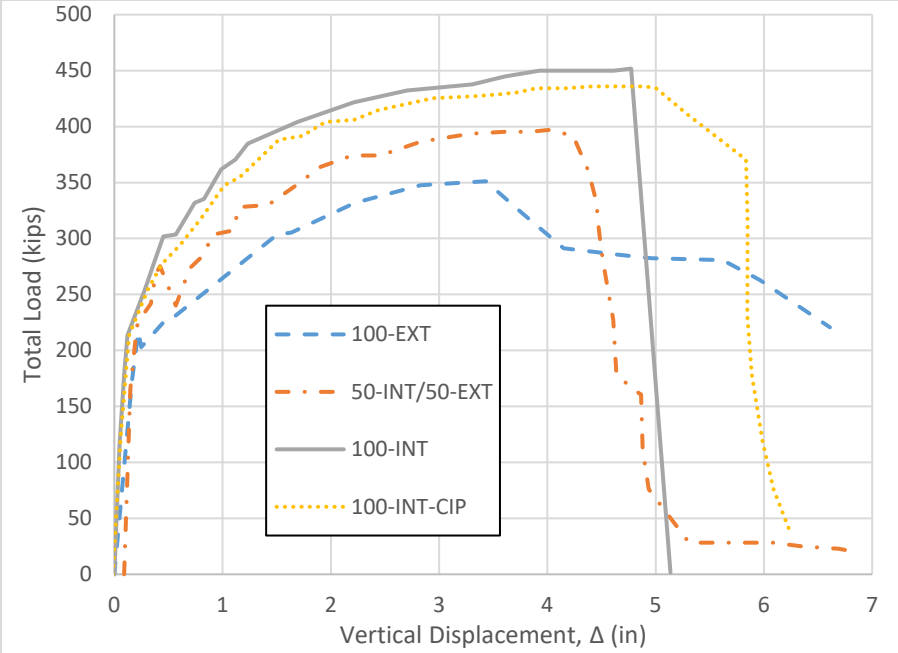

Figure 2.12 – Load-Deflection Curve of Segmental Girders Tested by Megally (2003)

The experimental results indicated that the ductility and displacement capacity can be substantially enhanced by use of 100% external post-tensioning, in agreement with the results by Hindi (Hindi et. al., 1995). Use of only external tendon can also minimize post-earthquake displacements as well as permanent openings of the segment-to-segment joints. Additionally,

epoxied segment-to-segment joints can experience significant repeated openings and closures under reverse cyclic loading without failure, even with no mild reinforcement within the joint. Combinations of internally bonded and externally unbonded tendons in precast segmental structures, as was allowed by AASHTO Guide Specifications at the time, should be avoided in high seismic zones due to the sudden, brittle failure that occurred due to rupture in the internal tendon. The flexural moment capacity of precast segmental bridge superstructures was reasonably predicted using provisions of the AASHTO Guide Specifications (1999) and AASHTO Standard Specifications for Highway Bridges (AASHTO, 1983).

A comprehensive parametric study was completed by J. Holombo to evaluate the current code requirements for the minimum flexural reinforcement of a structure (Holombo and Tadros, 2009). The objective if this research study was to develop recommended revision to the AASHTO LRFD Bridge Design Specifications for design of minimum reinforcement to prevent brittle failure of concrete sections. Four design methods were evaluated as part of this study, two of which can be considered strength methods and the other two are prescribed area methods. The two categories of design can be differentiated as follows:

(1) Strength Methods: The LRFD specifications and the Modified LRFD methods specified the minimum reinforcement by requiring that the flexural strength must be greater than cracking by an acceptable safety margin. Minimum prestressed reinforcement is determined through trial-and-error.

(2) Prescribed Area Methods: Leonhardt and Eurocode methods are based on providing minimum mild and/or prestressed reinforcement that is greater than the cracking

strength by an acceptable safety margin. These methods are further simplified so the amount of mild and/or prestressed reinforcement is calculated directly.

A concrete structure database was created with the intent to represent the range of structures commonly used for construction covered by the AASHTO LRFD Bridge design specifications. The concrete member database for this study, as well as the structural dimension limits are shown in Table 2.5.

Table 2.5 – Concrete Member Database Structural Dimension Limits by Holombo and Tadros (2009)

Bridge Types		Span - L (ft)		Depth/Span		Girder Spacing (ft)	
No.		Min	Max	Simple	Cont.	Min	Max
Cast-in-place Bridges							
2	Slab	20	45	0.07L	0.06L		
2	Reinforced concrete box	60	120	0.06L	0.055L	6.5	14
2	P/T Slab	40	70	0.03L	0.027L		
2	P/T Concrete Box	80	250	0.045L	0.040L	6	20
Precast Concrete Bridges							
2	Slabs	20	50	0.03L	0.03L		
2	Double tees	30	60	0.05L	0.05L	4	4
2	Box beams	50	120	0.033L	0.030L	3	4
2	I-girders	70	200	0.045L	0.040L	6	12
2	U-beams	80	200	0.045L	0.40L	12	26
Segmental Bridges (precast)							
2	Span x span	100	150	0.045L	0.040L	28	45
2	Balanced cantilever	100	200	N/A	0.025L	28	45
Concrete Substructure Elements							
2	Footings	12	35				
2	Cap beams	20	60	0.045L	0.04L		
26	**Total**						

A rational approach to the specification of minimum reinforcement was proposed, where variables are appropriately factored and include the maximum, rather than nominal strength, of the section as a true measure of ductile versus brittle response. The modified LRFD method provision was adopted by AASHTO Bridge Design Specifications, 8th edition and will be discussed in Section 2.4.1.

Following the parametric study, several conclusions were made based on the response of the reinforcement and prestressed concrete members. It was observed that the flexural cracking strength of concrete is dependent on many variables including curing methods, aggregates, compressive strength, and the overall member size. The suggested correlation with member depth and the modulus of rupture was also investigated by (Bosco et al., 1990; Carpinteri and Corrado, 2011). Additionally, precast segmental bridges exhibit lower flexural cracking strength than conventional concrete structures. Flexural cracks in these structures were typically initiated adjacent to the match-cast joint where an accumulation of fines and course aggregate led to a reduction of the tensile strength. This has been a consistent observation of the segmental concrete girder research within this section. The Modified LRFD method provided the most consistent level of safety provided for all concrete members within the database. This was largely due to the recognition that the ultimate strength of the member is a true measure of whether or not the section is ductile.

Holombo suggests that future testing of segmental bridge girders with external prestressing could provide additional data on the strength and ductility of externally prestressed sections and the cracking stress in the concrete layer adjacent to the match-cast joint. Additionally, large scale model testing would be beneficial to examine the identified correlation of member height to the modulus of rupture.

2.4 Code and design approaches to minimum flexural reinforcement requirement

In this section, a review and comparison of current U.S. and international standards for the minimum flexural reinforcement requirement is completed. This section will examine the differences in both philosophy and methodology of the various codes, as well as exemplify the necessity for further research.

2.4.1 AASHTO LRFD Bridge Design Specifications (8th Edition, 2017)

Art. 5.6.3.3 establishes the minimum flexural reinforcement requirement for bridge design. It was established based on the recommendation from (Holombo and Tadros, 2009). Additionally, the flexural cracking variability factor (γ_1) was reduced from 1.6 to 1.2 for precast segmental girders due to the findings of (Megally et al., 2003), where cracking occurred adjacent to the epoxy-bonded match-cast face. The factored flexural resistance, M_r, must be greater than or equal to the lesser of the following:

- 1.33 Times the factored moment required by the applicable strength load combination specified in Table 3.4.1-1;
- $M_{cr} = \gamma_3 \left[(\gamma_1 f_r + \gamma_2 f_{cpe}) S_c - M_{dnc} \left(\frac{S_c}{S_{nc}} - 1 \right) \right]$ (2.3)

Where:

M_{cr} = cracking moment (kip − in.)

f_r = modulus of rupture of concrete specified in Art. 5.4.2.6

f_{cpe} = compressive stress in concrete due to effective prestress forces only (after allowance for all prestress losses) at extreme fiber of section where tensile stress is causes by

externally applied loads

M_{dnc} = total unfactored dead load moment acting on the monolithic or noncomposite section (kip − in.)

S_c = section modulus for the extreme fiber of the composite section where tensile stress is caused by externally applied loads ($in.^3$)

S_{nc} = Section modulus for the extereme fiber of the monolithic or noncomposite section where tensile stress is caused by externally applied loads ($in.^3$)

Appropriate values for M_{dnc} and S_{nc} shall be used for any intermediate composite sections. Where the beams are designed for the monolithic or non-composite section to resist all loads, S_{nc} shall be substituted for S_c in the above equation for the calculation of M_{dnc}.

The following factors shall be used to account for variability in the flexural cracking strength of concrete, variability of prestress, and the ratio of nominal yield stress of reinforcement to ultimate:

γ_1 = flexural cracking variability factor

= 1.2 for precast segmental structures

= 1.6 for all other concrete structures

γ_2 = prestress variability factor

= 1.1 for bonded tendons

= 1.0 for unbonded tendons

$\gamma_3 =$ ratio of specified minimum yield strength to ultimate tensile strength of the reinforcement

= 0.67 for A615, Grade 60 reinforcement

= 0.75 for A706, Grade 60 reinforcement

= 1.00 for prestressed concrete structures

2.4.2 ACI 318-14 (ACI, 2014)

Art. 9.6.2.1 states for beams with bonded prestressed reinforcement, total quantity of mild reinforcement (A_s) and prestressed reinforcement (A_{ps}) shall be adequate to develop a factored load at least 1.2 times the cracking load calculated on the basis of the modulus of rupture (f_r), which is defined in Art. 19.6.2 as $7.5\sqrt{f'_c}$ (psi). The commentary of this section states that abrupt flexural failure immediately after cracking does not occur when the prestressing reinforcement is unbonded. Therefore, this requirement does not apply to members with unbonded tendon.

Additionally, Art. 9.6.2.3 states for beams with unbonded tendons the minimum area of bonded longitudinal reinforcement, $A_{s,min}$, shall be $0.004A_{ct}$, where A_{ct} is the area of that part of the cross section between the flexural tension face and the centroid of the gross section. This minimum bonded reinforcement is independent of reinforcement f_y. In this quantification, both prestressed and non-prestressed steel could be included to achieve the $A_{s,min}$. Under this current

code requirement, even in cases where unbonded reinforcement is provided, a minimum amount of bonded reinforcement, either non-prestressed or prestressed, is still required. Providing minimum amount of bonded reinforcement helps to ensure acceptable behavior at all loading stages.

2.4.3 BS 8110 (British Standards, 2007)

The British Standards states the design tensile stresses in flexure should not exceed $0.36\sqrt{f'c}$ [N/mm^2] for class 2 members. The resistance moment of a beam (M_r), containing bonded or unbonded tendons, all of which are located in the tension zone, may be obtained from the following equation:

$$M_r = f_{pb} A_{ps} (d - d_n) \quad [N - mm] \qquad (2.4)$$

Where f_{pb} is the design tensile stress in the tendons, A_{ps} is the area of prestressed tendons in the tensile zone, d is the effective depth to the centroid of prestressed tendon, and d_n is the depth to the centroid of the compression zone, which may be taken as 0.45x for a rectangular, or flanged beam in which the flange thickness is not less than 0.9x. Where x is the depth of the neutral axis.

For bonded tendons, values of f_{pb} and x may be obtained from Table 2.6. For unbonded tendons, values of f_{pb} and x may be obtained from equations (2.5) and (2.6). The value of f_{pb} should not be taken as greater than $0.7f_{pu}$.

$$f_{pb} = f_{pe} + \frac{7000}{\frac{l}{d}} \left(1 - 1.7 \left(\frac{f_{pu} A_{ps}}{f'_c bd}\right)\right) \quad \left[\frac{N}{mm^2}\right] \qquad (2.5)$$

$$x = 2.47 \left[\left(\frac{f_{pu} A_{ps}}{f'_c bd}\right)\left(\frac{f_{pb}}{f_{pu}}\right) d\right] \quad [mm] \qquad (2.6)$$

Where f_{pe} is the design effective Prestress in the tendons after all losses, l is the length of the tendons between end anchorages, and b is the width or effective width of the section or flange in the compression zone.

Table 2.6 – Conditions at the Ultimate Limit State for beams with Pre-tensioned or Post-tensioned Tendons having Effective Bond

$\frac{f_{pu}A_{ps}}{f_{cu}bd}$	Design stress in tendons as a proportion of the design strength, $f_{pb}/0.87f_{pu}$			Ratio of depth of neutral axis to that of the centroid of the tendons in the tension zone, x/d		
	f_{pe}/f_{pu}			f_{pe}/f_{pu}		
	0.6	0.5	0.4	0.6	0.5	0.4
0.05	1.00	1.00	1.00	0.12	0.12	0.12
0.10	1.00	1.00	1.00	0.23	0.23	0.23
0.15	0.95	0.92	0.89	0.33	0.32	0.31
0.20	0.87	0.84	0.82	0.41	0.40	0.38
0.25	0.82	0.79	0.76	0.48	0.46	0.45
0.30	0.78	0.75	0.72	0.55	0.53	0.51
0.35	0.75	0.72	0.70	0.62	0.59	0.57
0.40	0.73	0.70	0.66	0.69	0.66	0.62
0.45	0.71	0.68	0.62	0.75	0.72	0.66
0.50	0.70	0.65	0.59	0.82	0.76	0.69

2.4.4 Eurocode 2: Design of Concrete Structures (European Committee for Standardization, 2004)

A minimum amount of bonded reinforcement is required to control cracking in areas where tension is expected. Unless a more rigorous calculation shows lesser areas to be adequate, the required minimum areas of reinforcement may be calculated as follows. For profiled cross sections like box girders, minimum reinforcement should be determined for individual parts of the section (i.e. webs, flanges).

$$A_{s,min}\sigma_s = k_c k f_{ct,eff} A_{ct} \qquad (2.7)$$

Where,

$A_{s,min}$ = Minimum area of reinforcing steel within the tensile zone

A_{ct} = The area of concrete within the tensile zone

σ_s = The absolute value of the maximum stress permitted in the reinforcement immediately after formation of the crack. This may be taken as the yield strength of the reinforcement

$f_{ct,eff}$ = The mean value of the tensile strength of the concrete effective at the time when the cracks first occur

k = The coefficient which allows for the effect of non − uniform self − equilibrating stresses, which lead to a reduction of restraint forces

= 1.0 for webs with h ≤ 300 mm (11.8")

= 0.65 for webs with h ≥ 800 mm (31.5")

k_c = A coefficient which takes account of the stress distribtuion within the section immediately prior to cracking and of the change of the lever arm

- For pure tension: $k_c = 1.0$
- For bending or bending combined with axial forces:

$$k_c = 0.4\left[1 - \left(\frac{\sigma_c}{k_1\left(\frac{h}{h^*}\right)f_{ct,eff}}\right)\right] \leq 1 \qquad (2.8)$$

- For flanges of box sections and T-sections:

$$k_c = 0.9\frac{F_{cr}}{A_{ct}f_{ct,eff}} \geq 0.5 \qquad (2.9)$$

Where,

σ_c = the mean stress of the concrete acting on the part of the section under consideration:

$$\sigma_c = \frac{N_{ed}}{bh} \qquad (2.10)$$

N_{ed} = the axial force at the serviceability limit state acting on the part of the cross section under consideration. Should be determined considering the characteristic values of prestress and axial forces under the relevant combination of actions

$h^* = h$ (for $h < 1.0$ m) or 1.0 m (for $h \geq 1.0$ m)

k_1 = Coefficient considering the effects of axial forces on the stress distribution:

- $k_1 = 1.5$ if N_{ed} is a compressive force
- $k_1 = \frac{2h^*}{3h}$ if N_{ed} is a tensile force

F_{cr} = the absolute value of the tensile force within the flange immediately prior to cracking due to the the cracking moment calcuated with $f_{ct,eff}$

Bonded tendons in the tension zone may be assumed to contribute to crack control within a distance ≤ 150 mm (5.9”) from the center of the tendon. This may be taken into account by adding the term $\varepsilon_1 A'_p \Delta\sigma_p$ to the left hand side of equation 2.7.

Where:

A'_p = the area of pre or post − tensioned tendons within $A_{c,eff}$

$A_{c,eff}$ = the effective area of concrete in tension surrounding the reinforcement or prestressing tendons of depth $h_{c,eff}$

$h_{c,eff}$ = the lesser of $2.5(h - d)$, $\frac{h-x}{3}$, or h/2

ε_1 = the adjustment ratio of bond strength taking into account the different diameters of prestressing and reinforcing steel

$$= \sqrt{\varepsilon\left(\frac{\phi_s}{\phi_p}\right)} \qquad (2.11)$$

*Note: ε is established in Table 6.2 in Art. 6.8.2 (Eurocode 2, 2004)

ϕ_s = the largest bar diameter of reinforcing steel

ϕ_p = equivalent diameter of tendon:

$= 1.6\sqrt{A_p}$ for bundles

$= 1.75\phi_{wire}$ for single 7 wire strands

$= 1.2\phi_{wire}$ for single 3 wire strands

$\Delta\sigma_p$ = Stress variation in prestressing tendons from the state of

zero strain of the concrete at the same level

In prestressed members, no minimum reinforcement is required in sections where, under the characteristic combination of loads and the characteristic value of prestress, the concrete is compressed or the absolute value of tensile stress in the concrete is below $\sigma_{ct,p}$, which can be found in a specific countries National Annex.

$$A_{s,min} = 0.26\left(\frac{f_{ctm}}{f_{yk}}\right)b_t d \geq 0.0013 b_t d \quad [mm] \qquad (2.12)$$

Where b_t is the mean width of the tension zone and f_{ctm} is determined with respect to the relevant strength class according to Table 3.1 (Eurocode 2).

For members prestressed with permanently unbonded tendons or with external prestressing cables, it should be verified that the ultimate bending capacity is larger than the flexural cracking moment. A capacity of 1.15 times the cracking moment is sufficient.

2.4.5 Norwegian Standard (Norwegian Standards Association, 2003)

The Norwegian Standard (2003) required a minimum amount of reinforcement such that:

$$A_s \geq 0.25 k_w A_c \left(\frac{f_{tk}}{f_{sk}}\right) \qquad (2.13)$$

where,

$$k_w = 1.5 - \frac{h}{h_1} \geq 1.0$$

h_1 = 1.0 m [39.37 in]

f_{tk} = the tensile strength of concrete

f_{sk} = the steel yield strength

This standard is no longer utilized, as Eurocode 2 has been adopted by Norway. However, this requirement is included as it considers the parameter of beam depth in the computation.

2.4.6 Leonhardt's Method (1964)

Fritz Leonhardt proposed a method for solving the minimum reinforcement by equating the tensile forces in the concrete beam to the change in steel stresses (Leonhardt, 1964). The stresses are assumed to vary linearly across the section. Thus, the tensile force (T_{cr}) is directly correlated to the concrete's tensile strength. The tensile force is modified by a shape factor (κ) to represent the area under tension within the section. Change in the steel stresses occurs due to elongation after the beam has cracked. Figure 2.13 shows the stress distribution right before cracking occurs and at flexural capacity.

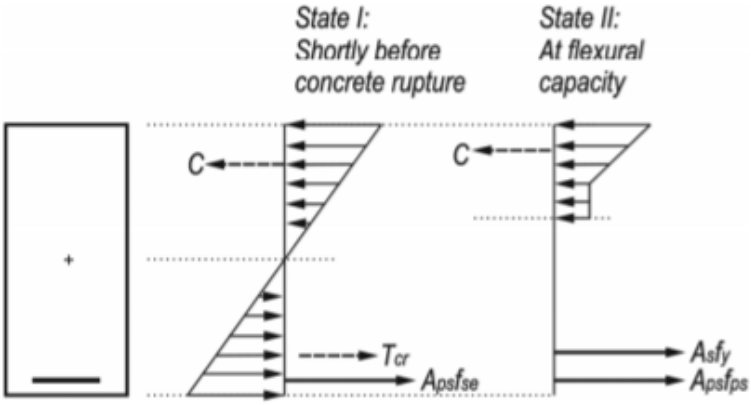

Figure 2.13 – Forces Present in Reinforced Concrete Member at Varying Load States from Brenkus and Hamilton (2014)

$$T_{cr} = \kappa \left[\frac{1}{2} b_w \left(\frac{h}{2}\right)\right] f_r \qquad (2.14)$$

$$A_{ps}\left(f_{ps} - f_{se}\right) + A_s f_y \geq T_{cr} \qquad (2.15)$$

Where A_{ps} is the area of prestressed reinforcement steel, f_{ps} is the prestressing stress associated with ultimate flexural capacity, f_{se} is the effective prestressing stress. This method is advantageous due to its simple nature. The procedure for calculating the minimum required steel becomes non-iterative and is independent of the cracking moment calculation. However, if a

non-rectangular section is utilized, computing the tensile force can become complex. Additionally, it should be noted that the depth of steel and the concrete's capacity are neglected.

Brenkus and Hamilton proposed a minimum reinforcement requirement for ACI based on modifying Leonhardt's approach (Brenkus and Hamilton, 2014). The modifications of the Leonhardt approach came from the assumptions used in the original formulation, which are the location of the steel depth at the resultant of the tensile force of the beam, the geometry of the beam under tension having a rectangular section, and ignoring the possible composite nature of a beam and deck section. It was noted that these assumptions are conservative for most cases, but that greater accuracy could be achieved by using a refined set of assumptions for the specific structure in question. When the member contains only prestressing steel, the minimum requirement for bonded prestressed reinforcement is simplified as follows:

$$A_{ps,min} = \frac{9\sqrt{f'_c}}{0.8\left(\frac{y_t}{I}\right)_{final} f_{ps} d_p - f_{se}\left(\frac{1}{A}+\frac{e y_t}{I}\right)_{transfer}} \qquad (2.16)$$

Rather than the requirement being based on the forces in the steel, Brenkus and Hamilton proposed a moment-based approach. The net cracking moment was defined as the moment beyond the decompression condition that required to cause flexural cracking in the member. Therefore, the design moment must be greater than the sum of the decompression and net cracking moments. A resistance factor (ϕ) is provided with the design moment and a factor of 1.2 is applied to the net cracking moment. The design moment was constructed based on an internal moment arm philosophy with the assumption that jd and ϕ are 0.9, where jd is the internal moment arm ratio. The greatest advantage of this proposed equation is that is avoids an interactive process. The proposed method consistently provided an overstrength moment ratio ($\phi M_n/M_{cr}$) of 1.16 or greater within the parametric study conducted (Brenkus and Hamilton, 2014).

2.5 Comparison of Beam Design with Various Code and Methodologies

A comparative study of the different codes and methodologies discussed was carried out using the typical cross section of a segmental post-tensioned concrete test girder of the experimental study, UNB3, shown in Figure 2.14. Note, the modified Leonhardt design method (Brenkus and Hamilton, 2014) was not included, as it is only applicable with bonded prestressing steel.

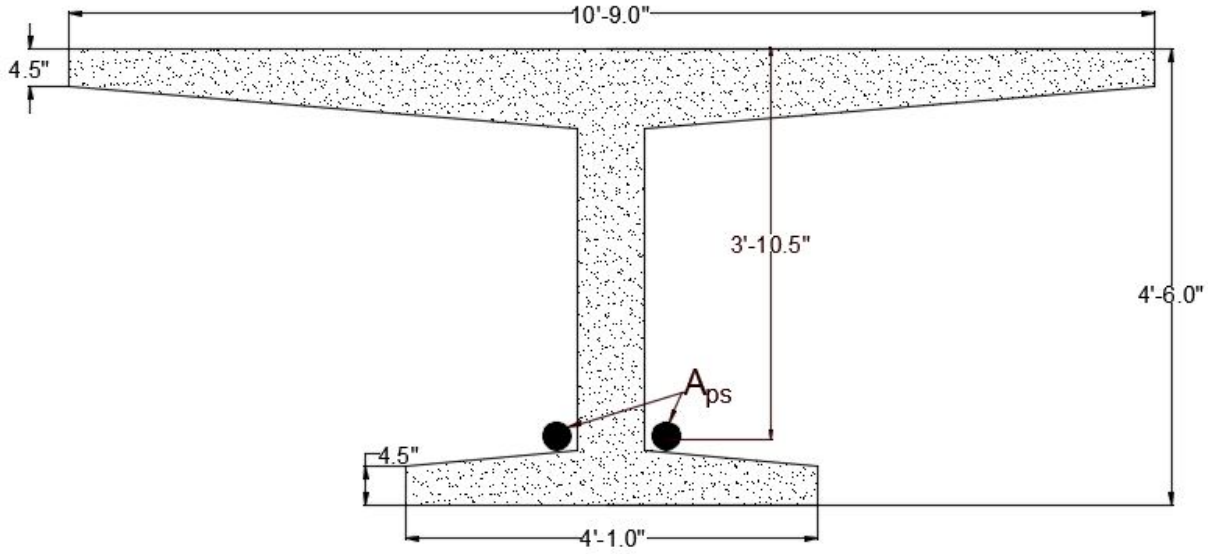

Figure 2.14 – Girder UNB3 Typical Cross Section

Table 2.7 exhibits the difference in the minimum reinforcement required for each aforementioned code ranging from 1.39 in^2, Norwegian Standard, to 4.81 in^2, British Standards. The mean $A_{ps,min}$ is 2.86 in^2 with a standard deviation of 1.15 in^2.The AASHTO requirement of 3.90 in^2 is above the average of all codes.

Table 2.7 – Comparison of Code Requirement for Minimum Reinforcement

Code	$A_{ps,min}$ (in^2)
AASHTO (8th Edition)	3.90
ACI 318-14	2.07
Leonhardt Method	2.61
BS 8110	4.81
Eurocode 2	2.36
Norwegian Standard	1.39
Average	2.86
St. Dev.	1.15

2.6 Summary of Findings

Important findings from the state-of-knowledge presented in this chapter as relevant to this project are summarized as follows:

- There has been very little experimental research to study the minimum flexural reinforcement requirements on bridge girders, specifically research involving prestressed concrete and segmentally constructed girders subjected to large-scale testing.

- Past research on minimally reinforced structures has used several measures to quantify the performance of a structure, such as moment ratios, ductility, brittleness number, deflection, etc.; however, there has been no consensus on what the best measure is for ensuring adequate safety of flexural members designed with minimum reinforcement after they experience flexural cracking. The most commonly used parameters are strength and ductility.

- Three parameters have been utilized in current code to limit the minimum flexural reinforcement in flexural members: ductility and strength ratio (mainly for safety) as well as crack width. Due to the emphasis on safety, crack width is not considered as a main controlling parameter in the current project since different provisions are used in AASHTO LRFD Design Specifications to evaluate this.

- Minimum flexural reinforcement requirements in the current codes, standards, and specifications vary significantly and are based on different assumptions.

CHAPTER 3 - EXPERIMENTAL STUDY AND BEHAVIOR ANALYSIS OF TEST GIRDERS WITH MINIMUM FLEXURAL REINFORCEMENT

3.1 Introduction

This chapter presents a summary of the completed experimental and analytical investigation of the segmental post-tensioned concrete girder portion of the NCHRP 12-94 research project. In total, three unbonded post-tensioned segmental concrete girders and one bonded post-tensioned segmental girder were tested. All girders represented the full-scale girder at either a 1/2 or a 1/3 scale of a 9 ft deep typical AASHTO box girder. For all tested girders, analytical models were developed then validated through the experimental results. Various conclusions were made at the commencement of the experimental study. This chapter was prepared to be submitted as a stand-alone research article, and thus there may be some redundancies with other chapters within the thesis.

3.2 Proposed revisions to minimum flexural reinforcement requirements

The current AASHTO minimum flexural reinforcement requirements was presented in Section 2.4.1. This section presents the proposed revisions for the current code requirement on minimum flexural reinforcement.

3.2.1 Proposed revisions to AASHTO LRFD Specifications (NCHRP 12-94)

The research study detailed within this chapter was completed as part of a larger research project examining the minimum flexural reinforcement requirement through the National Cooperative Highway Research Program (NCHRP). The following are the changes the project team recommended based on the experimental results for Article 5.6.3.3 of AASHTO LRFD regarding minimum flexural reinforcement provisions in the AASHTO LRFD specifications (Sritharan et. al, 2018):

Deletions are shown as a single ~~strikethrough~~.

Additions are shown as <u>underlined</u>.

Unless otherwise specified, at any section of a non-compression-controlled flexural component, the amount of prestressed and non-prestressed tensile reinforcement shall be adequate to develop a factored flexural resistance, M_r, ~~greater than or equal to the lesser of the following~~ <u>at least equal to the lesser of:</u>

- ~~1.33~~ *α times the factored moment required by the applicable strength load combination specified in Table 3.4.1-1;*

$$M_{cr} = \gamma_3 \left[(\gamma_1 f_r + \gamma_2 f_{cpe}) S_c - M_{dnc} \left(\frac{S_c}{S_{nc}} - 1 \right) \right] \quad (3.1)$$

where:

<u>α = *strength factor for minimum reinforcement* $1.0 \leq \alpha = 1.0 + \frac{.33(\varepsilon_t - \varepsilon_c)}{(\varepsilon_{tl} - \varepsilon_{cl})} \leq 1.33$</u>

<u>ε_t = *net tensile strain in the extreme tension steel at nominal resistance, per AASHTO LRFD.*</u>

f_r = *modulus of rupture of concrete specified in Article 5.4.2.6.*

f_{cpe} = *compressive stress in concrete due to effective prestress forces only (after allowance for all prestress losses) at extreme fiber of section where tensile stress is caused by externally applied loads (ksi)*

M_{dnc} = *total unfactored dead load moment acting on the monolithic or noncomposite section (k-in.)*

S_c = *section modulus for the extreme fiber of the composite section where tensile stress is caused by externally applied loads (in.^{3})*

Appropriate values for M_{dnc} and S_{nc} shall be used for any intermediate composite sections. Where the beams are designated for the monolithic or noncomposite section to resist all loads, substitute S_{nc} for S_c in the above equation for the calculation of M_{cr}.

The following factors account for variability in the flexural cracking strength of concrete, variability of prestress and the ratio of nominal yield stress of reinforcement to ultimate.

γ_1 = *flexural cracking variability factor*

= $1.2\ (h/12)^{-0.15}$ *for precast segmental structures*

= $1.6\ (h/12)^{-0.15}$ *for all other concrete structures, where h is the member depth (in.)*

γ_2 = *prestress variability factor*

= *1.1 for bonded tendons*

= *1.0 for unbonded tendons*

γ_3 = *ratio of specified minimum yield strength to ultimate tensile strength of the nonprestressed reinforcement*

= *0.67 for AASHTO M 31 (ASTM A615), Grade 60 reinforcement*

= *0.75 for ASTM M 31 (ASTM A615), Grade 75 reinforcement*

= *0.76 for ASTM M 31 (ASTM A615), Grade 80 reinforcement*

= *0.75 for A706, Grade 60 reinforcement*

= *0.80 for A706, Grade 80 reinforcement*

As seen in the proposed revision, a variable h, member depth, is introduced as a factor to determine the flexural cracking variability factor. The depth of the member, h, influences the modulus of rupture, which has been supported by the fracture mechanics theory and some experimental work (Bosco et al., 1990; Bruckner and Eligehausen, 1998; Ferro et al., 2007; Rao et al., 2008; Carpinteri and Corrado, 2011). However, due to lack of sufficient experimental data, the current code requirements ignore the influence of the member depth, which can lead to unnecessarily high amount of minimum flexural reinforcement in real-world examples. Including this effect of depth may significantly influence the minimum flexural reinforcement because of their basis in the cracking moment, which is dependent on the modulus of rupture.

Additionally, segmentally constructed girders appear to have lower modulus of rupture (Megally, 2003). This research concluded that the lower modulus of rupture is due to the soft layer of concrete at the ends of the segments adjacent to the epoxied joints, where large aggregates are hardly present. Thus, if a primary goal in prescribing minimum flexural reinforcement is to ensure the stability of the structure after flexural cracking, it is imperative to consider the influence of the depth and type of construction of the member for accuracy. Segmental girders tested for minimum flexural reinforcement are absent from the experimental literature.

3.3 Design process of test girders with minimum flexural reinforcement

All test girders were designed at full-scale using a 9 ft deep typical AASHTO box girder section. The test girders were then scaled to 1/3 (i.e. UNB1 and UNB2) and 1/2 (i.e. UNB3 and BON2) scale for testing. Additional modifications were made to the test girders to ensure the formwork and construction was cost effective. Table 3.1 summarizes the experimental test matrix.

Table 3.1 – Experimental Test Matrix

Type	Section ID	Depth	Span Length (ft)	Span-to-Depth Ratio	Target f'_c (ksi)	Target ρ_{design}
Unbonded Post-Tensioned	UNB1	3'-0"	66	22	6	75% AASHTO Min
	UNB2	3'-0"	54	18		
	UNB3	4'-6"	54	12		
Bonded Post-Tensioned	BON2	4'-6"	54	12		

The segmental girder's overall profiles are detailed in Figure 3.1. The unbonded post-tensioned segmental girders contained external harped tendons, which deviate at the deviator segments. The bonded post-tensioned segmental girder contained an internal parabolic tendon. Figure 3.2 through Figure 3.4 detail the cross-section of a typical, deviator, and end block segment for each girder. Additionally, Appendix A contains the structural drawings for all test girders. Note, only the unbonded post-tensioned test girders will have deviator segments to create the harped profile of the prestressed tendon.

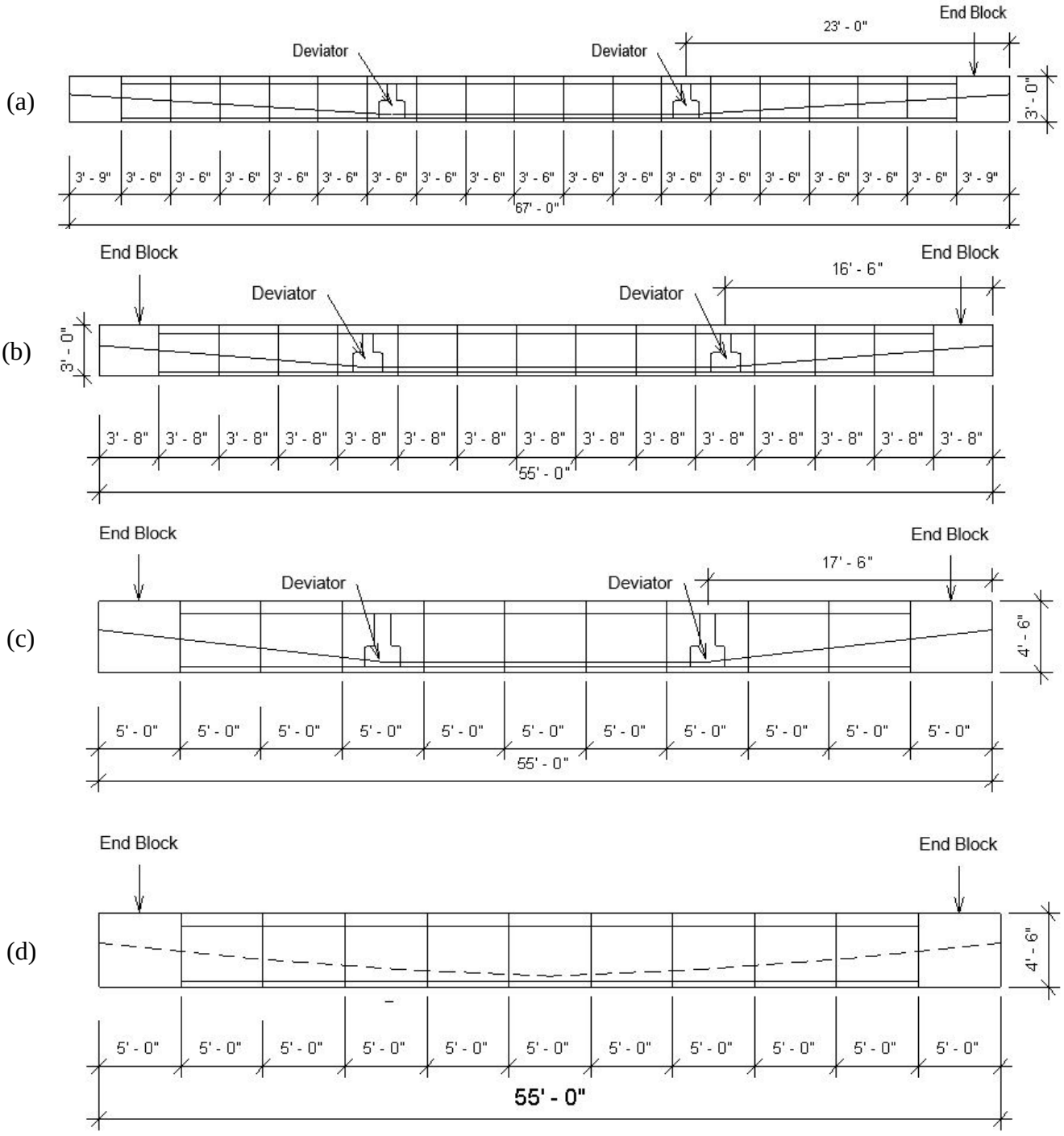

Figure 3.1 – Segmental Profile of (a) UNB1 (b) UNB2 (c) UNB3 (d) BON2 Girders

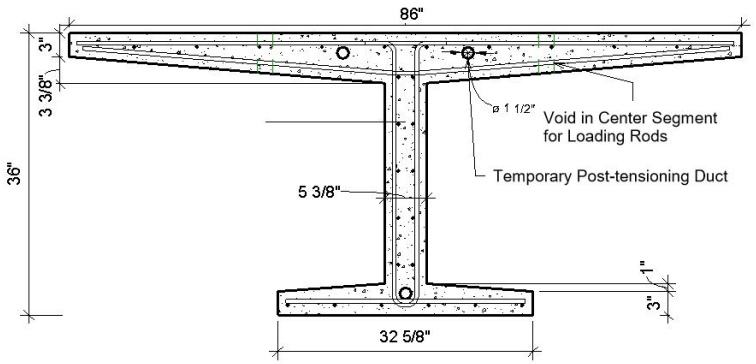

(a)

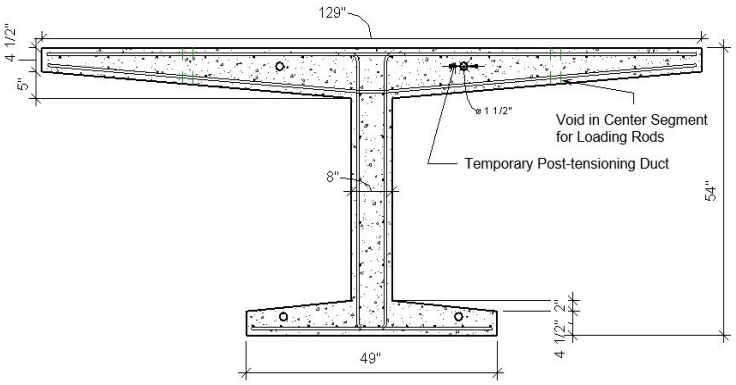

(b)

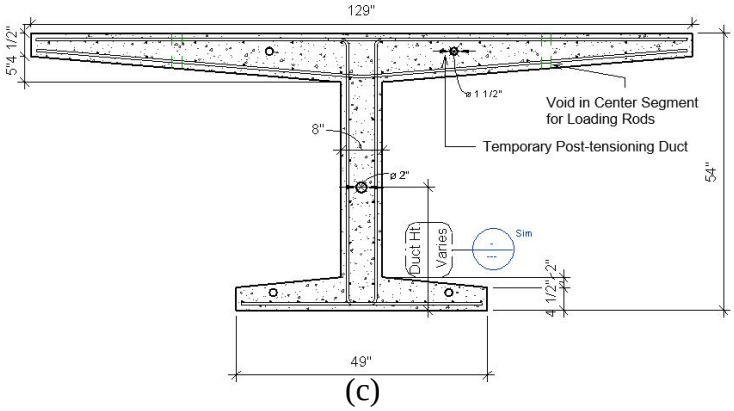

(c)

Figure 3.2 – Typical Segment Cross-Section (a) UNB1, UNB2 (b) UNB3 (c) BON2

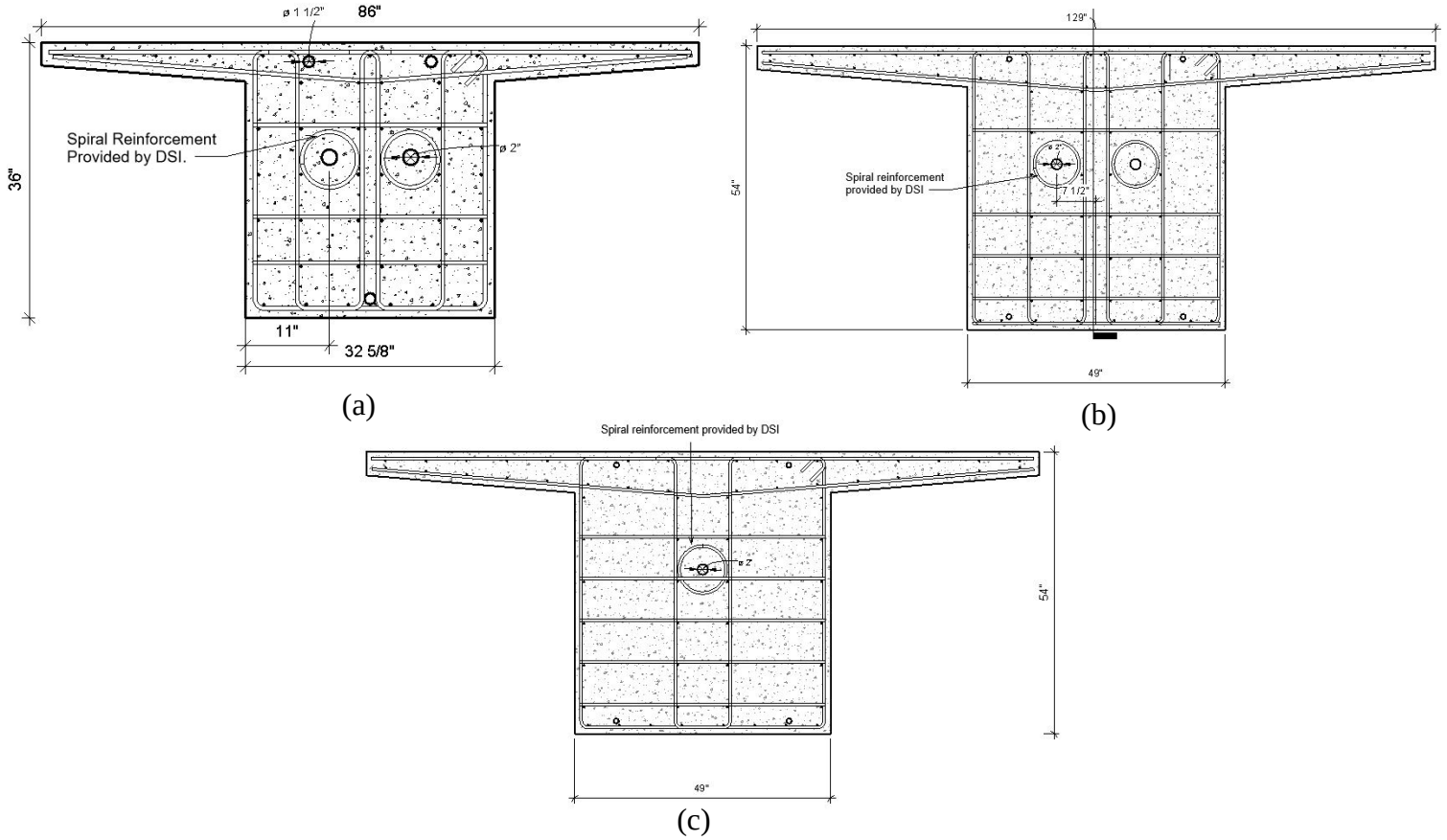

Figure 3.3 – End Block Cross-Section (a) UNB1, UNB2 (b) UNB3 (c) BON2

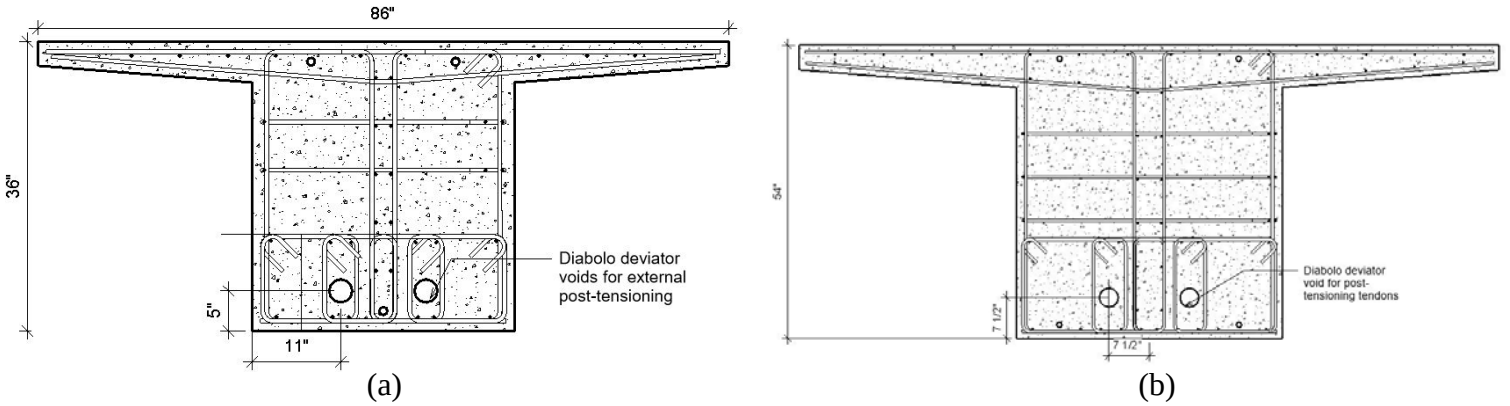

Figure 3.4 – Deviator Segment Cross-Section (a) UNB1, UNB2 (b) UNB3

In all cases, the minimum reinforcement was determined at the full-scale, however, the minimum reinforcement solution did not converge at test scale when re-evaluated for UNB1 and UNB2. The nominal moment (ϕM_n) did not exceed the cracking moment (M_{cr}) (i.e. $\frac{\phi M_n}{M_{cr}} < 1$) regardless of the amount of prestressed reinforcement added. To address this issue, UNB1 was constructed with less reinforcement and UNB2 was constructed with more reinforcement than the required minimum according to the AASHTO LRFD Specifications (AASHTO, 2017). Comparing the responses of UNB1 and UNB2 with each other, as well as to the response of UNB3 would determine if the use of Leonhardt's method, a common method practiced in industry, for designing the minimum reinforcement is appropriate when utilization of the AASHTO LRFD method for designing the minimum reinforcement leads to no convergence.

Leonhardt's Method is a method produced by Fritz Leonhardt for solving the minimum reinforcement by equating the tensile forces in the concrete beam to the change in steel stressed (Leonhardt, 1964). The stresses are assumed to vary linearly across the section. Thus, the tensile force (T_{cr}) is directly correlated to the concrete's tensile strength. The tensile force is modified by a shape factor (κ) to represent the area under tension within the section. Change in the steel stresses occurs due to elongation after the beam has cracked. Figure 3.5 illustrates the stress distribution right before cracking occurs and at flexural capacity.

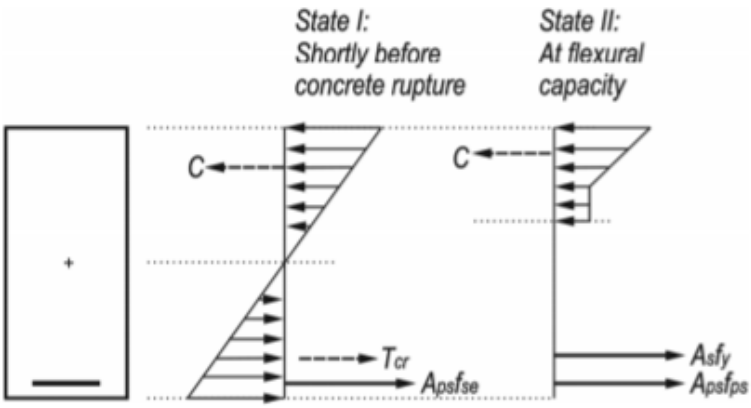

Figure 3.5– Forces Present in Reinforced Concrete Member at Varying Load States from Brenkus and Hamilton (2014)

$$T_{cr} = \kappa\left[\frac{1}{2}b_w\left(\frac{h}{2}\right)\right]f_r \qquad (3.2)$$

$$A_{ps}(f_{ps} - f_{se}) + A_s f_y \leq T_{cr} \qquad (3.3)$$

This method is advantageous due to its simple nature. The procedure for calculating the minimum required steel becomes non-iterative and is independent of the cracking moment calculation. However, if a non-rectangular section is utilized, as typically the case in segmental girders, computing the tensile force can become complex. Additionally, it should be noted that the depth of steel and the concrete's capacity are neglected.

3.4 Experimental study

This section details the work completed in the experimental study portion of the research project. Specifically, this section summarizes the construction process, material testing conducted, instrumentation of the test girders, and the experimental test results.

3.4.1 Construction

Construction of the segmental girders was completed in-house at Iowa State University Structural Laboratory. Table 3.2 summarizes properties of the tested segmental post-tensioned girders.

Table 3.2 – Summary of Segmental Post-Tensioned Test Girders

% Minimum Flexural Reinforcement			Strands			
Beam	ρ_{design}	$\rho_{experimental}$	Diameter (in)	Quantity	f_{pi} (ksi)	f_{pi}/f_{pu}
UNB1	81.0%	66.4%	0.6	10	204.7	0.76
UNB2	130.9%	115.9%	0.6	14	196.9	0.73
UNB3	73.8%	59.3%	0.5	18	186.2	0.69
BON2	56.3%	47.8%	0.5	12	153.5	0.57

Casting of segments was completed using the long-line approach. Meaning, after casting of a segment was complete, it was left in place for the next pour to be match-cast against the end of the previous segment. Match-casting was employed to ensure the segments' joints would be properly placed together when they are epoxied. Each segment was provided a minimum curing time of 48 hours to ensure adequate strength during form removal. Debonding agent was applied on the segment prior to match-casting to inhibit bonding between the concrete surfaces. Figure 3.6 shows the match-casting process described.

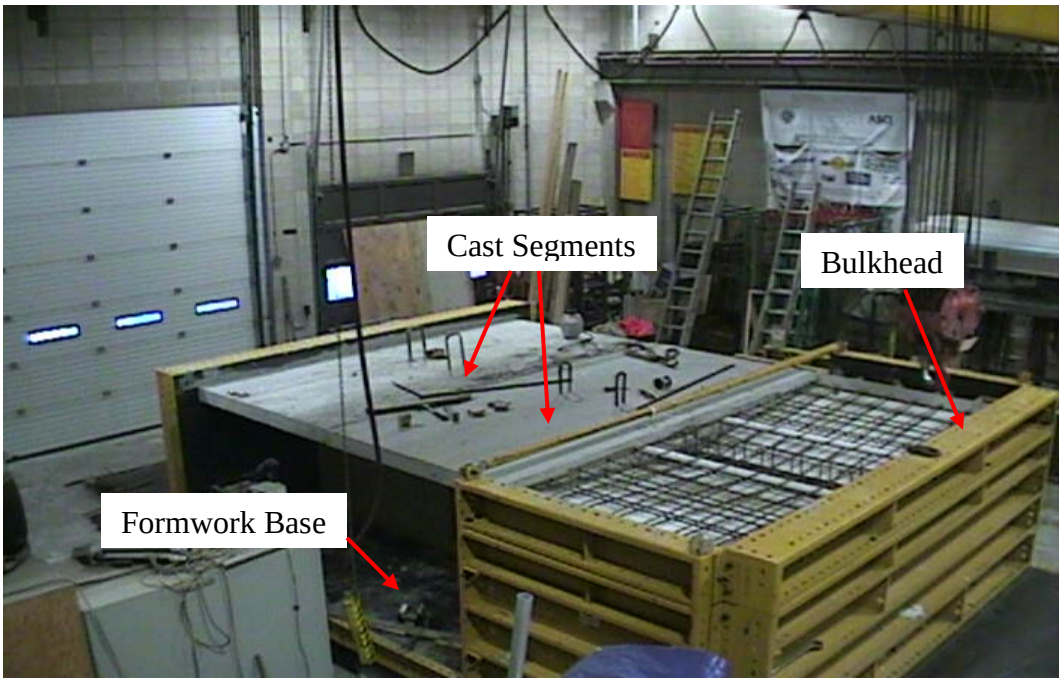

Figure 3.6 – Segment Match-casting Setup (Sritharan et. al., 2018)

Following the casting of all segments of a test girder, the segments were individually removed and the shear key surface of each segment was prepared by pressuring washing each face at 3,500 psi, in accordance with epoxy specifications. In order to allow adequate time for the application of the epoxy, a slow set epoxy suitable for 55° F - 75° F temperature range was selected.

To ensure suitability of the selected epoxy, a tensile test was conducted on concrete cylinders connected with the slow set epoxy to examine the failure surface. The results of the tests was a consistent fracture in the concrete adjacent to the epoxy layer, not within the epoxy layer, as seen in Figure 3.7. This validated the suitability of the epoxy for use in construction. Additional testing of materials completed within the project is detailed in section 3.4.2.

Figure 3.7 – Failure of Cylinders Connected with Epoxy from Tensile Test (Sritharan et. al., 2018)

The epoxy process was started at the midspan section and moved outward, concluding with the end block sections. Prior to epoxying, the midspan section was secured in place utilizing vertical rods placed through voids in the section's flanges to ensure proper placement on the temporary shoring. An epoxy layer of approximately 1/16 in. thick was applied to each concrete face, totaling to 1/8 in. of epoxy within each joint, in accordance with FHWA Standards

(FHWA, 2014). Once epoxy was applied, the girders were moved into place and a temporary post-tensioning force was applied to generate a stress of 0.04 ksi across the joint, in accordance with the AASHTO Specification Art. 5.12.5.4.2 (AASHTO, 2017), as seen in Figure 3.8. The epoxied segments were then cured for a minimum of 48 hours before the temporary force was removed and the next segments were set in place to repeat the aforementioned process. Figure 3.9 shows joint interfaces after the curing process.

Figure 3.8 – Application of Temporary Post-tensioning Force (Sritharan et. al., 2018)

Figure 3.9 – Joint Interfaces after Curing (Sritharan et. al., 2018)

Once the epoxy within all joints of the girder reached the minimum strength requirement of 6 ksi, the steel tendons, composed of either 0.5 in. or 0.6 in. 7-wire diameter strands were placed. The target stress of each tendon was 75% of f_{pu}, where f_{pu} is the specified ultimate strength of 270 ksi. To ensure no cracking within the girder during the post-tensioning, the unbonded girder's (UNB1, UNB2, UNB3) tendons were stressed at alternating steps of 25% of f_{pu} between each tendon until the target stress of 75% f_{pu} was reached.

Once post-tensioning was completed, the end supports were put into place and the temporary shoring was removed from under the girder. Following the removal of the temporary shoring, the unbonded girders were ready to be instrumented and tested. However, the BON2 girder required an additional step in which the internal duct containing the prestressed tendon was grouted. The grout was pumped from one end of the girder to the other, with an additional outlet located at the midspan of the girder, the low point of the tendon profile, to ensure proper flow. Grout flowing out of the opposite end, as well as the build-up of pressure following closure of all outlet valves ensure proper grouting of the tendon.

3.4.2 Material testing

The test girders used self-consolidating concrete to ensure proper casting with minimal voids, a specific area of concern was the bottom flange of the girder. The specified concrete compressive strength (f'c) was 6,000 psi at 28 days. The concrete strength of each segment was evaluated periodically over the 28-day period following casting, as well as the day of testing, denoted as TD. Table 3.3 through Table 3.6 report the concrete compressive strengths over the period described. Additional tests were conducted on the middle three segments of each girder to obtain the rupture strengths.

Table 3.3 - Measured Material Properties for Midspan Segments of Girder UNB1

Segment	Age (days)	Compressive Strength, f'_c (psi)	Modulus of Rupture Strength, f_r (psi)	Splitting Strength, f_{sp} (psi)	$f_r/\sqrt{f'_c}$ (ksi)	$f_{sp}/\sqrt{f'_c}$ (ksi)
9	1	2,401	N/A	N/A	N/A	N/A
	7	5,241				
	14	6,345				
	28	7,689				
	134 (TD)	9,102	N/A	N/A	N/A	N/A
10	1	2,344	N/A	N/A	N/A	N/A
	7	5,729				
	14	7,291				
	28	8,546				
	130 (TD)	9,538	1,251	857.7	0.405	0.278
11	1	1,867	N/A	N/A	N/A	N/A
	7	5,332				
	14	6,977				
	28	8,870				
	126 (TD)	9,468	N/A	N/A	N/A	N/A

Table 3.4 - Measured Material Properties for Midspan Segments of Girder UNB2

Segment	Age (days)	Compressive Strength, f'_c (psi)	Modulus of Rupture Strength, f_r (psi)	Splitting Strength, f_{sp} (psi)	$f_r/\sqrt{f'_c}$ (ksi)	$f_{sp}/\sqrt{f'_c}$ (ksi)
7	1	2074	N/A	N/A	N/A	N/A
	7	4572				
	14	6142				
	28	7185				
	123 (TD)	8665	1,328	845	0.451	0.287
8	1	1446	N/A	N/A	N/A	N/A
	7	4462				
	14	5662				
	28	7318				
	119 (TD)	7830	1,367	739	0.489	0.264
9	1	1525	N/A	N/A	N/A	N/A
	7	5123				
	14	6074				
	28	7145				
	117 (TD)	8477	1,334	822	0.458	0.282

Table 3.5 – Measured Material Properties for Midspan Segments of Girder UNB3

Segment	Age (days)	Compressive Strength, f'_c (psi)	Modulus of Rupture Strength, f_r (psi)	Splitting Strength, f_{sp} (psi)	$f_r/\sqrt{f'_c}$ (ksi)	$f_{sp}/\sqrt{f'_c}$ (ksi)
5	1	1605	N/A	N/A	N/A	N/A
	7	5793				
	14	7191				
	28	8278				
	105 (TD)	9631	1,416	839	0.456	0.270
6	1	1051	N/A	N/A	N/A	N/A
	7	5779				
	14	6967				
	28	8404				
	102 (TD)	9501	1,237	809.5	0.401	0.262
7	1	872	N/A	N/A	N/A	N/A
	7	5190				
	14	6231				
	28	8033				
	98 (TD)	8844	1,383	739.5	0.465	0.249

Table 3.6 - Measured Material Properties for Midspan Segments of Girder BON2

Segment	Age (days)	Compressive Strength, f'_c (psi)	Modulus of Rupture Strength, f_r (psi)	Splitting Strength, f_{sp} (psi)	$f_r/\sqrt{f'_c}$ (ksi)	$f_{sp}/\sqrt{f'_c}$ (ksi)
5	1	1230	N/A	N/A	N/A	N/A
	7	4927				
	14	6109				
	28	6562				
	150 (TD)	8807	1,329	727	0.448	0.245
6	1	1186	N/A	N/A	N/A	N/A
	7	4279				
	14	6029				
	28	6432				
	141 (TD)	8444	1,160	794.9	0.399	0.274
7	1	1267	N/A	N/A	N/A	N/A
	7	5672				
	14	7379				
	28	8430				
	139 (TD)	9633	1,293	881.9	0.416	0.284

To obtain accurate data on the prestressing strand utilized, a uniaxial tensile test was conducted on 3-ft long samples of 0.6 in. diameter strand, used in UNB1 and UNB2, and 0.5 in. diameter strand, used in BON2 and UNB3. Figure 3.10 and Figure 3.11 present the average result of these tests, respectfully. The yield strength was determined using a 0.2% offset strain. The strand material properties of Young's modulus (E_s), yield stress (f_{py}), ultimate stress (f_{pu}), and ultimate strain (ε_s) for each strand size is tabulated in Table 3.7 and Table 3.8.

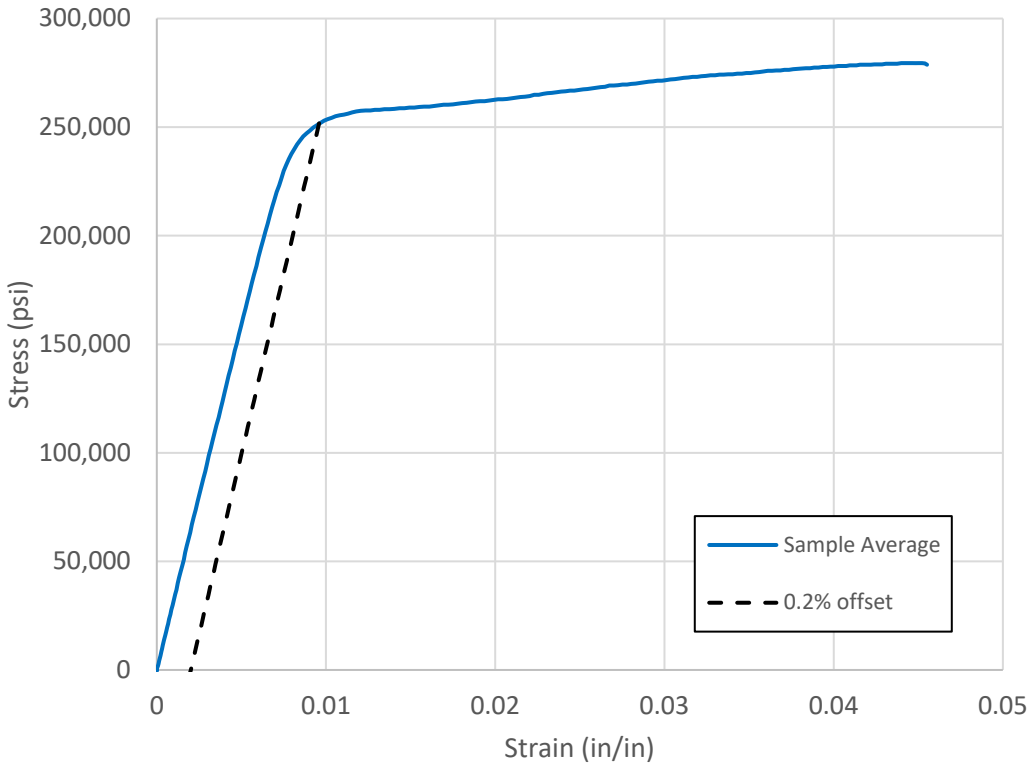

Figure 3.10 – Stress vs. Strain Diagram for the 0.6 in. diameter Prestressing Strand

Table 3.7 – Material Properties of 0.6 in. diameter Prestressing Strand

E_{ps} (ksi)	f_{py} (ksi)	f_{pu} (ksi)	ε_u (in/in)
31,100	251	277.4	0.046

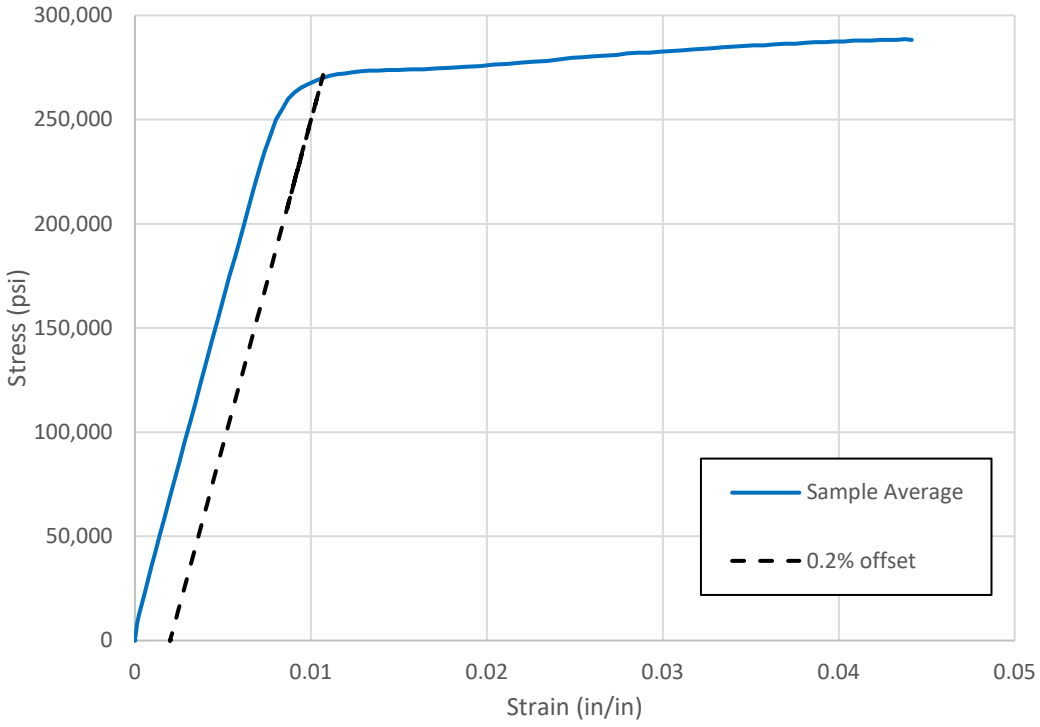

Figure 3.11 – Stress vs. Strain Diagram for the 0.5 in. diameter Prestressing Strand

Table 3.8 – Material Properties of 0.5 in. diameter Prestressing Strand

E_{ps} (ksi)	f_{py} (ksi)	f_{pu} (ksi)	ε_u (in/in)
31,200	251	268.5	0.043

Additional material tests were conducted on grout specimens for BON2 and the epoxy utilized on all test girders. Grout samples for girder BON2 were utilized to obtain the compressive strength over time. Grout compressive strength over time is presented in Figure 3.12 and Table 3.9. Epoxy cubes were also tested to evaluate the strength. The average compressive strength at 28 days for the epoxy is 8,183 psi.

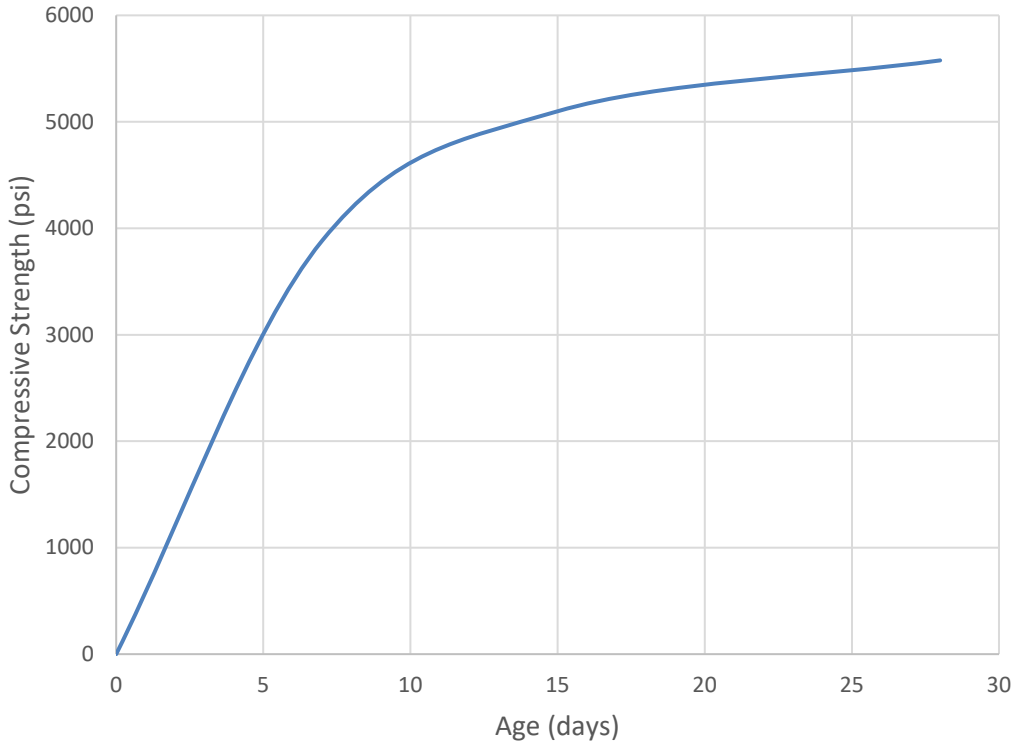

Figure 3.12 – Increase in Compressive Strength with Time for Girder BON2 Grout

Table 3.9 - Measured Compressive Strength of Girder BON2 Grout

Age (days)	Compressive Strength, f'_c (psi)
7	3884
15 (TD)	5099
28	5577

3.4.3 Instrumentation

Data acquisition instruments were applied to the test girders prior to testing in order to capture the overall behavior. Specific areas of interest were the behavior at the segmental joints near the midspan. The girders were externally instrumented with displacement transducers at critical joints near the midspan to measure the crack opening. String potentiometers were applied underneath the girders to monitor the deflection along the length of the girder. An Optoktrak 3D LED system was utilized at the midspan section, as seen in Figure 3.13, to capture the critical joint openings and vertical slip between segments. Tiltmeters were applied at the end blocks to evaluate the rotation during testing. Strain gauges were placed along the length of the prestressing tendons, on specific rebar within the middle segment, and on the concrete of the middle segment near the loading apparatus. The strain gauges were applied prior to the initial prestressing in order to record the strain increase from the post-tensioning process, as well as during the test. The strain gauges were protected with a coating of polyurethane and tape to ensure adequacy through testing.

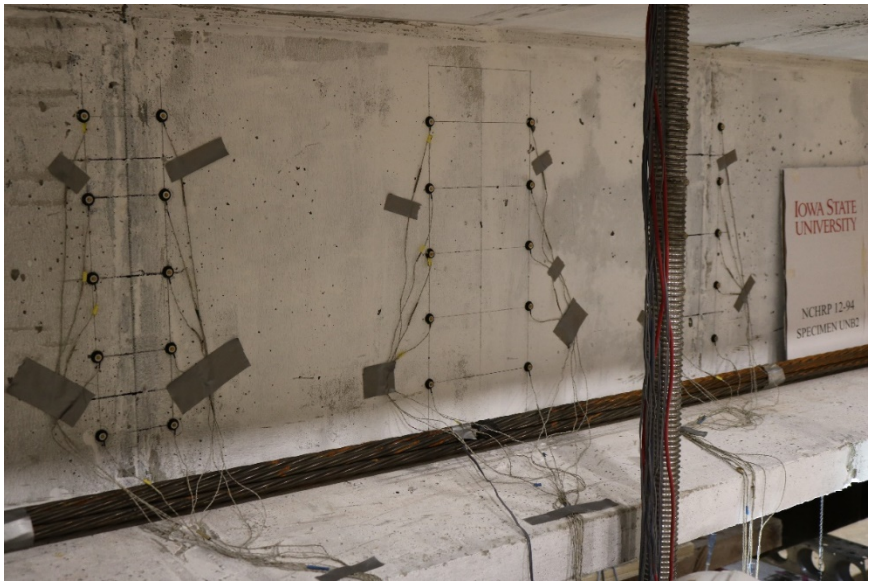

Figure 3.13 – Optoktrak 3D LED layout for Girder UNB2 (Sritharan et. al., 2018)

There were differences in the instrumentation used between the externally unbonded and internally bonded post-tensioned segmental test girders. The post-tensioning and testing of UNB1 and UNB2 was monitored using load cells at each end of the beam. However, for UNB3 and BON2 the prestressing tendon diameter exceeded that of the load cell, thus additional strain gauges were mounted on the tendons. Strain gauges were applied to the internal tendon of girder BON2 prior to entry into the duct. Due to the grouting of the internal tendon, the strain gauges were only used to evaluate the tendon strain during the post-tensioning process.

3.4.4 Testing

All segmental post-tensioned concrete test girders were tested by applying a load at the midspan, detailed in Figure 3.14. The load was applied in a quasi-static manner incrementally at specific load steps, as show in Figure 3.15. After each load step, the test was paused, visual inspection was conducted, and cracks were located and marked on the front (South) and back (North) sides of the girder, as well as on the bottom surface of the girder near the midspan. The test girders were subjected to quasi-static loading rather than introducing fatigue loading due to the research conducted by Rao and Frantz (Rao and Frantz, 1996). In this research, prestressed concrete box girders that had been in service for 27 years were subjected to fatigue loading. The study concluded that fatigue may need not be a concern as long as the beam is uncracked.

Figure 3.14 – Test Setup for Segmental Girders (Sritharan et. al., 2018)

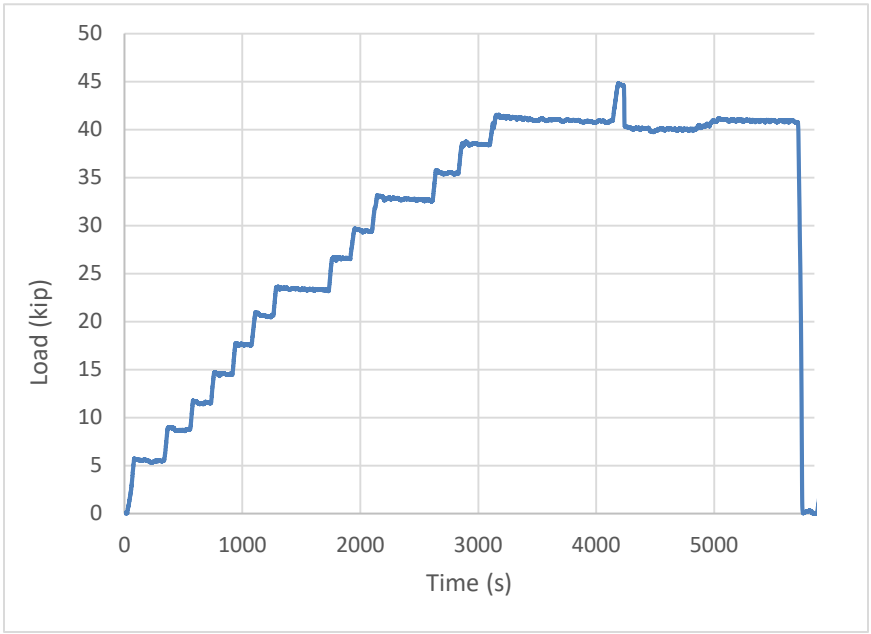

Figure 3.15 – UNB1 Loading vs. Time

The experimental testing led to a better understanding of the behavior of post-tensioned segmental girders with unbonded and bonded tendons, specifically with reinforcement amount both above (UNB2) and below (UNB1, UNB3, BON2) the current required amount by the

AASHTO LRFD Bridge Design Specifications (AASHTO, 2017). The overall responses of the test girders helps to assess if the goal of the minimum flexural reinforcement requirement, which is to ensure adequate safety by providing sufficient warning prior to failure, is met. In addition to providing adequate safety, it is important to verify that the maximum moment resisted by the test girder is greater than the cracking moment. Table 3.10 presents a visual summary of the responses of the tested girders. A detailed account of the testing of each girder is presented in the subsequent sections.

Table 3.10– Summary of Responses of Test Girders

Name	Height	Span (ft)	Cracking Load (kip)	Failure Load (kip)	fr/√f'c (ksi)	Failure Mode
UNB1	3'-0"	66	42	45	0.19	Tendon Rupture
UNB2	3'-0"	54	91	108	0.15	Shear Slip
UNB3	4'-6"	54	116	164	0.14	Shear Slip
BON2	4'-6"	54	60	122	0.09	Tendon Rupture

3.4.5 Experimental test results

3.4.5.1 Girder UNB1

Flexural cracking first developed in girder UNB1 at the midspan when the applied load reached 42 kips with a corresponding displacement of just under 1 inch. The initial crack was confined to the bottom flange. As the load was increased to 45 kips, this crack extended to the mid-height of the web. An additional crack developed in the same precast segment (i.e., Segment 10) adjacent to the epoxy interface that connected the segment on the left (i.e., Segment 11). Formation of this crack, which was located about 3 in. from the joint interface, is consistent with expectation that cracking in segmental beams would not be at the epoxy interface, but rather

develop in the concrete laitance near the ends of the segment, where large aggregates are hardly present. This crack ran up the bottom flange up to the mid height of the web as a flexural crack and then as an inclined shear crack. Although the load was expected to be increased further, this was not possible. Instead, the displacement increased further, which was associated with another crack forming at a distance of about 2 in. from the Segment 10 to Segment 11 joint interface. The width of this crack increased approximately to 1/8 in. when the recorded beam displacement reached 1.35 in. Additionally, this crack formation was non-symmetric along the length and only occurred near the east side of the 10 to 11 joint interface. There was no increase in the width of the two cracks that were previously observed. At this point, the beam was unloaded due to time constraints in the lab.

The following day, the beam was reloaded with the load applied in a 6 kip increment until it reached 1.35 in. vertical displacement. From this point onward, the beam was loaded under displacement control in increments of 0.25 in. At a displacement of 1.5 in., the cracking closest to the epoxy interface extended toward the top flange, which then propagated horizontally at the web-flange interface. At 1.75 in. of displacement, the larger crack seen beside the segment 10 to 11 interface continued to widen. Additionally, a new crack was observed in the middle of segment 11 on the bottom flange. At a displacement of 2 in. and beyond, widening of the crack only occurred to the one adjacent to joint 10 to 11 interface. This crack reached a width of 0.25 in. at a mid-span deflection of 2 in. As the displacement was increased to 3 in. and then 4 in., the cracks extended to the bottom of the top flange, which was unexpected and appeared to suggest that the beam response was deviating from simple beam behavior. At a displacement of around 4 in., one of the strands on the south side fractured at the anchorage location. From this point onward, the test was continued using a displacement control increment of 1 in. without visual

inspection due to safety concerns. When the mid-span deflection reached approximately 10 in., two other strands on the south side fractured near the anchorage on the west end; the width of the main crack at this point was about 1.5 in. The test was subsequently terminated. The progression of the crack development in the midspan region is shown in Figure 3.16 while the deflected shape of the beam at 10 in. of displacement is presented in Figure 3.17. When the applied load was removed, all cracks were closed, and the beam did not exhibit any significant permanent deformation. The condition of the test girder after the removal of the load is presented in Figure 3.18.

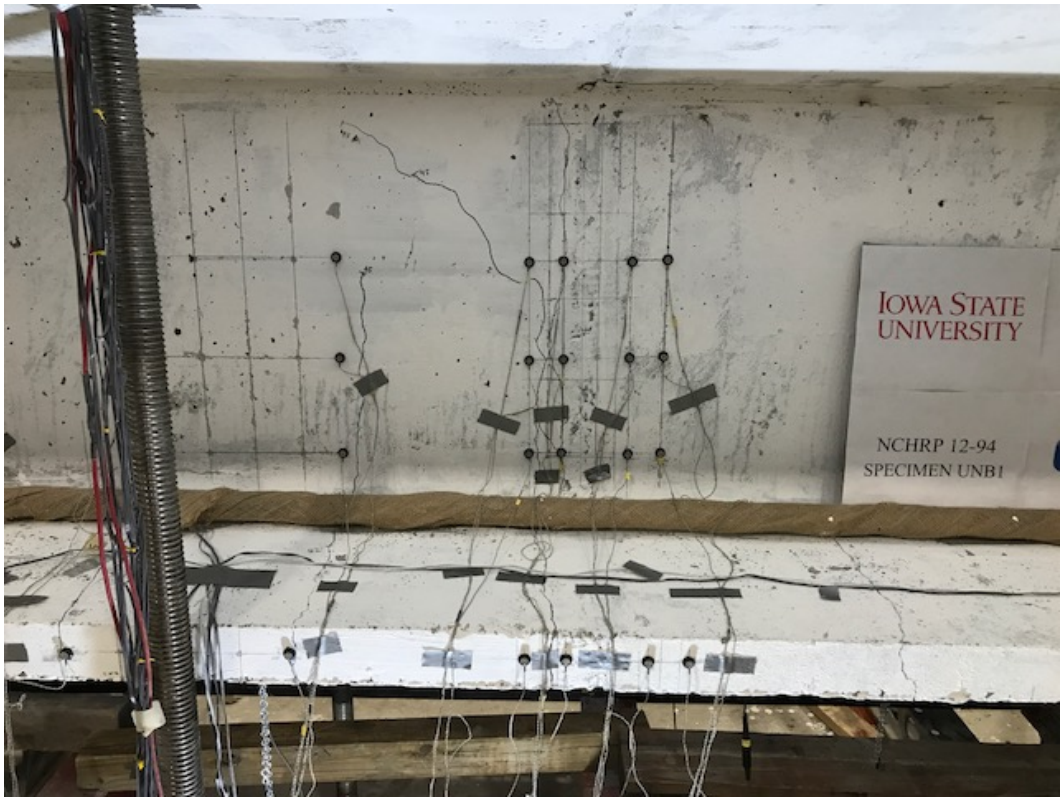

(a)

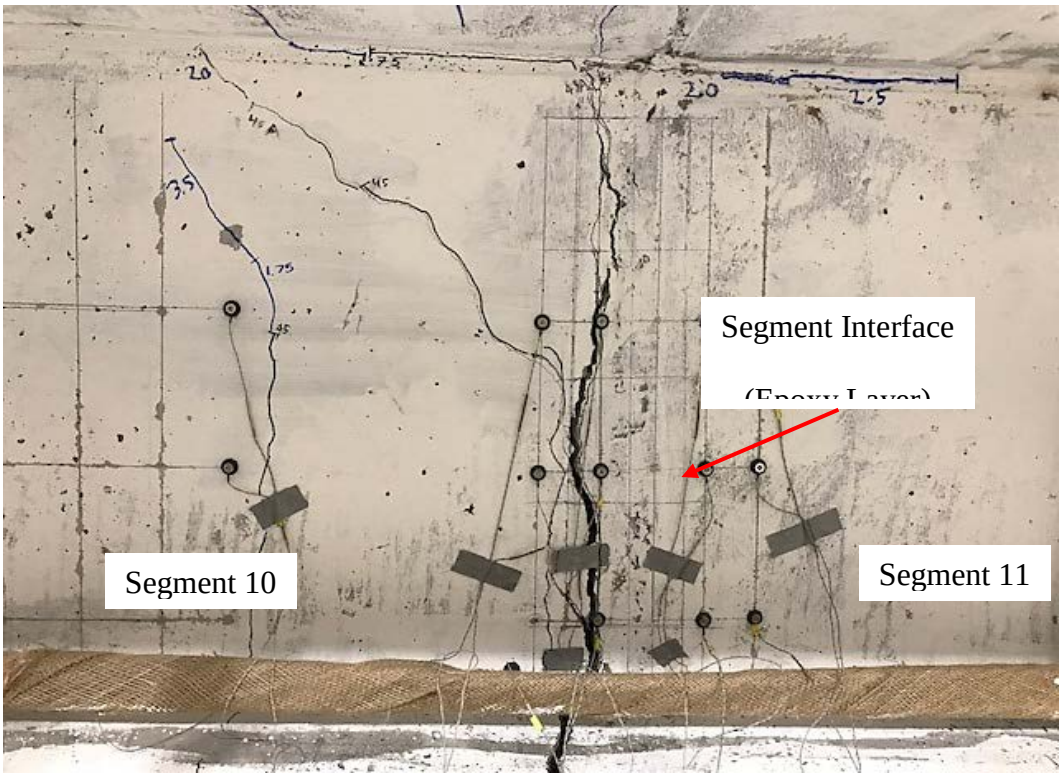

(b)

(c)

Figure 3.16 – Progression of Crack Formation and Opening beside the Segment Joint Interface (Sritharan et. al., 2018)

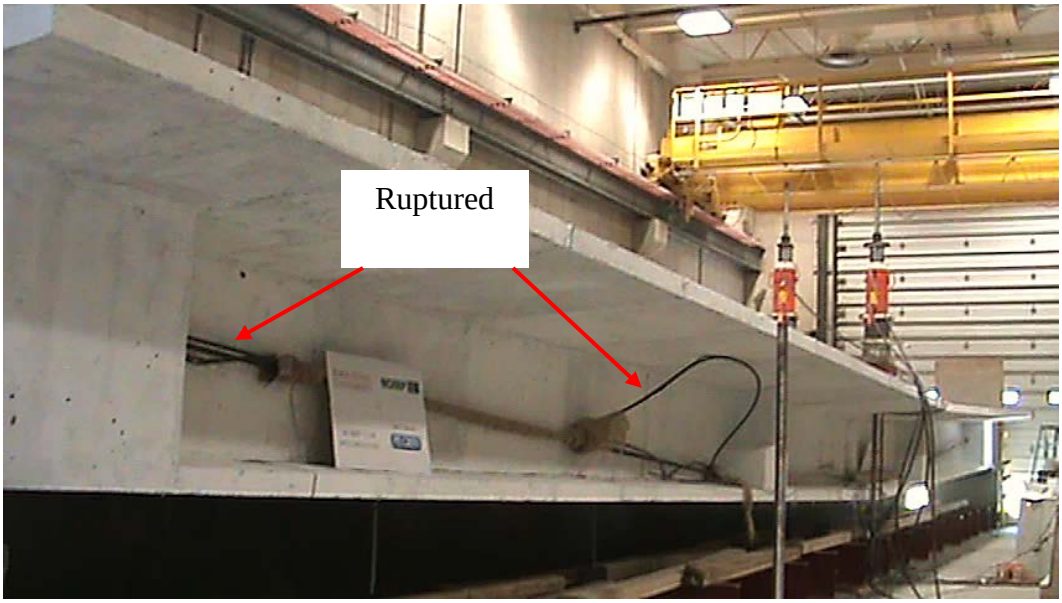

Figure 3.17 – Girder UNB1 at 10 in. of Displacement (Sritharan et. al., 2018)

Figure 3.18 – Midspan Condition after Removal of Applied Load to Girder UNB1 after the Test (Sritharan et. al., 2018)

The prestressing strand had an initial strain, prior to testing, of slightly over 6 mε (microstrain) from post-tensioning. The maximum recorded strain, occurring prior to the first strand rupture, was about 7.5 mε. The deflection profiles of the girder for various applied loads are shown in Figure 3.19. while the load vs. midspan deflection plot is presented in Figure 3.20, with the maximum recorded applied load of 45.45 kips. There was no sign of any change in stiffness until the load caused first flexural cracking to develop. The response of UNB1 produced M_u/M_{cr} of 1.08 with Δ_u/Δ_{cr} of 4.17.

Closely examining Figure 3.20 suggests that the beam experienced a small stiffness change due to cracking and reached 44.8 kips with a displacement of 1.08 in., which is followed by a drop in strength. This loss is suspected to be due to the beam shifting from the conventional flexural beam theory mechanism to what appeared to be a hinging mechanism, which is detailed further in Section 3.5.1.

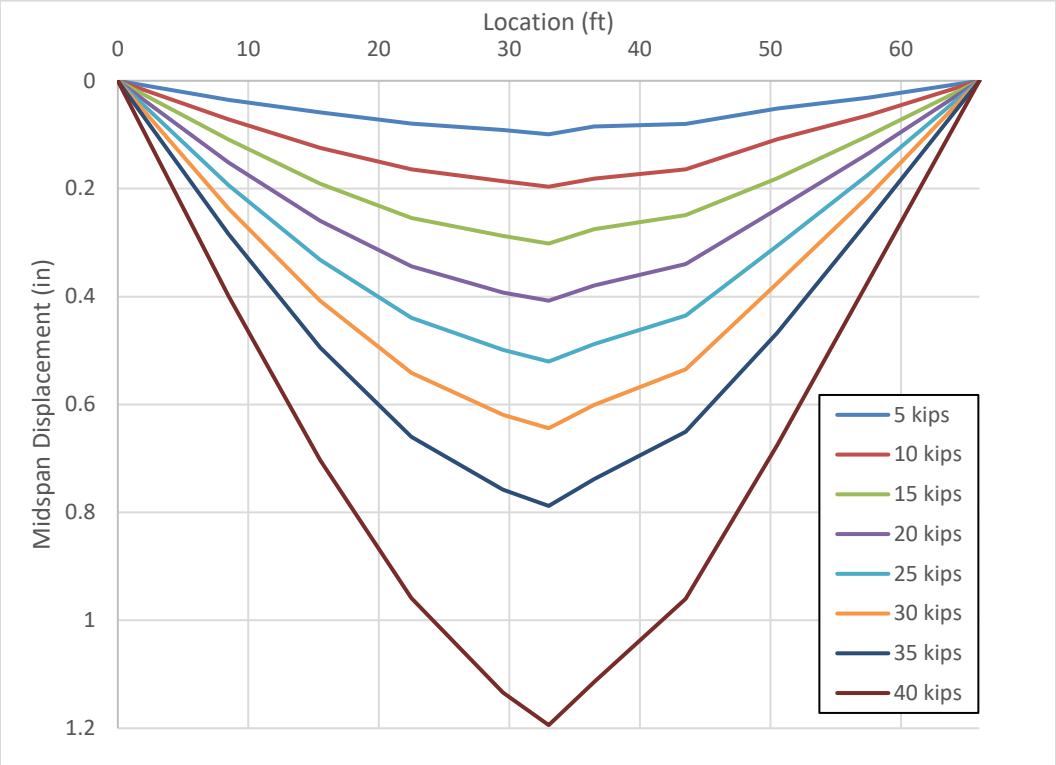

Figure 3.19 – Deflection Profiles at Various Loads for UNB1

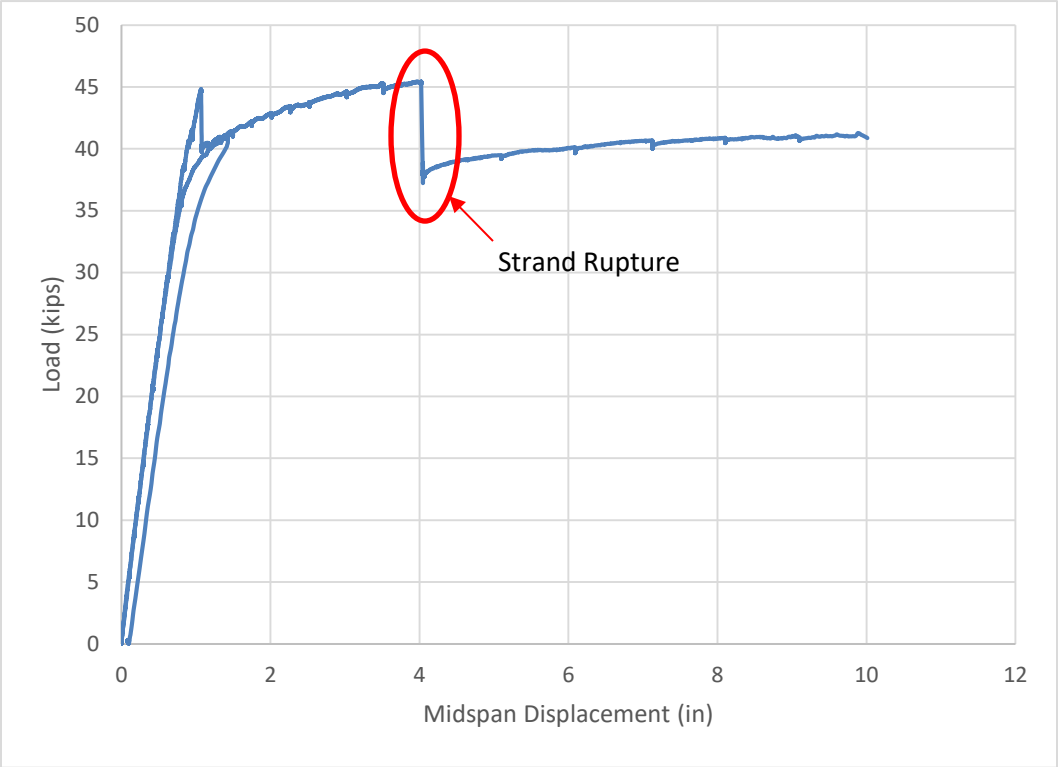

Figure 3.20 – Load vs. Midspan Displacement Curves for UNB1

3.4.5.2 Girder UNB2

Girder UNB2 was loaded incrementally over a two day period, similar to UNB1. On the first test day, the girder was loaded in 3 kip load steps until 90 kips of load. The first hairline flexural crack was observed at the midspan on the bottom of the girder during the last load step, with an applied load of 90 kip. Due to time constraints, the girder was unloaded. When testing resumed, the beam was reloaded at a load step of 6 kips until the load reached 90 kips. The girder was visually inspected for damage after applying 30, 60, and 90 kips. No further crack was observed, except for the hairline crack noted from day one. Once reaching 90 kips of load, the load step was reduced to 3 kips. Formation and propagation of new hairline cracks occurred at a slow rate on the bottom face of the girder. Flexural cracking first developed on the sides of the girder, propagating from the hairline crack observed at the bottom surface, in the midspan

segment (i.e. segment 8) at a load of 102 kips, with a corresponding displacement of 1.315 in. Four visible cracks located near the midspan of segment 8 propagated from the bottom flange of the beam to the mid-height of the web as flexural cracks. The crack development was symmetric on the north and south sides of the girder. As the load was increased to 105 kips, new cracking occurred approximately 1 in. from the segment 7-8 joint interface in segment 8, within the concrete laitance. This observation is consistent with cracking observed in UNB1. Flexural cracking in the midspan segment began to incline at approximately 45° as inclined shear cracks after propagating to mid-height of the web at the displacement of approximately 1.38 in.

After reaching 105 kips of load, Girder UNB2 experienced large displacements, also consistant with the observations of UNB1. This appears to be when the hinging mechanism developed. Therefore, from this point onward, the beam was loaded under displacement control. At a displacement of 1.75 in., the cracking adjacent to the epoxy layer continued to propagate up the web into inclined shear cracking. The crack had a width of approximately 0.1 in. on the bottom flange. Due to safety concerns, no additional visual inspection was conducted from this point onwards. At a displacement of 2 in., the width of the crack had widened to approximately 0.5 in. After 2 in. displacement, the beam was loaded at displacement increments of 0.5 in. At 4.72 in. of displacement, shear cracking from the beam continued as a horizontal crack along the bottom of the top flange at the midspan (i.e. segment 8). Failure of the beam occurred at a displacement of 5.81 in. due to the large crack at Segment 7 to 8 joint interface causing the midspan segment to tilt from and drop from loading. The width of the crack at Segment 7 to 8 joint interface was approximately 0.75 in. The post-tensioning force compressed the segments preventing it from falling off to the ground. The test was subsequently terminated. The

progression of the interface crack development detailed above is shown in Figure 3.21 while the failure mode of the girder is presented in Figure 3.22.

Figure 3.21 – Progression of Crack Formation beside the Segment Interface in UNB2 (Sritharan et. al., 2018)

Figure 3.22 – Girder UNB2 after Failure (Sritharan et. al., 2018)

The load vs. midspan displacement plot is presented in Figure 3.24, while the deflection profile obtained for UNB2 at various loads is presented in Figure 3.23. The maximum recorded load was 108 kips. There was no sign of any change in stiffness until the load caused the first flexural cracking at 90 kips, yielding M_u/M_{cr} ratio of 1.20. A drop of the load at approximately 103 kips occurred after the flexural cracks developed on the web, similar to the results of UNB1. This, presumably, is the result of the development of the hinging mechanism. Had the test been conducted under force control, there would have been a sudden increase in displacement at 103 kips. At this point, UNB2 would have had reserve capacities of 5.05 kips and 3.05 in., which are better than those observed for UNB1 and could be considered adequate, in terms of safety. Note, however, that UNB2 did not experience failure of strands at the anchorage, as observed for UNB1. The initial strain recorded due to prestressing was approximately 6.5 mε. The net tensile strain when the test was concluded was recorded to be 7.6 mε.

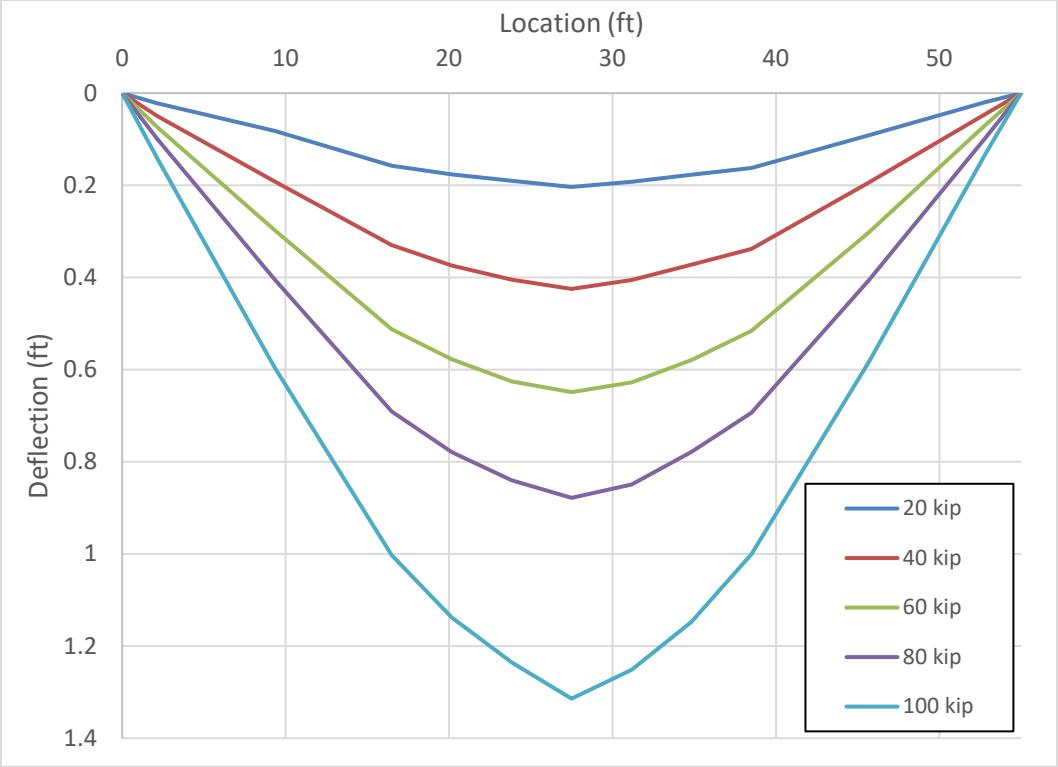

Figure 3.23 – Deflection Profiles at Various Loads for UNB2

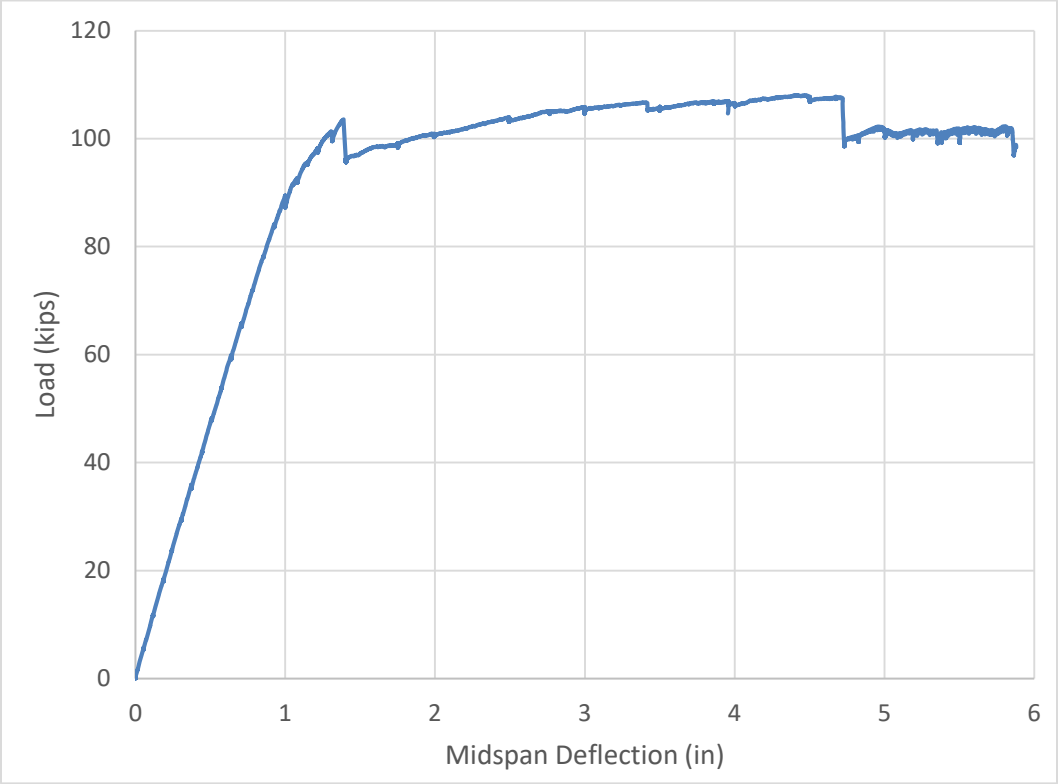

Figure 3.24 – Load vs. Midspan Displacement Curves for UNB2

3.4.5.3 Girder UNB3

Flexural cracking first developed at the midspan of the girder, propagating from the bottom flange to the bottom of the web through the north and south loading holes of the girder. The applied load was 116 kips with a corresponding displacement of 0.27 in. The crack continued to propagate up the web as loading increased. No additional cracks were observed until an applied load of 133 kips was reached, when cracks developed at the midspan in Segment 6. Loading of the girder continued to 136 kips with a corresponding displacement of 0.44 in. The girder sustained the load for approximately 30 seconds, then a large crack developed near the joint interface between Segment 5 and Segment 6, approximately 0.5 in. from joint interface, similar to the large cracks observed in UNB1 and UNB2. The crack development led to the load drop from 136 kips to 108 kips, and a displacement increase from 0.44 in. to 0.49 in. As described previously, this drop in load is presumably when the hinging mechanism develops. The crack propagated vertically from the bottom flange to approximately half way up the web then began to incline as shear cracks towards midspan. Additionally, it was observed that the formation of the large crack near the joint interface led to the almost complete closure of other existing cracks.

From this point onward, the beam was loaded under displacement control. At a displacement of 0.75 in., additional cracks formed near the joint interface of Segment 5 and Segment 6. At displacement 1.0 in., the cracks near the joint interface continued to propagate up the web and formed a concentrated crack that continued to widen with increased displacement. Figure 3.25 presents the widening of the concentrated crack as the displacement increased. Due to safety concerns and no additional crack formations, no further visual inspections were conducted after 2 in. displacement was reached. At a displacement of 6.0 in, with a

corresponding load of 158.6 kips, concrete in the top flange of the girder began to crush in Segment 6. At a displacement of 9.5 in., the actuators were stroked out. The beam was unloaded, the loading frame tightened back down, and the beam was reloaded until failure. Failure occurred at a displacement of 9.68 in., with a corresponding load of 161.1 kips, due to the large concentrated crack at Segment 5 to 6 joint interface, similar to that of UNB2. The failure mode of UNB3 is presented in Figure 3.26.

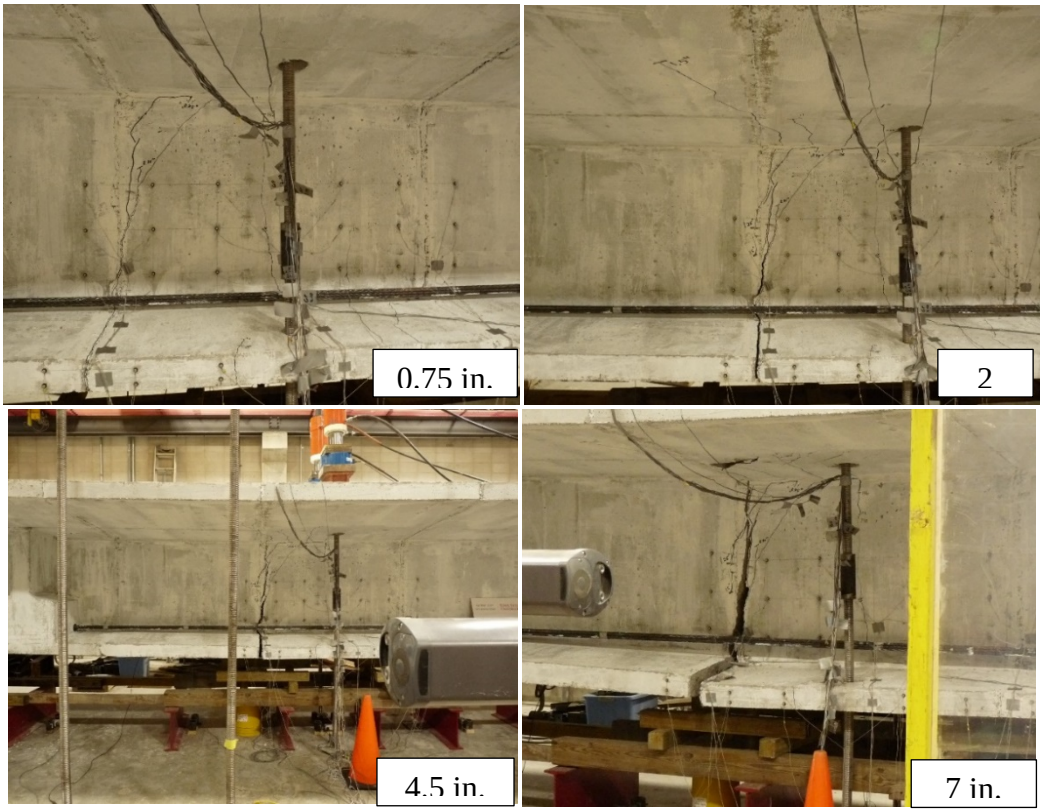

Figure 3.25 – Progression of Crack Formation beside the Segment Joint Interface for UNB3 (Sritharan et. al., 2018)

Figure 3.26 – Failure Mode of UNB3 (Sritharan et. al., 2018)

Figure 3.27 presents the deflection profile of girder UNB3 at various loads. Figure 3.28 presents the load vs. midspan deflection curve for UNB3. As can be seen in this figure, the formation of hinging dropped the load by 26.6 kips. If the test had been done under load control, the deflection would have increased to 2.86 in., leaving significant displacement and load-resisting capacities beyond formation of the hinging mechanism. For UNB3, M_u/Mc_r and Δ_u/Δ_{cr} ratios of 1.41 and 19.6, respectively. The initial prestressing strain from post-tensioning was approximately 6.3 mε with the recorded strain at failure of 8 mε.

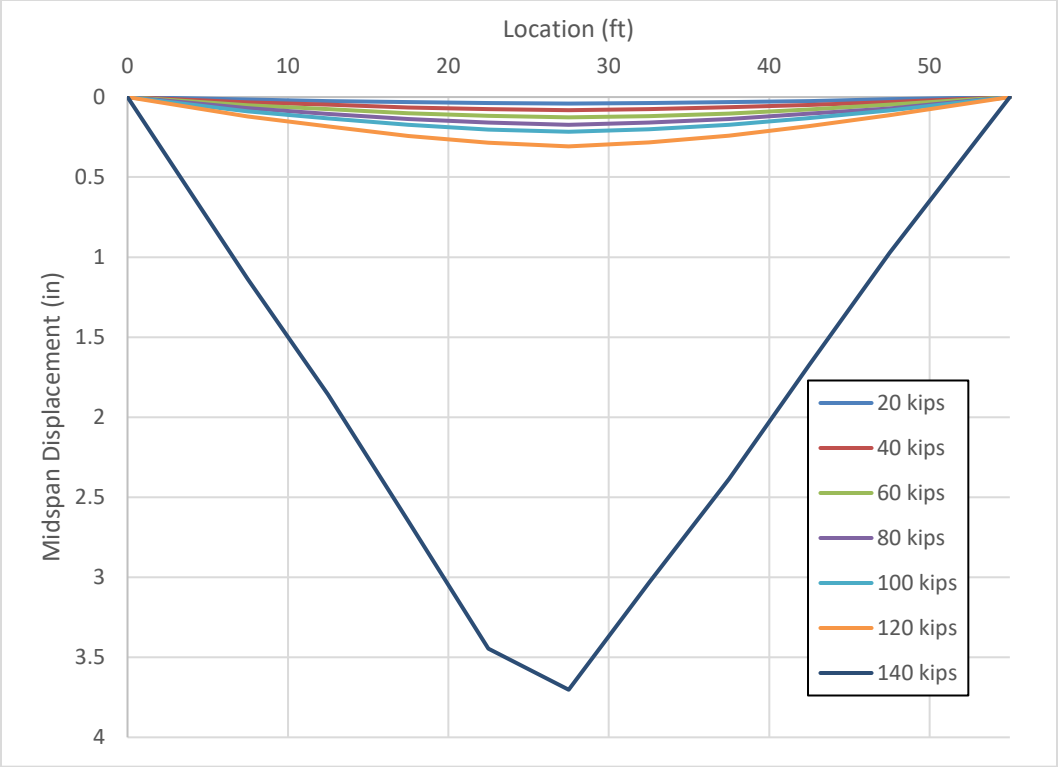

Figure 3.27 – Deflection Profiles at Various Loads for UNB3

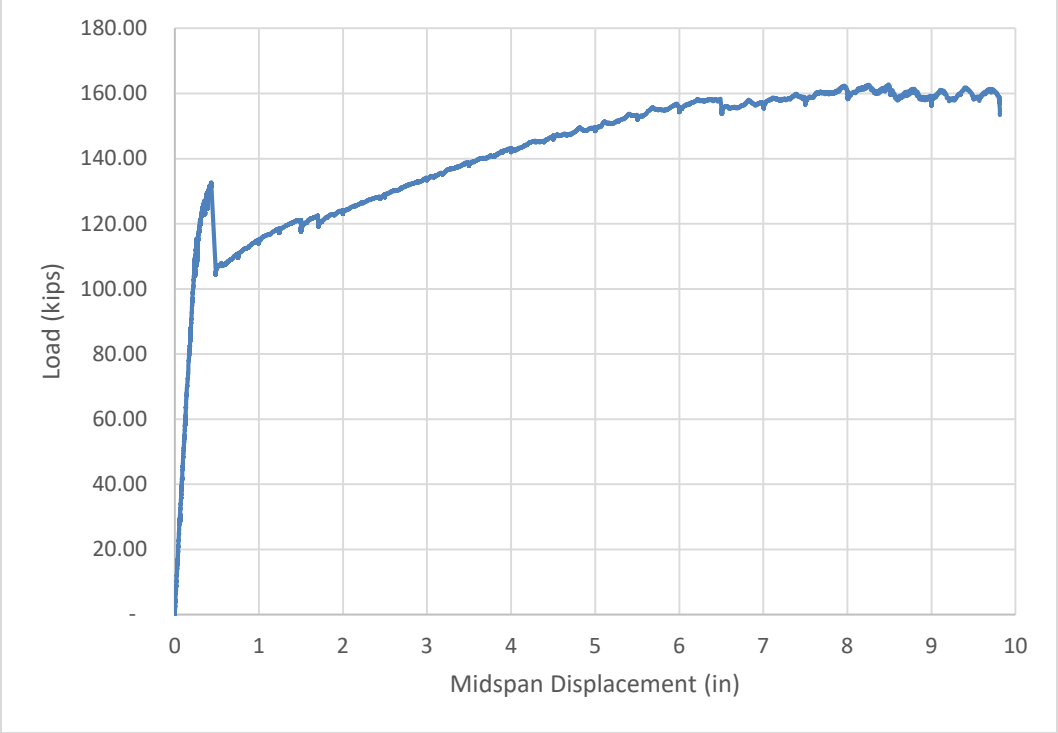

Figure 3.28 – Load vs. Midspan Displacement Curves for UNB3

3.4.5.4 Girder BON2

On the first day of testing, first cracking occurred at a load of 60 kips, with a corresponding displacement of 0.26 in. The cracking occurred at the midspan (i.e., Segment 6) on the north side of the girder, as well as near the joint interface of Segment 4 and Segment 5 on both sides of the girder. Similar to UNB3, the midspan crack propagated from the bottom flange through the holes within the bottom flange of the girder for loading. Loading resumed to a load of 65 kip, when new cracks formed approximately 2" adjacent to the Segment 6 to 7 joint interface. Similar to the unbonded post-tensioned girders, the cracking near the joint interface propagated approximately half way up the web then began to incline as shear cracks towards the midspan. After this point, the girder was loaded under displacement control. No new crack formations were observed until a displacement of 1 in. was reached. At 1 in. displacement, cracks formed near the joint interface of Segment 5 to 6 on both sides of the girder, with propagation similar to existing cracks near the Segment 6 to 7 joint interface. Cracking near the joint interface of Segment 6 to 7 was accompanied with a load drop from 72 kips to 62 kips. Crack development was very similar on both sides of the girder and both sides of the midspan, as expected for bonded specimens. At this point the beam was unloaded and reloaded the following day.

The following day, the beam was reloaded incrementally to 1 in. of displacement reached the previous day and load application under displacement control resumed. As the displacement increased, many new cracks developed within Segment 4 to Segment 8. Cracking continued to be symmetric on each side of the girder. This differs from the unbonded segmental girders, where a large concentrated crack dominated the response. At a displacement of 1 in., cracks developed

near the joint interface of Segment 7 to 8, accompanied with a drop of load from 90 kips to 80 kips. The presence of multiple load drops also differs from the response of the unbonded segmental girders, which only experienced one load drop. At a displacement of 5 in., new cracks developed near the joint interface between Segment 8 and Segment 9. The cracking was again accompanied with a load drop, from 112 kips to 105 kips. At a displacement of 6 in., cracks developed near the joint interface between Segment 3 and Segment 4. Cracking continued to be symmetric and similar on both sides of the girder. Due to safety concerns, no more visual inspection was conducted after 6 in. of displacement. Even without up close visual inspection, crack propagation was apparent as displacement increased. Figure 3.29 presents crack propagation over the duration of the test. Failure of girder BON2 occurred at a load of 119.3 kips and a center displacement of 11.66 in. The failure mode occurred at the crack near the joint interface between Segment 5 and Segment 6. The failure mode of girder BON2 is presented in Figure 3.30.

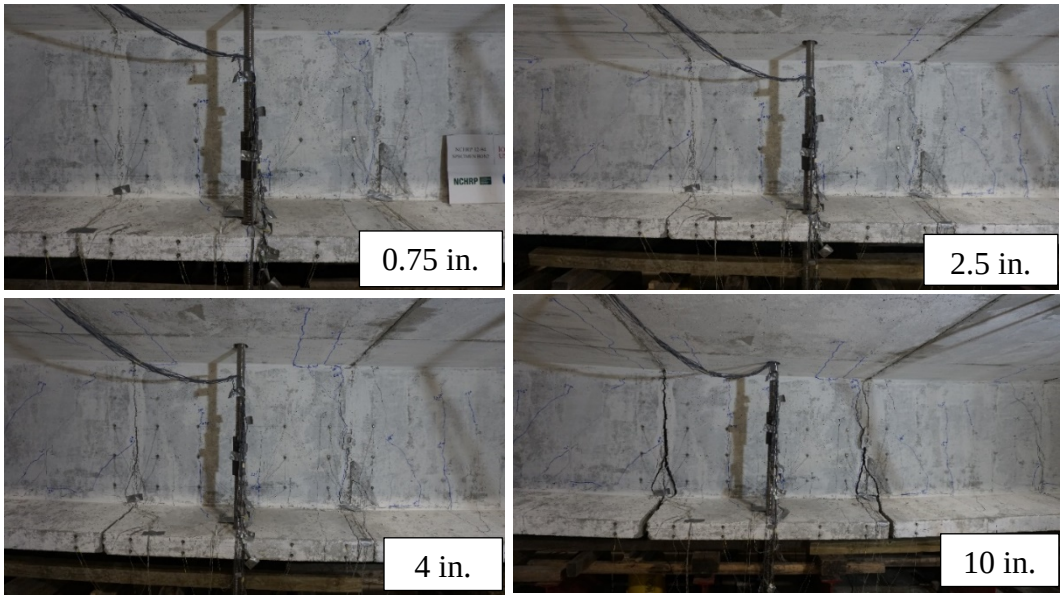

Figure 3.29 - Progression of Crack Formation for BON2 (Sritharan et. al., 2018)

Figure 3.30 - Girder BON2 after Failure (Sritharan et. al., 2018)

Figure 3.32 presents the load vs. midspan deflection curve of girder BON2 for both days of testing. Figure 3.31 presents the deflection profile of girder BON2 at various loads. The M_u/Mc_r and Δ_u/Δ_{cr} ratios of 1.99 and 44.8, respectively. No strain data was available during testing due to the internal tendon being grouted. The observed response, which was similar to those of pretensioned girders, exhibited no safety concerns for experiencing a brittle failure despite designing it with lower than the requirement in the current specifications of AASHTO (AASHTO, 2017) for the minimum reinforcement.

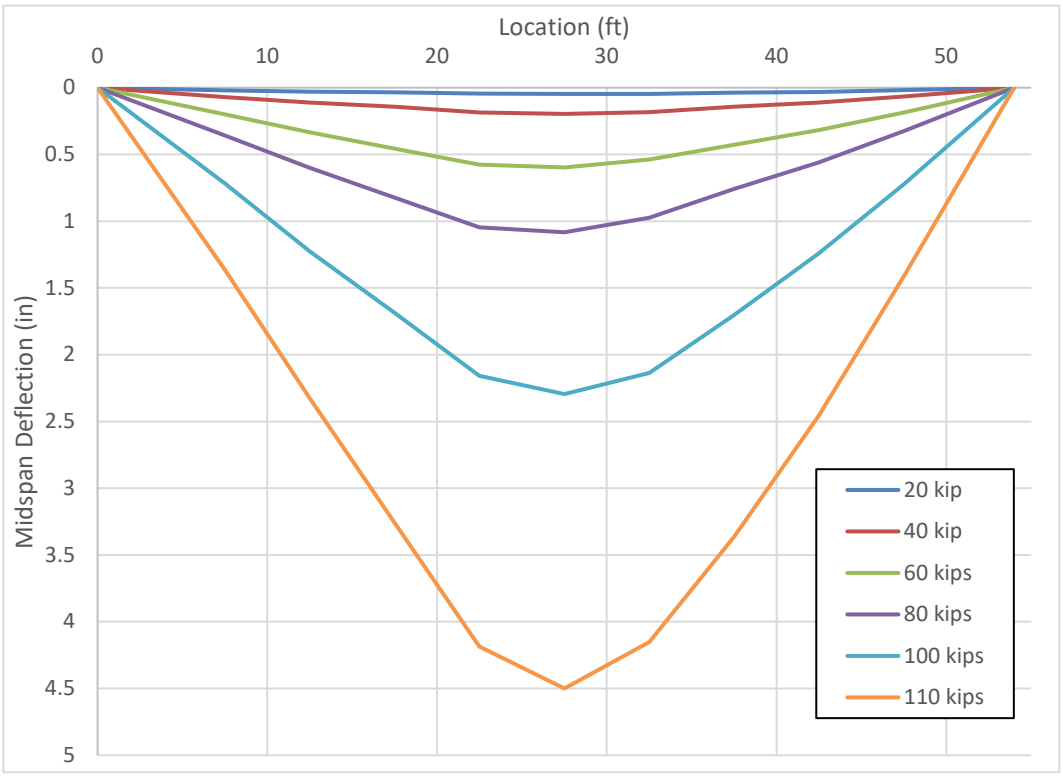

Figure 3.31 – Deflection Profiles at Various Loads for BON2

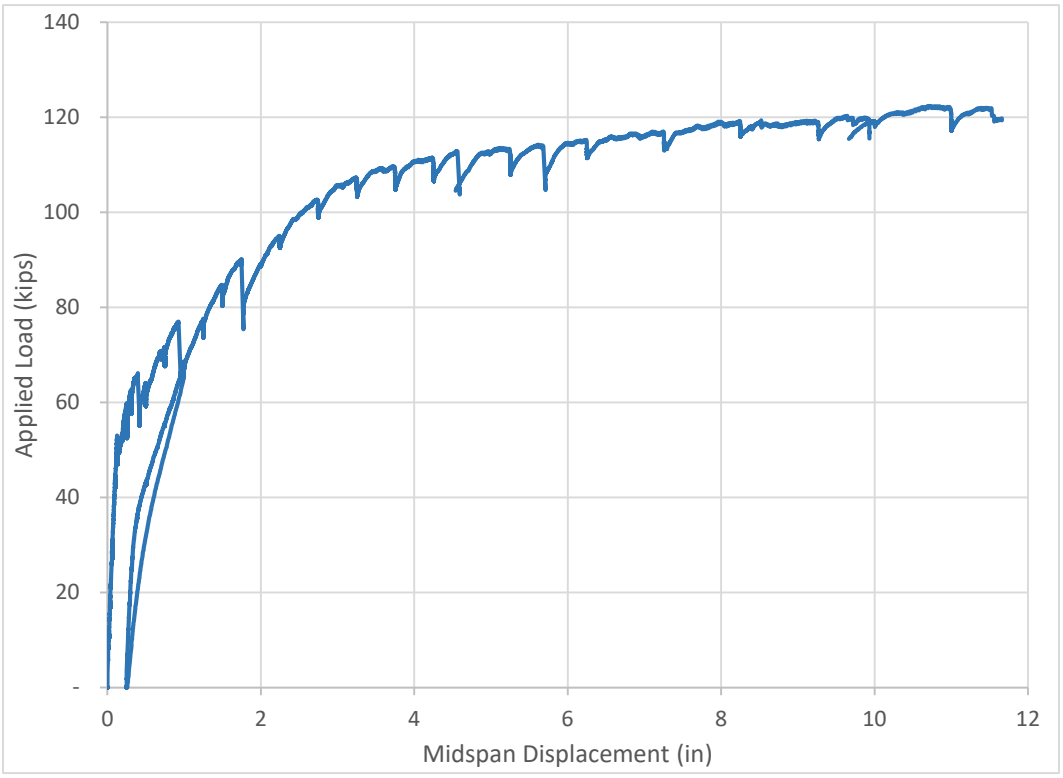

Figure 3.32 – Load vs. Midspan Displacement Curves for BON2

3.5 Analytical study

In order to further understand the behavior of the segmental post-tensioned concrete girders and ensure adequacy in design, an analytical method is proposed and validated through comparison to the experimental results. Additional analysis was conducted on the prestressed tendon stress at nominal strength in unbonded girders. Finally, an investigation into the affect the depth factor has on segmental girders was conducted. These results of these analytical studies are presented in this section.

3.5.1 Response validation of unbonded post-tensioned segmental girders

As discussed briefly in the test results, a reduction in resistance for the unbonded segmental girders occurred right after the formation of a major flexural crack adjacent to a joint interface, which was claimed to be associated with the formation of a hinging mechanism. Visual evidence of the propagation and widening of these concentrated crack as displacement increased for UNB1, UNB2, and UNB3 is shown in Figure 3.33 through Figure 3.35, respectfully.

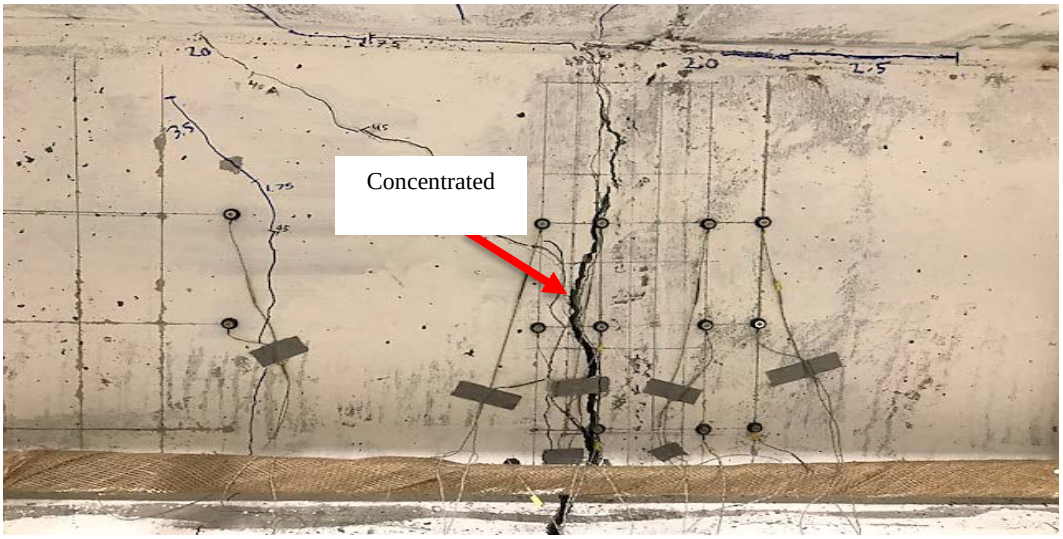

Figure 3.33 – Concentrated Crack Observed in UNB1 (Sritharan et. al., 2018)

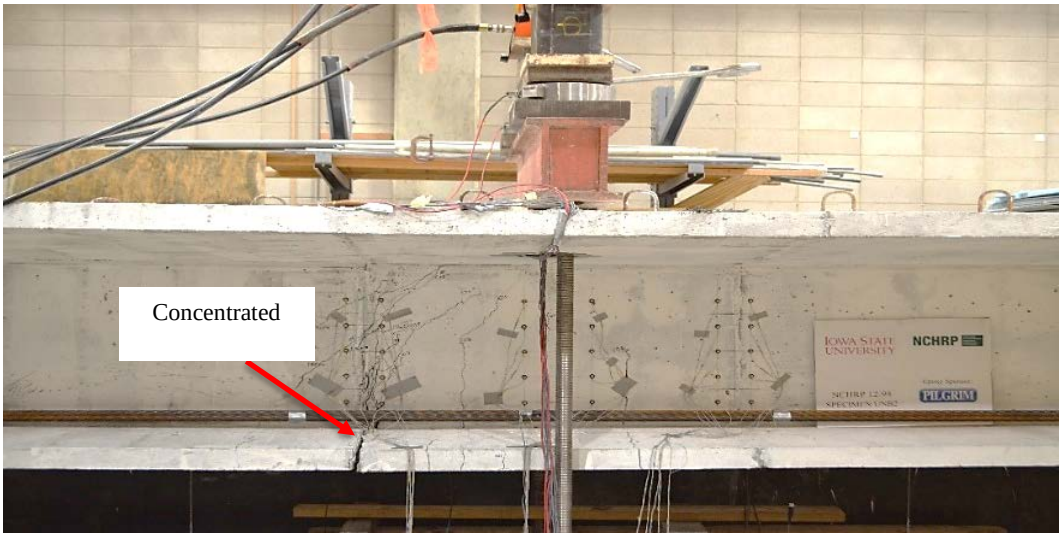

(a)

(b)

Figure 3.34 – Progression of Concentrated Crack Developed in UNB2 (Sritharan et. al., 2018)

(a)

(b)

Figure 3.35 – Progression of Concentrated Crack Observed in UNB3 (Sritharan et. al., 2018)

To provide additional evidence of a mechanism change, one specific deflection within the flexural response region (i.e., prior to experiencing drop in load resistance) and one from the proposed hinging mechanism response region were selected to compare the overall girder profile. They are presented in Figure 3.36 through Figure 3.38. Deflection values were measured

during the test using string potentiometers placed underneath the girder along the length. The deflection profiles were normalized to better visually exemplify the difference in profiles. The beam profile within the flexural response region follows much more of a parabolic profile, while the profile within the hinge region is practically linear from each support to the concentrated crack location.

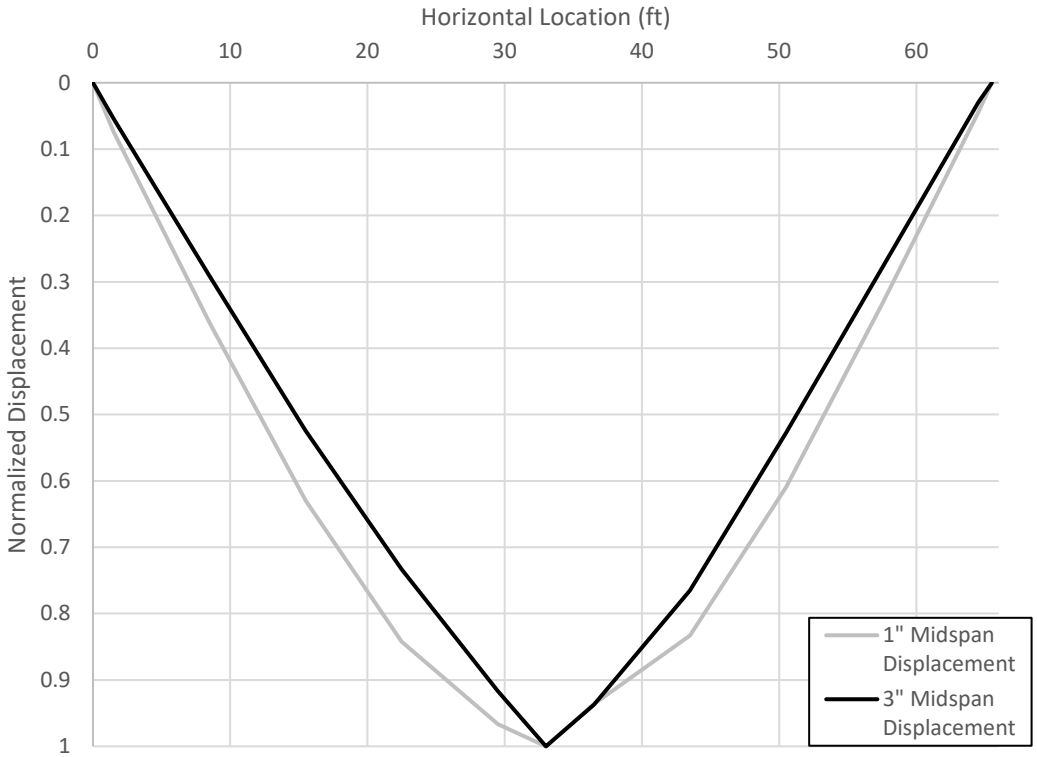

Figure 3.36 – Comparison of Normalized Deflection Profiles for UNB1

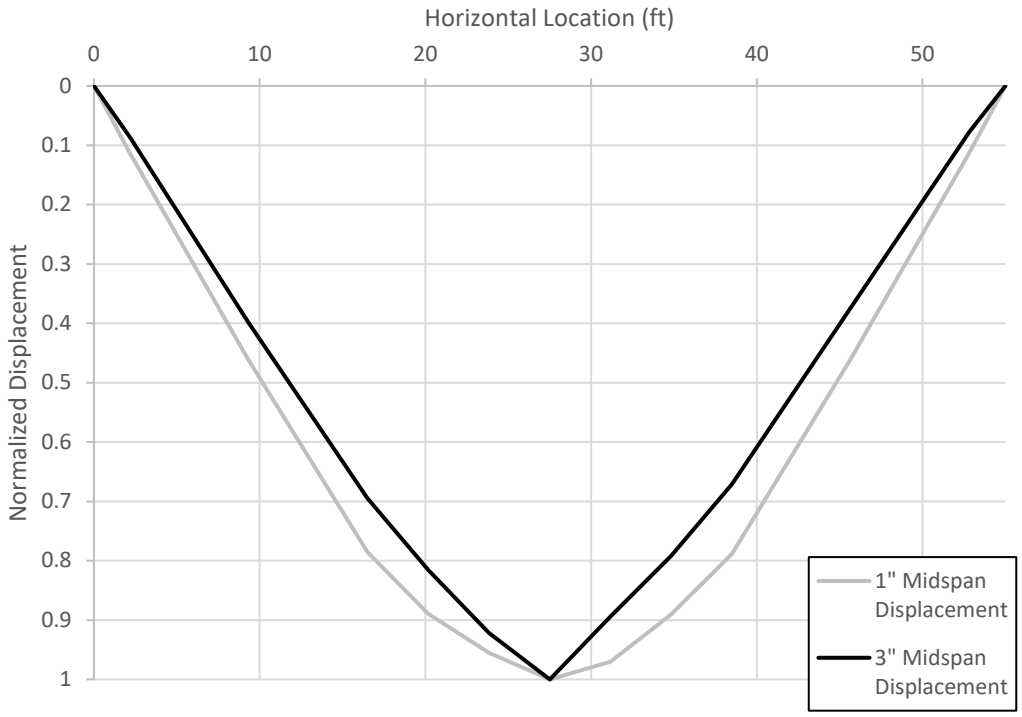

Figure 3.37 – Comparison of Normalized Deflection Profiles for UNB2

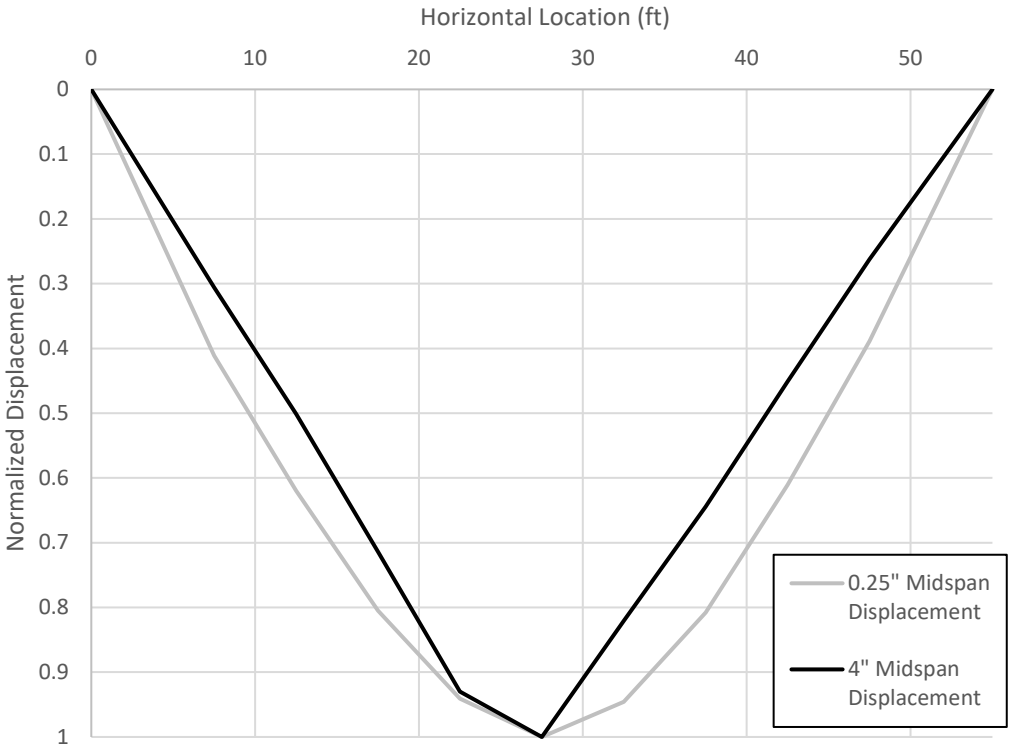

Figure 3.38 – Comparison of Normalized Deflection Profiles for UNB3

As discussed in Section 3.3, an issue with the current AASHTO LRFD Specifications (2017) method for prestressed girders is that in certain situations the minimum reinforcement solution does not converge to a solution. Resulting in the nominal Moment (ϕM_n) not exceeding the cracking moment (M_{cr}) regardless of the amount of prestressed reinforcement added. Leonhardt's method was stated as one method that could be utilized to address this issue, however many assumptions made by Leonhardt are not accurate for most segmental post-tensioned box girder designs. To ensure sufficient strength and ductility in design, another method is presented in the subsequent sections. This method, taking into account the observation of two distinct response regions, was then validated with the experimental data of the study.

It is important to note that the proposed analysis method relies on the assumptions of flexural theory. We assume that no slip occurs between the steel and concrete. However, based on our observed response of the girders, slip does occur in the prestressed strand. Additionally, the tensile strength of the concrete in neglected following first cracking. In reality, the concrete within the tensile region may still influence the response. The actual material properties may differ from typical models, such as strand and concrete stress-strain relationship. The compressive concrete is assumed to remain in the linear state following the cracking moment until the formation of the hinging mechanism response. If desired, an analysis could incorporate the non-linear state of the compressive concrete into the analysis. Finally, strain hardening in the high-strength steel tendons, as well as the dynamic effects of loading are neglected in the analysis.

3.5.1.1 Flexural response region analysis

Figure 3.39 exhibits a schematic of a typical flexural response of an unbonded post-tensioned segmental girders. The analysis of the flexural response region was separated into

three stages to accurately analyze the girders. The first stage is from zero applied load to an applied load inducing decompression in the extreme bottom fiber. The second stage is from the decompression applied load to the cracking load. The final, or third, stage is from the cracking load to the formation of the concentrated crack associated with the transition to a hinging mechanism response.

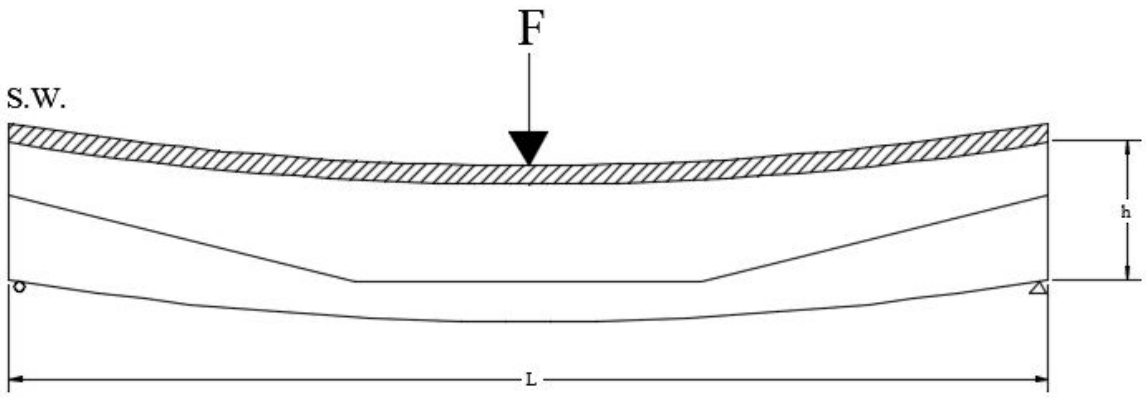

Figure 3.39 – Flexural Response of an Unbonded Segmental Post-Tensioned Girder

To validate the analytical model it was necessary to determine the concrete strain (ε_c), concrete stress (σ_c), and tensile force from the prestressed reinforcement (T_{pt}) as the applied load (F) increased. Values of the concrete strain were obtained utilizing data from the LEDs mounted at the midspan of the girder and extrapolated to the extreme compressive and tensile fibers. The concrete stress was then determined using the unconfined concrete stress-strain model developed by (Karthic and Mander, 2011). Mander's unconfined concrete stress-strain model can be utilized to estimate concrete stress and strain if no test data is available. The tensile force from the prestressed tendon was determined by interpolating the strain gage data to the stress-strain data from the direct tensile tests of the 0.5 in. diameter and 0.6 in. diameter strands. If no test data is available, the change in the strain due to the applied load is calculated from section geometry and the total change in the length of the tendon over the total length. Figure 3.39

through Figure 3.41 detail the transition of the internal forces within the unbonded girders for each aforementioned stage, respectfully.

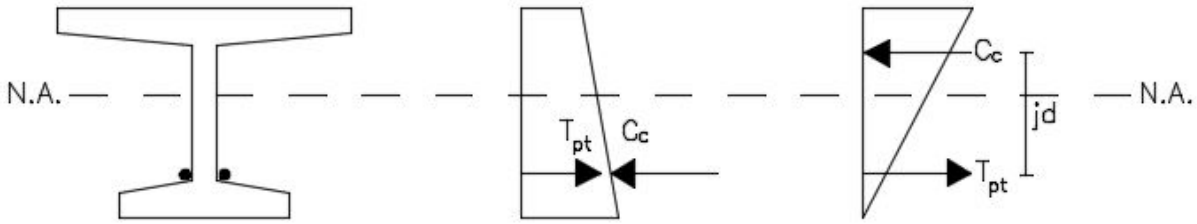

Figure 3.40 – Internal Forces in Unbonded Girders from Zero Moment to Decompression Moment (Stage 1)

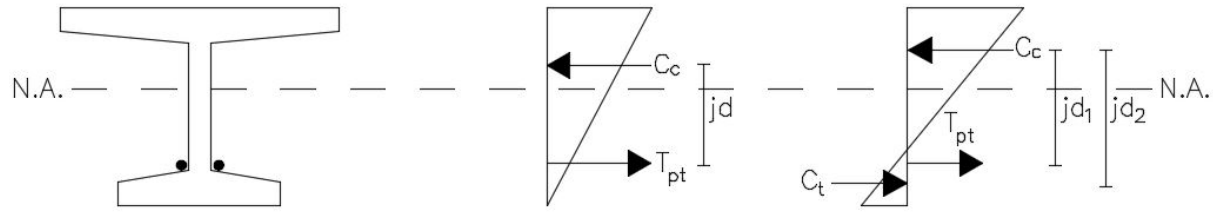

Figure 3.41 – Internal Forces in Unbonded Girders from Decompression Moment to Cracking Moment (Stage 2)

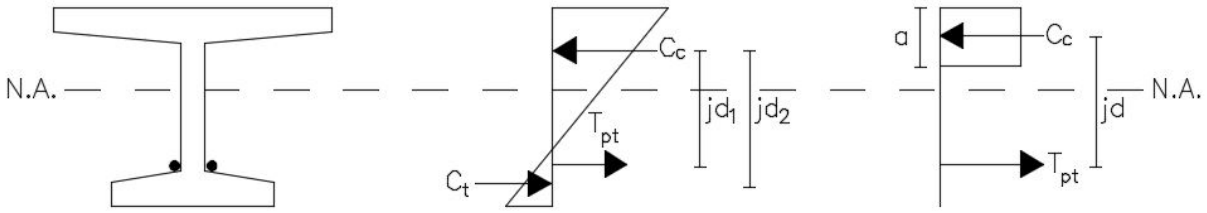

Figure 3.42 – Internal Forces in Unbonded Girders from Cracking Moment to Formation of Hinging Mechanism Response (Stage 3)

The resulting moment (M) can be calculated from taking the moment about the compressive concrete resultant force (C_c):

$$\text{(Stage 1 and 3)} \quad \sum \text{Moments about } C_C = T_{pt}(jd) - M = 0 \qquad (3.4)$$

$$\text{(Stage 2)} \quad \sum \text{Moments about } C_C = T_{pt}(jd_1) + C_t(jd_2) - M = 0 \qquad (3.5)$$

Figure 3.43 shows the free body diagram of the girder cut at the midspan during testing in the flexural response region. Utilizing know section properties of each unbonded post-tensioned

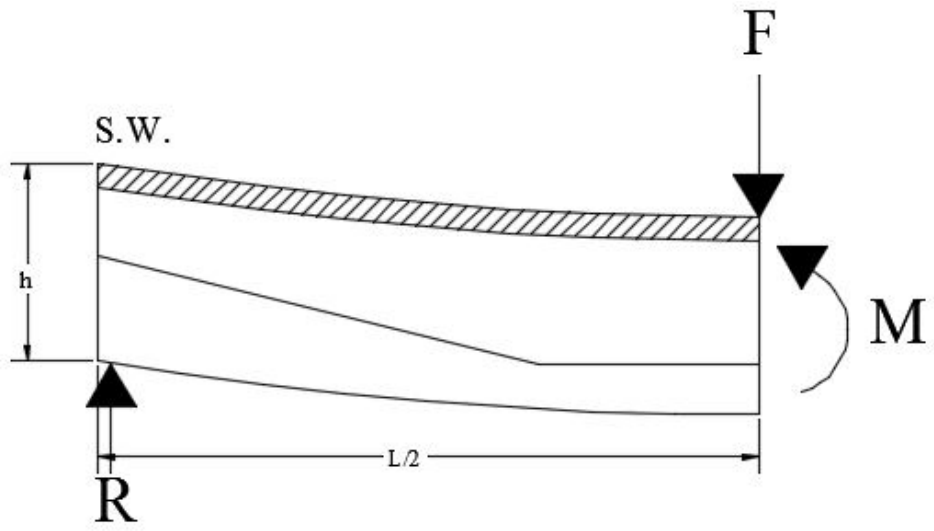

segmental girder, the applied load (F) can be calculated:

Figure 3.43 - Free Body Diagram of Unbonded Segmental Girder in Flexural Response Region

$$\sum \text{Moments about the midspan} = = -R\left(\frac{L}{2} - 0.5\right) + M = 0 \qquad (3.6)$$

Rearrange the equation above to solve for the applied load (F):

$$F = \frac{(2M - wL)}{\left(\frac{L}{2} - 0.5\right)} \qquad (3.7)$$

All distances are in feet, where w is the self-weight of the girder in kip per foot and L is the total length of the girder. In order to make the equation determinant, it was assumed the support reaction is the sum of half total force and self-weight (ie., $R = \frac{F}{2} + \frac{wL}{2}$).

3.5.1.2 Hinging mechanism response region analysis

Figure 3.44 displays a schematic of the hinging mechanism response of an unbonded post-tensioned segmental girders. The beam segments with lengths L_1 and L_2 experience rotations θ_1 and θ_2, respectfully, but do not undergo a flexural response after the concentrated crack formation. Additional validation of the proposed hinging mechanism response analysis method is provided prior to determination of the applied load (F)

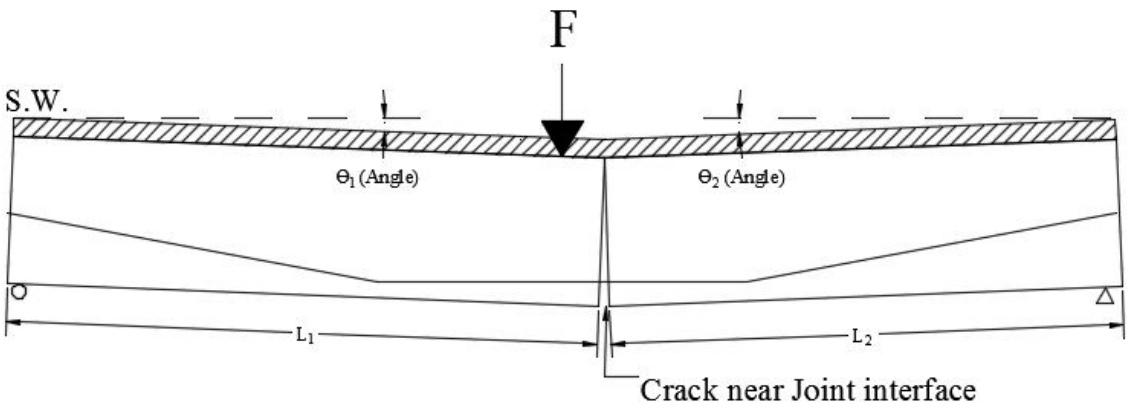

Figure 3.44 – Hinging Mechanism of an Unbonded Segmental Post-Tensioned Girder

Comparing the experimental crack width of the concentrated crack to an analytical crack width presents evidence to validate the proposed hinging response mechanism. As previously mentioned, the experimental crack width was determined using data from LEDs mounted along the face of the girder at the concentrated crack location. The analytical crack width is a function of rotation (θ), which was calculated from a known displacement. Crack width vs. midspan

displacement plots for UNB1, UNB2, and UNB3 are presented in Figure 3.45 through Figure 3.47, respectfully. The analytical crack width was determined as follows:

$$\text{Crack Width } (W_{cr}) = (Y - \text{hinge}) \sin(\theta_1 + \theta_2) \quad (3.8)$$

where (Y-hinge) is the distance from the centroid of the compression zone to the bottom of the girder. θ_1 and θ_2 are the rotations of the girder on each side of the concentrated crack due to the applied load. As seen in the figures, good agreement is seen for UNB3, which implies that the hinging mechanism developed as soon as the load dropped. In other cases, it suggests that a flexural mechanism changed to a hinging mechanism gradually as the displacement was increased. When the two lines become parallel is an indication of a fully developed hinging mechanism

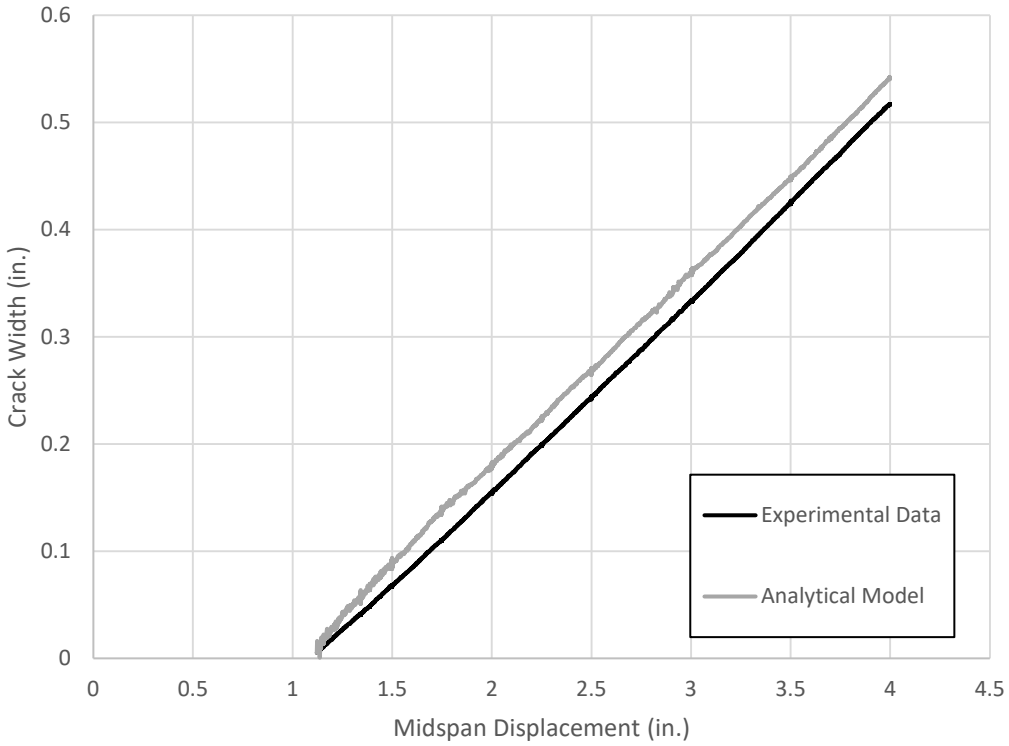

Figure 3.45 – Crack Width vs. Midspan Displacement for UNB1

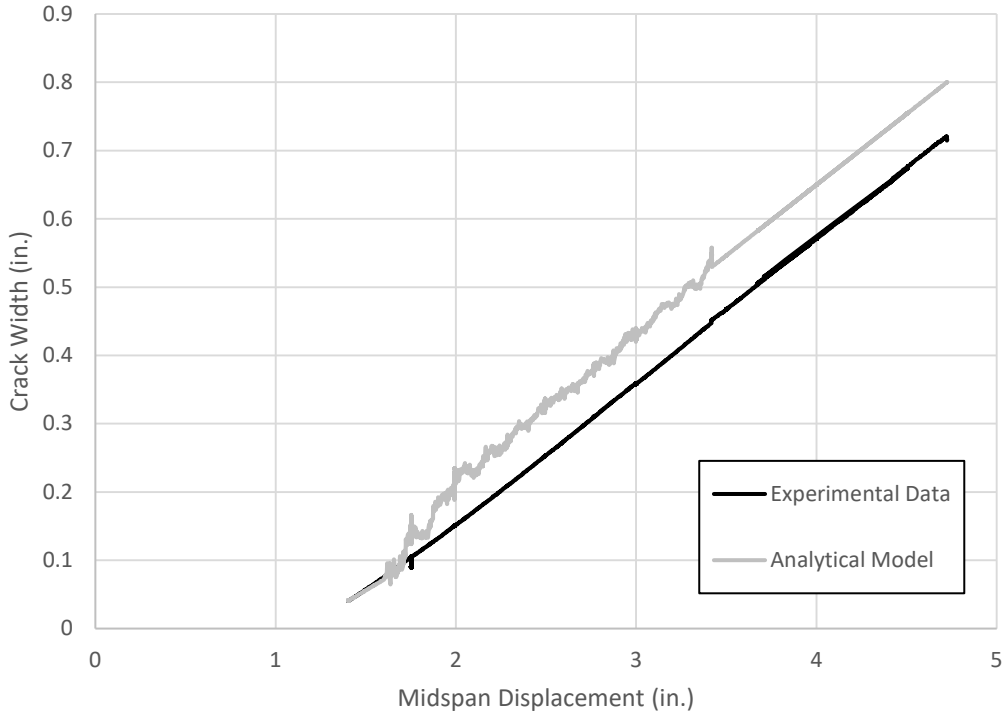

Figure 3.46 – Crack Width vs. Midspan Displacement for UNB2

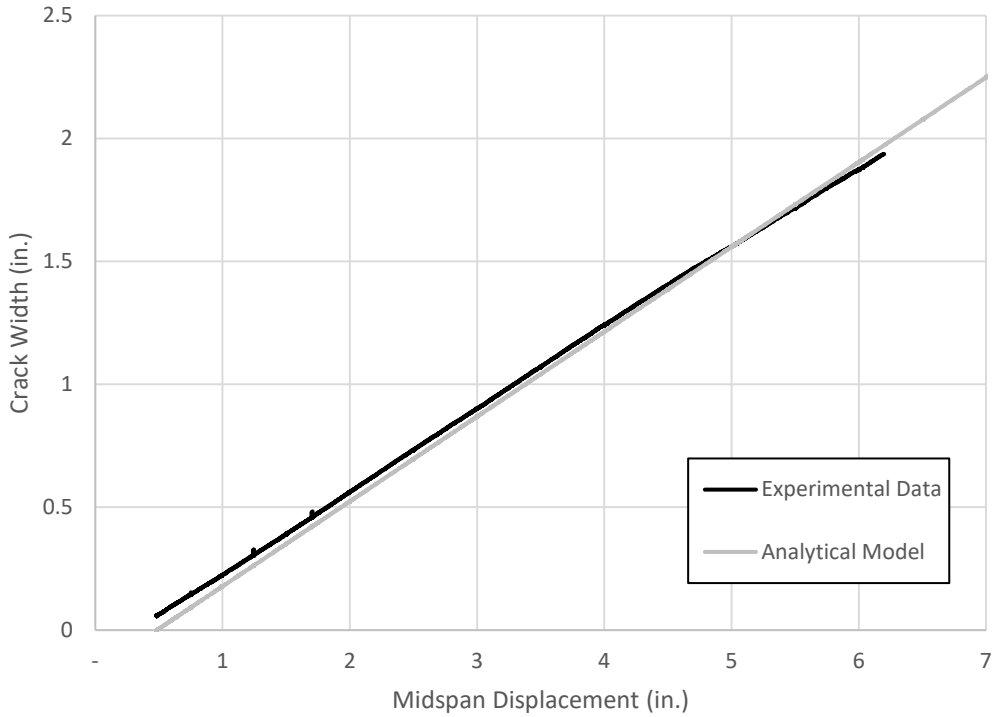

Figure 3.47 – Crack Width vs. Midspan Displacement for UNB3

Figure 3.48 through Figure 3.50 present the incremental prestressed strand strain (ε_{pt}) versus midspan displacement for each segmental girder from the experimental data and analytical model. The analytical prestressed strand strain was determined as follows, assuming the strain increase is only due to the crack opening at the hinge location:

$$\varepsilon_{pt} = \frac{W_{cr}}{l_{pt}} \qquad (3.9)$$

where l_{pt} is the length of the unbonded prestressed strand, in inches. The experimental data was collected using high-yield strain gages mounted on the prestressed strands near the midspan. Again, a good agreement in the calculated and measured strain is seen for UNB3, confirming that there was no flexural action as soon as the hinging mechanism formed. In UNB1 and UNB2, the analytical strain became equal to the measured strain when the hinging mechanism was fully formed. There observations confirm that strain measured in the tendon was primarily influenced by the concentrated crack width once the hinging mechanism is formed. In contrast, a flexural mechanism would produce higher strains due to additional elongation in the tensile region of the girder.

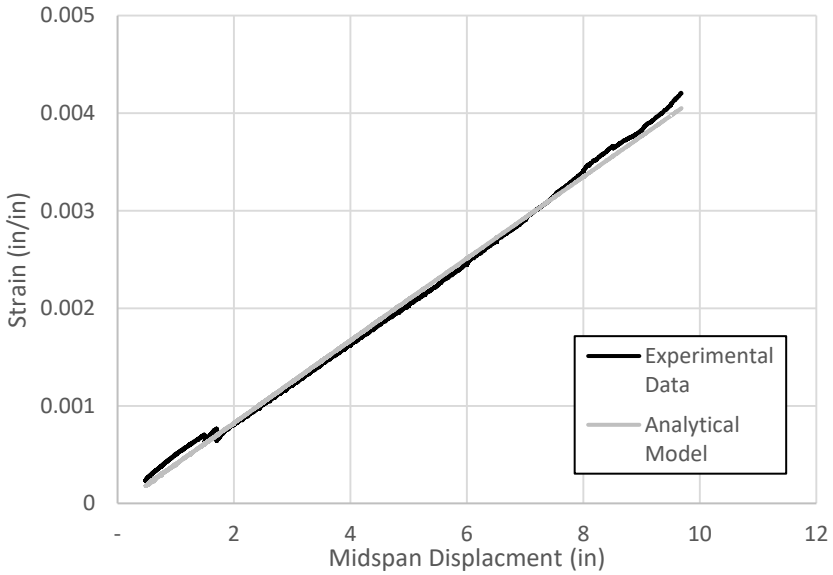

Figure 3.48 – Incremental Prestressing Strand Strain vs. Midspan Displacement for UNB1

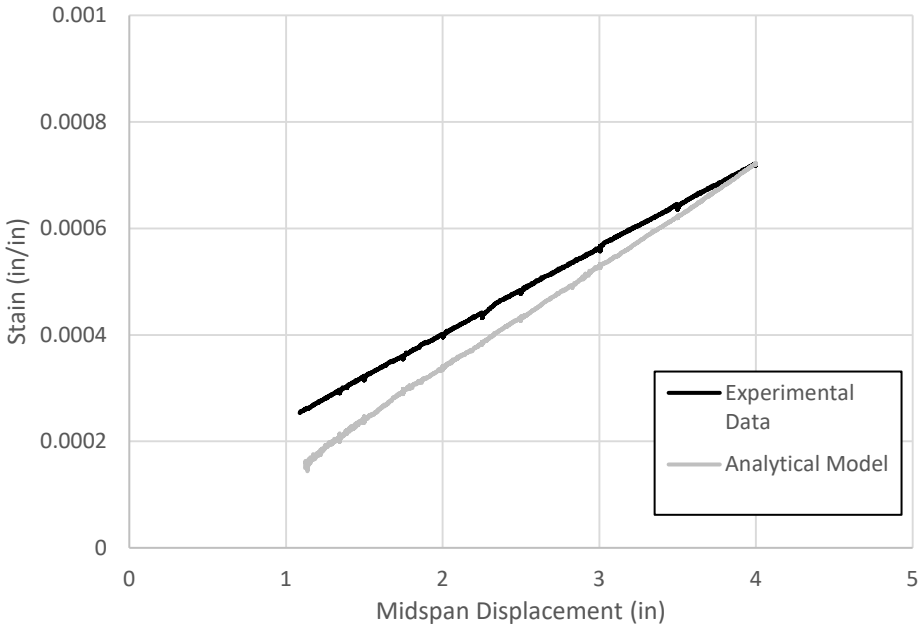

Figure 3.49 – Incremental Prestressing Strand Strain vs. Midspan Displacement for UNB2

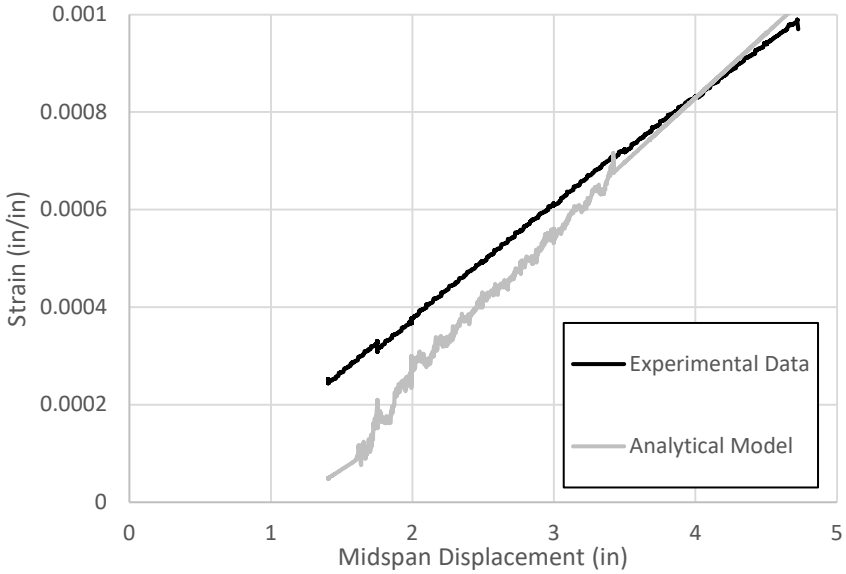

Figure 3.50 – Incremental Prestressing Strand Strain vs. Midspan Displacement for UNB3

From the known displacement and Y-hinge location, the rotation (θ) about each support can be determined. Figure 3.51 presents the free body diagram of the girder during testing after development of the concentrated crack and the proposed hinging response has begun. Once again,

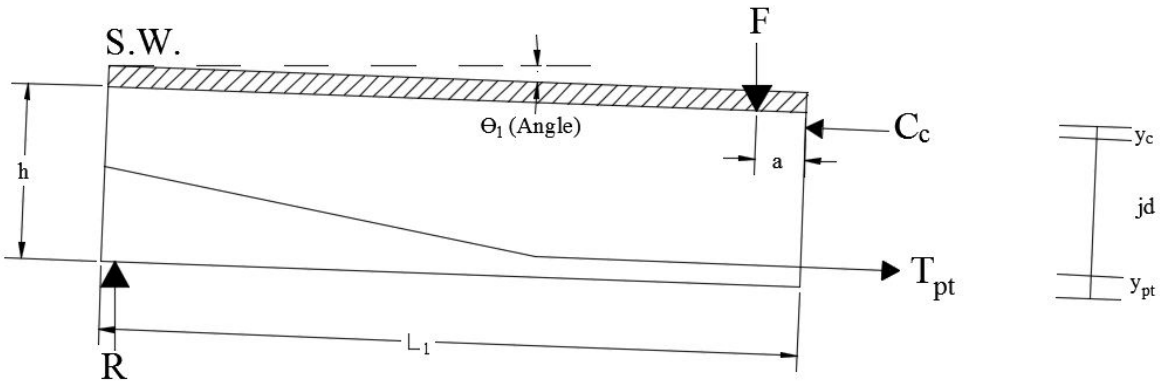

utilizing known section properties for each segmental post-tensioned girder, the applied load (F) can be calculated with similar to that in the flexural response region:

Figure 3.51 - Free Body Diagram of Unbonded Segmental Girder after the Hinging Mechanism Formed

$$\sum \text{Moments about } C_C = T_{pt}(jd) + F\cos\theta_1(a) - F\sin\theta_1(y_c) + wL_1\left(\frac{L_1}{2}\right) - \left(\frac{F}{2} + \frac{wL}{2}\right)\sin\theta_1(y_{pt} + jd) - \left(\frac{F}{2} + \frac{wL}{2}\right)\cos\theta_1(L_r) = 0 \qquad (3.10)$$

Rearrange the equation above to solve for the applied load (F):

$$F = \frac{T_{pt}(jd) + wL_1\left(\frac{L_1}{2}\right) - \frac{wL}{2}\sin\theta_1(y_{pt} + jd) - \frac{wL}{2}\cos\theta_1(L_r)}{y_c\sin\theta_1 + \left(\frac{1}{2}\right)\sin\theta_1(y_{pt} + jd) + \left(\frac{1}{2}\right)\cos\theta_1(L_r) - a\cos\theta_1} \qquad (3.11)$$

All distance values are in feet, where h is the height of the girder, y_{pt} is the distance from the center of the prestressed strand to the bottom of the girder, jd is the distance between the centroid of the compression zone and the tensile force due to post-tensioning (T_{pt}), y_c is the distance from the centroid of the compression zone to the bottom of the girder, L is the total

length of the girder, L_1 is the distance from the end of the girder to the concentrated crack, L_r is the distance from the support to the concentrated crack, a is the distance from the loading frame to the concentrated crack, and W is the distributed self-weight of the girder, in kip/ft. Once again, in order to make the equation determinant, it was assumed the support reaction is the sum of half total force and self-weight (ie., $R = \frac{F}{2} + \frac{wL}{2}$).

The applied load vs. midspan displacement plots comparing the experimental results to the calculated flexural response and hinge mechanism response for all unbonded segmental girders are be presented in Figure 3.52 through Figure 3.54. The analytical model for the flexural response was completed from zero displacement until the load drop, where the hinging mechanism was only completed using displacements after the load drop in each girder, respectfully. As can be seen, these plots further confirm the flexural response prior to the formation and transition to the hinge mechanism in segmental girders with unbonded post-tensioning. Additionally, in each case the strength within hinging mechanism response exceeds that experienced at the load drop, where the hinging mechanism began to form. This demonstrates that nominal moment (ϕM_n) does in fact exceed the cracking moment (M_{cr}) (i.e. $\frac{\phi M_n}{M_{cr}} < 1$).

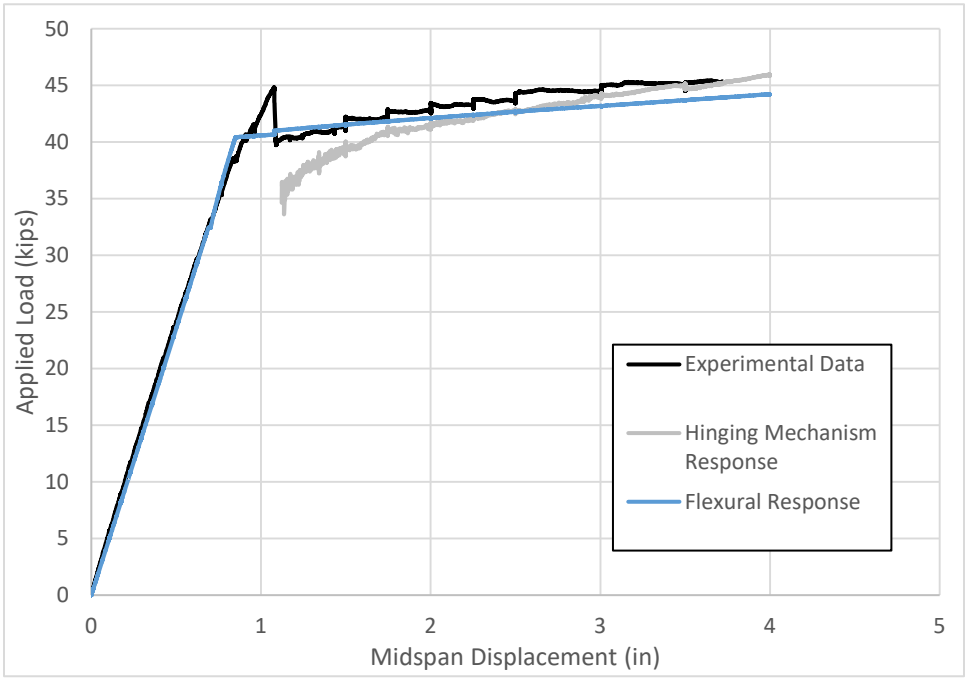

Figure 3.52 – Comparison of Applied Load vs. Midspan Displacement for UNB1

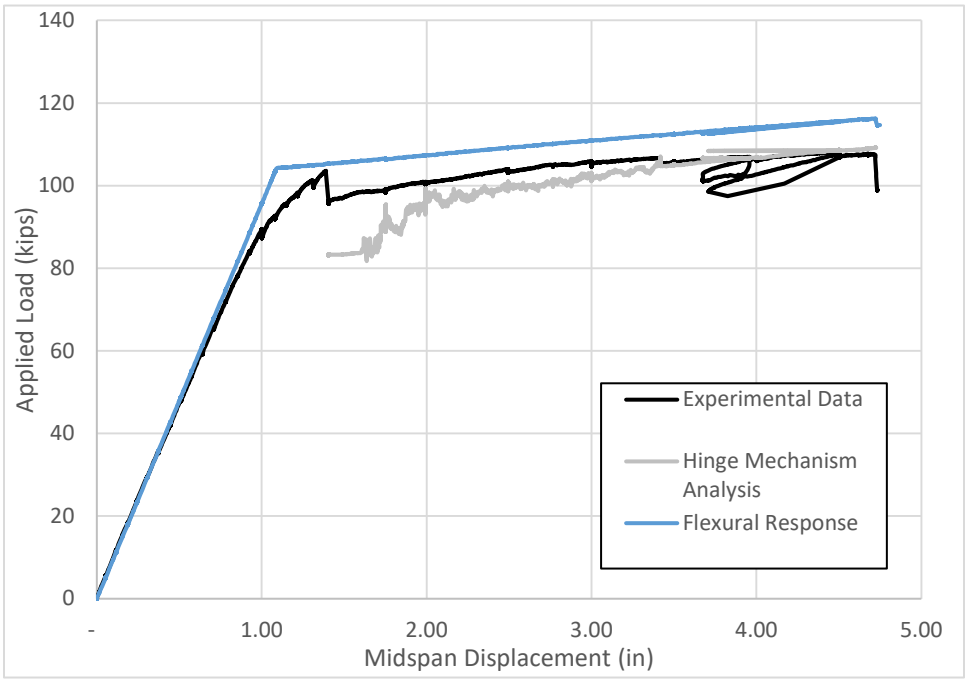

Figure 3.53 – Comparison of Applied Load vs. Midspan Displacement for UNB2

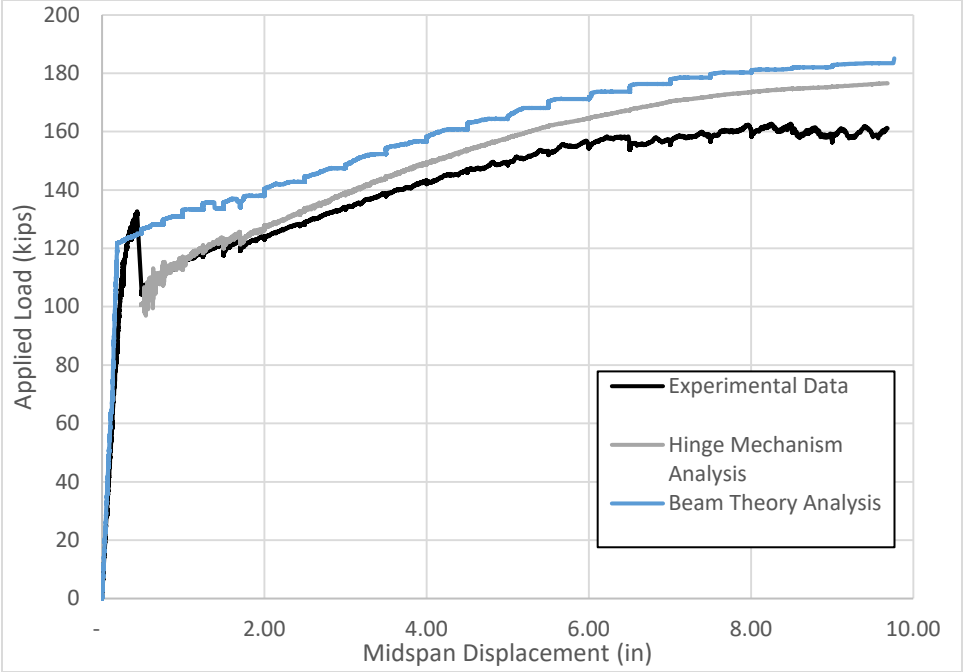

Figure 3.54 – Comparison of Applied Load vs. Midspan Displacement for UNB3

3.5.2 Unbonded prestressed tendon stress analysis

There are key differences in the determination of the nominal strength of a girder with external unbonded tendons compared to a girder with internal bonded tendons. The only contact the external unbonded tendons make with the concrete section are at deviation or support points along the girder. This leads to the tendon strains being independent of the strains in the adjacent concrete section. Compared to in a fully bonded system, where the tendon is completely encased in the concrete section and effectively grouted, resulting in the tendon strains being assumed to be the same as the concrete section at the level of the tendon. Assuming no friction with the surrounding duct of an external tendon, the tendon strain is constant for the full length between anchorages. The change in the strain due to the applied load is calculated from the total change in the length of the tendon (ΔL) over the total length (L).

Art. 5.7.3.1.2 of the AASHTO LRFD Bridge Design Specifications (AASHTO, 2017) establishes the following method for evaluating the average stress in unbonded prestressing steel for a rectangular or flanged section at nominal strength subjected to flexure about one axis based on research conducted by MacGregor (MacGregor et. al., 1989):

$$f_{ps} = f_{pe} + 900\left(\frac{d_p - c}{l_e}\right) < f_{py} \qquad (3.12)$$

Where:

f_{ps} = the tendon stress corresponding to nominal strength (ksi)

f_{pe} = effective stress in the prestressed reinforcement after all prestress losses (ksi)

f_{py} = yielding stress in the prestressed reinforcement (ksi)

d_p = distance from the extreme compression fiber to center of prestressed reinforcement (in)

c = distance from the extreme compression fiber to the neutral axis calculated using factored material strengths and assuming tension reinforcement has yielded (in)

l_e = effective length of the tendon for calculation on nominal strength

$$l_e = \left(\frac{2l_i}{2+N_s}\right) \text{ [in]} \qquad (3.13)$$

Where:

l_i = the length of the tendon between anchorages (in)

N_s = the number of support hinges crossed by the tendon (draped tendons only)

The commentary within Art. 5.7.3.1.2 states that a first estimate of the average stress in unbonded prestressing steel may be made as:

$$f_{ps} = f_{pe} + 15.0 \text{ (ksi)} \qquad (3.14)$$

In order to solve for the value of f_{ps} in eq. (3.5) the equation of force equilibrium at ultimate is needed. Thus, two equations with two unknowns (f_{ps} and c) need to be solved simultaneously to achieve a closed-form solution.

Building Code Requirements for Structural Concrete (ACI 318) (ACI, 2014) also provided an approximate method for evaluating the value of nominal flexural strength of an unbonded tendon shown in Table 3.11.

Table 3.11 – Approximate Values of f_{ps} at nominal flexural strength for unbonded tendons

l_n/h	f_{ps} (psi)	
≤ 35	The least of	f_{se}+ 10,000 + $f'_c(100\rho_p)$
		f_{se} + 60,000
		f_{py}
>35	The least of	f_{se}+ 10,000 + $f'_c(300\rho_p)$
		f_{se} + 30,000
		f_{py}

Where l_n is the span length, h is the height, f_{se} is the effective stress, and ρ_p is the ratio of A_{ps} to bd_p. Using the tendon strain data from the experimental testing along with data from the direct tensile tests completed, the nominal strength of the tendons of the unbonded UNB1, UNB2, and UNB3 were determined. Table 3.12 compares the experimental data to the current

approximate methods. The comparison indicates that the AASHTO approximate method is more accurate, yet still conservative when utilizing the method for design. The AASHTO approximate for UNB2 is larger than the experimental result, however the difference is less than 1%.

Table 3.12 – Comparison of Experimental Tendon Stress at Nominal Strength to Approximate Methods

Name	Experimental f_{ps} (ksi)	ACI 318 f_{ps} (ksi)	AASHTO f_{ps} (ksi)
UNB1	239	212	226
UNB2	224	212	226
UNB3	256	237	243

3.5.3 Response validation of bonded post-tensioned segmental girder

Analytical validation of the flexural response of the bonded post-tensioned segmental girder BON2 was completed utilizing the same analysis method for the flexural response region of the unbonded girders. As mentioned in the test results, no load drop or change in response was observed. Figure 3.55 presents the comparison of the analytical response to the experimental data. As can be seen, the plot further confirms the flexural response of the girder.

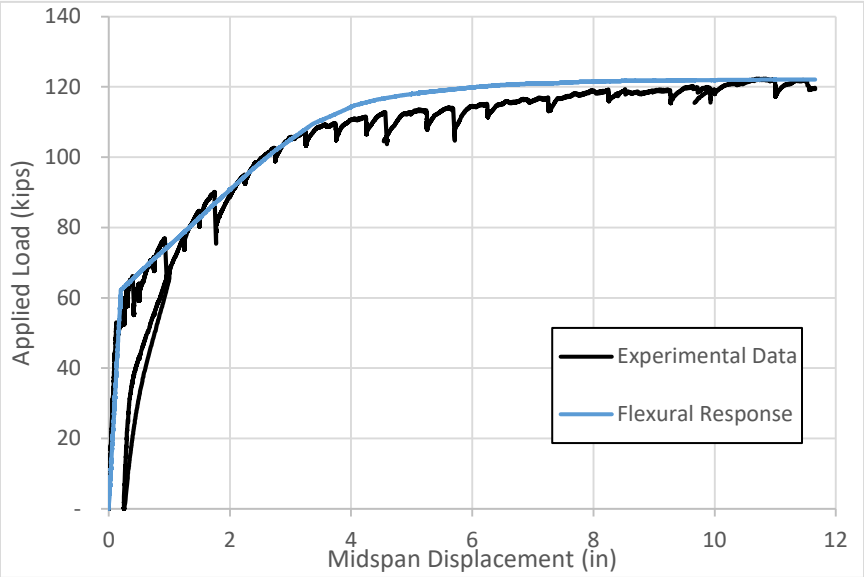

Figure 3.55 - Comparison of Applied Load vs. Midspan Displacement for BON2

3.6 Influence of Depth Factor

During testing, the onset of flexural cracking was carefully identified, and the corresponding modulus of rupture was established for each test girder. Figure 3.56 includes these modulus of rupture values as a function of member depth together with test data available from literature of previous studies. The data from the segmental portion of the NCHRP 12-94 study are seen in the figure as orange diamonds (♦). Also presented in the figure are the modulus of rupture values of $0.24\sqrt{f_c'}$ (ksi) and $0.37\sqrt{f_c'}$ (ksi), which represent the current and the past coefficients for modulus of rupture in AASHTO LRFD Bridge Specifications. In addition, the recommendation of Carpinteri and Corrado (2011) is plotted showing the possible variation in modulus of rupture with member depth, including $\pm 0.079\sqrt{f_c'}$ variation based on their recommendation. Overall, it is seen that plotted data corroborate the notion that the modulus of rupture decreases with increasing member depth. The most significant scatter in the data is seen among the modulus of rupture data that used 6 in. deep test units.

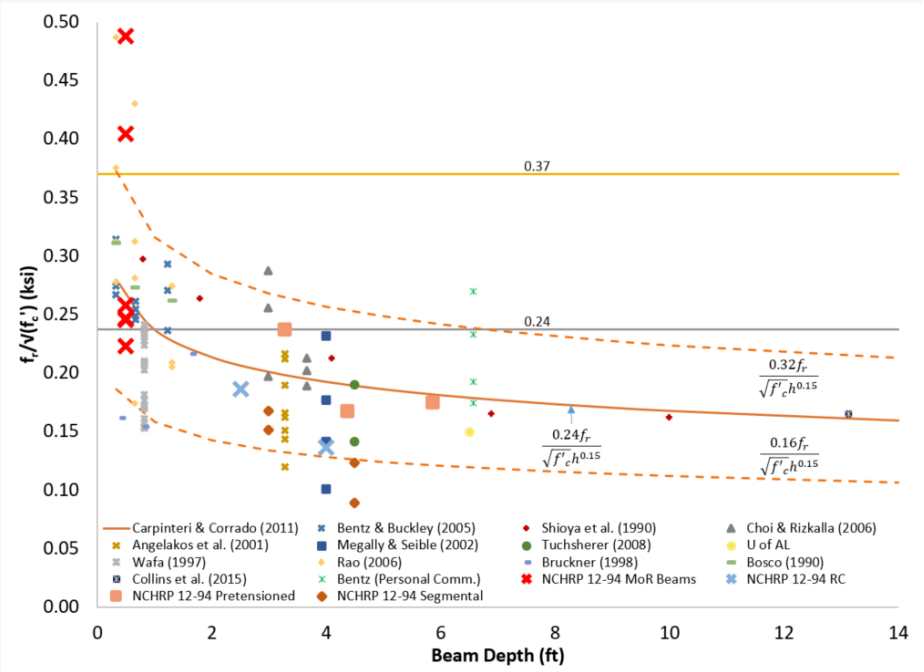

Figure 3.56 – Modulus of Rupture Values from Test Specimens (Sritharan et. al., 2018)

3.7 Conclusions of experimental study

This chapter has summarized the research completed by the project team at Iowa State University. The major indications from the experimental study of the three unbonded and one bonded post-tensioned segmental girders are as follows:

1. Of the girders that were designed with flexural reinforcement less than that required by the current AASHTO LRFD Specifications (UNB1, UNB3, BON2), all exhibited adequate safety margins beyond the experimental cracking limit state. UNB1 exhibited a limited reserve capacity following cracking, however its failure was dictated by premature failure of the strands at the anchorage. Yet, UNB1 still exhibited a minimum overstrength moment ratio $(\frac{M_u}{M_{cr}})$ of 1.08.

2. The unbonded post-tensioned segmental girders experienced flexural behavior at the beginning, followed by hinging mechanism forming and eventually dominating the response following the formation of a large concentrated flexural crack adjacent to a segment joint. The initiation of the hinging mechanism was associated with a drop in load resistance, which was regained as displacement increased. Identifying the formation of the hinging mechanism is imperative to predict the response of unbonded post-tensioned segmental girders.

3. An alternative analysis method to determining the adequacy of an unbonded segmental post-tensioned concrete girder is detailed if convergence is not met when utilizing the AASHTO LRFD Bridge Specification (AASHTO, 2017). This analysis method may be

more advantageous to use compared to Leonhardt's method, as the assumptions are more realistic for current segmental post-tensioned concrete girder designs. Validation of the proposed analytical method is provided for the unbonded test girders of the experimental study.

4. The stress accompanied with an unbonded prestressed tendon at nominal strength was analyzed using strain data within the unbonded test girders. Results were compared to the current approximate methods described in the AASHTO LRFD Bridge Specifications (AASHTO, 2017) and ACI 318 (ACI, 2014). While both methods were able to estimate the stress (f_{ps}) with a fair amount of accuracy, AASHTO LRFD approximation method provides more accurate results, while remaining conservative for design.

5. There was one bonded post-tensioned segmental girder tested (BON2) and its behavior differed from that of the unbonded girders. This is due to BON2 experiencing distributed cracking over the duration of testing rather than a concentrated crack forming, as was observed in the unbonded segmental girders. The moment ratio and ductility of the girder, 1.99 and 44.8, respectfully, display more than adequate ductility and strength gain. BON2 exhibited no safety concerns for experiencing a brittle failure despite designing it with lower than the requirement in the current AASHTO LRFD Specifications (2017) for the minimum reinforcement.

6. An investigation into the affect member depth (h) has on the modulus of rupture was conducted by NCHRP 12-94. Data collected by the segmental post-tensioned test girders further validated the claim that the modulus of rupture decreases with increasing member depth.

CHAPTER 4 – SUMMARY OF FINDING, CONCLUSIONS, AND RECOMMENDATIONS

4.1 Summary of findings

The overall objective of this study was to examine the performance of segmental post-tensioned concrete girders designed with minimum flexural reinforcement. Additionally, an alternative method to determine adequacy of an unbonded segmental post-tensioned concrete girder when convergence was unobtainable using the current AASHTO LRFD Specifications (AASHTO, 2017) was presented.

Previous research into prestressed concrete girders by (McClure and West, 1983; Rabbat and Sowlat, 1987; MacGregor et. al., 1989; and Aparicio et. al., 2001) provided valuable insight into the expected failure modes of prestressed concrete girders. Specifically, a failure mode involving a large concentrated crack at or near a segmental joint was detailed by McClure (McClure and West, 1983), as well as MacGregor (MacGregor et. al., 1989). MacGregor also detailed an approximate method for determining the stress within an external prestressed tendon at nominal strength, which was later adopted by the AASHTO LRFD Specifications (AASHTO, 2017). U.S. and International code requirements for the minimum flexural reinforcement in prestressed girders were also evaluated to exemplify the variety and inconsistencies in the requirements around the world.

The experimental testing, which consisted of a quasi-static load being applied at the midspan of a simply supported test girders. The test girders consisted of four 1/3 scale (UNB1, UNB2) or 1/2 scale (UNB3, BON2) typical 9 ft AASHTO box girders. Additional section modifications were made for construction ease and cost efficiency. Three of the test girders were

constructed with exterior unbonded tendons (UNB1, UNB2, UNB3) and one test girder was constructed with an internal bonded tendon (BON2). The test girders were instrumented prior to testing to evaluate the overall performance of the girder, as well as evaluate specific components, such as the prestressed tendons. Prior to testing, additional material testing was conducted to evaluate material properties of the concrete, high-strength steel strand, grout, and epoxy utilized.

The experimental results revealed consistent behavior of the unbonded segmental post-tensioned girders. A flexural response dominated the response initially, followed by a load drop accompanied with the formation of a large crack adjacent to an epoxy joint at the midspan. The large crack formation initiated a change to a hinging mechanism response, which gradually dominated the girder response until failure occurred. The failure mode of UNB1 was tendon rupture near the anchorage, while the failure mode of UNB2 and UNB3 was due to the aforementioned concentrated crack. The bonded segmental post-tensioned girder's, BON2, response was dominated by a flexural response throughout the duration of the test. Cracking of the bonded girder differed from that of the unbonded girders. Where a large number of cracks formed along the length of the girder, rather the formation of the concentrated crack, as seem in the unbonded girders.

An analytical study was conducted to validate the responses described in the girders. Additionally, to provide an alternative method to determine if an unbonded segmental post-tensioned girder provides sufficient strength and ductility to prevent sudden, brittle failure. The method was then validated utilizing the test data from the experimental study.

4.2 Conclusions

The following are the major conclusions drawn from the experimental study:

1) Of the girders that were designed with flexural reinforcement less than that required by the current AASHTO LRFD Specifications (UNB1, UNB3, BON2), all exhibited adequate safety margins beyond the experimental cracking limit state. UNB1 exhibited a limited reserve capacity following cracking, however its failure was dictated by premature failure of the strands at the anchorage. Yet, UNB1 still exhibited a minimum overstrength moment ratio $(\frac{M_u}{M_{cr}})$ of 1.08.

2) The unbonded post-tensioned segmental girders experienced flexural behavior at the beginning, followed by hinging mechanism forming and eventually dominating the response following the formation of a large concentrated flexural crack adjacent to a segment joint. The initiation of the hinging mechanism was associated with a drop in load resistance, which was regained as displacement increased. Identifying the formation of the hinging mechanism is imperative to predict the response of unbonded post-tensioned segmental girders.

3) An alternative analysis method to determining the adequacy of an unbonded segmental post-tensioned concrete girder is detailed if convergence is not met when utilizing the AASHTO LRFD Specification (AASHTO, 2017). This analysis method may be more advantageous to use compared to Leonhardt's method, as the assumptions are more realistic for current segmental post-tensioned concrete girder designs. Validation of the

proposed analytical method is provided for the unbonded test girders of this research study.

4) The stress accompanied with an unbonded prestressed tendon at nominal strength was analyzed using strain data within the unbonded test girders. Results were compared to the current approximate methods described in the AASHTO LRFD Bridge Specifications (AASHTO, 2017) and ACI 318 (ACI, 2014). While both methods were able to estimate the stress (f_{ps}) with a fair amount of accuracy, AASHTO LRFD approximation method provides more accurate results, while remaining conservative for design.

5) There was one bonded post-tensioned segmental girder tested (BON2) and its behavior differed from that of the unbonded girders. This is due to BON2 experiencing distributed cracking over the duration of testing rather than a concentrated crack forming, as was observed in the unbonded segmental girders. The moment ratio and ductility of the girder, 1.99 and 44.8, respectfully, display more than adequate ductility and strength gain. BON2 exhibited no safety concerns for experiencing a brittle failure despite designing it with lower than the requirement in the current AASHTO LRFD Specifications (AASHTO, 2017) for the minimum reinforcement.

6) An investigation into the affect member depth (h) has on the modulus of rupture was conducted by NCHRP 12-94. Data collected by the segmental post-tensioned test

girders further validated the claim that the modulus of rupture decreases with increasing member depth.

4.3 Recommendations for further research

The following are areas of importance were further studies would be beneficial:

I. Additional validation of the described hinging mechanism of an unbonded segmental post-tensioned girders and proposed analysis method.

II. Experimental investigation into additional parameters that may affect the strength and ductility adequacy of segmental post-tensioned girders

III. A more accurate approximation method of the prestressed tendon stress at nominal strength should be investigated.

REFERENCES

AASHTO (2017). *AASHTO LRFD Bridge Design Specifications, 8th edition*. Washington, DC: American Association of State Highway and Transportation Officials.

AASHTO (1973). *Standard Specifications for Highway Bridges, 11th edition*. Washington, DC: American Association of State Highway and Transportation Officials

AASHTO (1983). *Standard Specifications for Highway Bridges, 13th edition*. Washington, DC: American Association of State Highway and Transportation Officials

ACI Committee 318. (2014). *Building Code Requirements for Reinforced Concrete (ACI 318-14)*. Detroit: American Concrete Institute.

Aparicio, A., Ramos, G., and Casas, J. (2001). *Testing of Externally Prestressed Concrete Beams*. Engineering Structures, 24, pp.73-84.

Bosco, C., Carpinteri, A., and Debernardi, P. G. (1990). Minimum Reinforcement in High-Strength Concrete. *Journal of Structural Engineering ASCE*, 116 (2), pp. 427-437.

Brenkus, N. and Hamilton, H. (2014). *Proposed Minimum Steel Provisions for Prestressed and Non-prestressed Reinforced Sections*. ACI Journal, March-April 2014, pp. 431-440.

Bruckner, M. and Eligehausen, R. (1998). Minimum Reinforcement in RC Beams. *Proceedings of 2nd Int. Ph. D. Symposium in Civil Engineering*, Budapest, Hungary.

British Standards Institution. (2007). *Structural Use of Concrete- Part 1: Code of Practice for Design and Construction*. London: British Standards Institution.

Carpinteri, A. and Corrado M. (2011). Upper and Lower Bounds for Structural Design of RC Members with Ductile Response. *Engineering Structures*, 33 (12), pp. 3432-3441.

European Committee for Standardization. (2004). *Eurocode 2: Design of Concrete Structures- Part 1-1: General Rules and Rules for Buildings*. Brussels: European Committee for Standardization.

Ferro, G., Carpinteri, A., and Ventura, G. (2007). Minimum Reinforcement in Concrete Structures and Material/Structural Instability. *International Journal of Fracture*, 146 (4), pp. 213-231.

FHWA (2014). *Standard Specifications for Construction of Roads and Bridges on Federal Highway Projects*. Washington, DC: U.S. Department of Transportation - Federal Highway Administration.

Hindi, A., MacGregor, R., Kreger, M., and Breen, J. (1995). *Enhancing Strength and Ductility of Post-Tensioned Segmental Box Girder Bridges*. ACI Structural Journal, January-February 1995, pp.33-44.

Holombo, J. and Tadros, M. (2009). *Recommended LRFD Minimum Flexural Reinforcement Requirements, NCHRP Web-Only Document 149*. Washington, DC: NCHRP.

Japan Society of Civil Engineers. (2010). *Standard Specification for Concrete Structures*. Tokyo: Japan Society of Civil Engineers.

Leonhardt, F. (1964). *Prestressed Concrete: Design and Construction,* 2nd Ed., Translated by C. van Amerongen. Berlin: Wilhelm Ernst & Sohn.

MacGregor, R. J. G., Kreger, M., Breen, J. (1989). *Strength and Ductility of a Three-span Externally Post-tensioned Segmental Box Girder Bridge Model*. Austin, TX: University of Texas at Austin.

Madhu, M. Karthik, and Mander, B. John (2011). *Stress-Block Parameters for Unconfined and Confined Concrete Based on Unified Stress-Strain Model*. Journal of Structural Engineering., V.127, No. 2, pp 270-273

McClure, R. and West, H. (1984). *Full-scale testing of a prestressed concrete segmental bridge*. Can. J. Civ. Eng., 11, pp.505-515.

Megally, S., Seible, F., and Dowell, R. K. (2003). *Seismic Performance of Precast Segmental Bridges: Segment-to-Segment Joints Subjected to High Flexural Moments and Low Shears*. Precast/Prestressed Concrete Institute Journal, V. 48, No. 2, March-April 2003, pp. 80-96.

Norwegian Standards Association. (2003). *Concrete Structures Design and Detailing Rules*. Lysaker: Standards Norway.

Precast/Prestressed Concrete Institute. (2011). *PCI Bridge Design Manual 3rd Edition, First Release, November 2011*.

Rabbat, B. and Sowlat, K. (1987). *Testing of Segmental Concrete Girders with External Tendons*. PCI Journal, March-April 1987, pp.86-107.

Rao, C. and Frantz, C. G. (1996). *Fatigue Tests of 27-Year-Old Prestressed Concrete Bridge Box Beams.* PCI Journal, September-October 1996, pp. 74-83.

Rao, G. A., Vijayanand, I., and Eligehausen, R. (2008). *Studies on Ductility and Evaluation of Minimum Flexural Reinforcement in RC Beams.* Materials and Structures, 41 (4), pp. 759-771.

Rosenthal, Michael (2018). *An Evaluation of Minimum Flexural Reinforcement in Concrete Girders with an Emphasis on Post-Tensioned Segmental Members.* Thesis. Iowa State University. (in preparation).

Sritharan, S., Wibowo, H., Rosenthal, M. J., Eull, J. N., and Holombo, J. (2018). *LRFD Minimum Flexural Reinforcement Requirements*. Washington, DC: Transportation Research Board. (in preparation).

Warwaruk, J., Sozen, M., Siess, C. J. (1960). *Strength and Behavior in Flexure of Prestressed Concrete Beams*. University of Illinois at Urbana Champaign.

APPENDIX – TEST GIRDER DRAWINGS

Total prestress is based on 72.6% f's, f's = 270 ksi and As = 0.217 in^2

All prestressing strands shall conform to ASTM A416 Grade 270 Low Relaxation Strands
All beams are to be increased in length to compensate for elastic shortening, creep, and shrinkage

All concrete strengths shall not be greater than 1,000 psi greater than the specified concrete strength

Rebar dimensions are taken from edge to edge, not centerline to centerline

Lifting points as measured from end of girder	
Girder	Distance* (ft)
A34	13
BTC 60	20
BTE 70	25

Cracking will be detrimental to the girders, therefore girders shall be lifted at the points described in the Lifting points as measured from end of girder table

12 modulus of rupture cylinders shall be cast per girder and cured with the girder

Precaster provides girders, girder reinforcement (including hooks), and test cylinders (deck and deck reinforcement are not to be provided by the precaster)

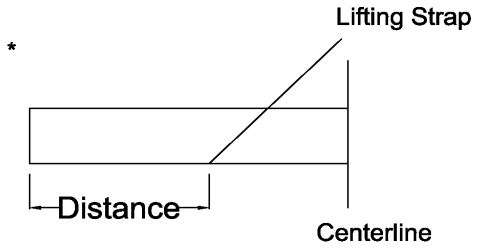

NCHRP 12-94	Cover Page			Dr. Sri Sritharan Principal Investigator	BRIDGE NO. — POST MILES — 05-05-2015 Test Units DISREGARD PRINTS BEARING EARLIER REVISION DATES REVISION DATES (PRELIMINARY STAGE ONLY) X SHEET 1 OF

Figure A.1 – RC and Pretensioned Girder Drawing Cover Page

Sheet List	
Sheet Number	Sheet Name
01	GENERAL NOTES
02	REBAR DETAILS
03	SEGMENTAL BEAMS
04	UNB1 TYPICAL SEGMENT
05	UNB1 END BLOCK
06	UNB1 DEVIATOR
07	UNB2 TYPICAL SEGMENT
08	UNB2 END BLOCK
09	UNB2 DEVIATOR
10	UNB3 TYPICAL SEGMENT
11	UNB3 END BLOCK
12	UNB3 DEVIATOR
13	BON2 TYPICAL SEGMENT
14	BON2 END BLOCK
15	DEVIATOR DETAILS
16	DEVIATOR SEGMENT ISOMETRIC
17	SHEAR & ALIGNMENT KEY DETAILS
18	SHEAR & ALIGNMENT KEY DETAILS 2

General Notes

All reinforcement bars are #4 unless noted otherwise.

The clear cover is 1 inch unless noted otherwise.

For UNB1 and UNB2 the maximum aggregate size is 1/2 inch. For UNB3 and BON2 the maximum aggregate size is 3/4 inch.

No concrete will enter the ducts during the pouring of the segments.

The 28 day compressive strength of the concrete will be at least 6 ksi and not more than 7 ksi.

The mild reinforcement used in the segments is A615 Grade 60 steel.

All transverse sections are symmetrical about their centerlines.

Short reinforcement bars may be placed to secure the tendon ducts.

Concrete will have a compressive strength of at least 2.5 ksi before the forms are stripped (AASHTO 5.14.2.4.2).

In addition to the needs of the precaster, provide 18 - 4x8 inch cylinders and 4 - 6 inch x 6 inch x 36 inch modulus of rupture beams for each pour.

All anchorage systems are Muliplane Anchorage from DSI. UNB1: use two 5-0.6". UNB2: Use two 7-0.6". UNB3: Use two 9-0.5". BON2: Use 12-0.5".

The segments will be match cast to ensure proper geometric placement during testing.

Provide lifting hooks at equal distance longitudinally from the center of the segments. (See detail below)

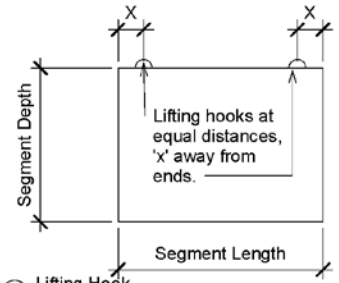

1 Lifting Hook
1/2" = 1'-0"

IOWA STATE UNIVERSITY	GENERAL NOTES	NCHRP 12-94	Dr. Sri Sritharan, Principal Investigator Drawn by Michael Rosenthal, mjr@iastate.edu, 319-210-7435	BRIDGE NO. / POST MILES 05-20-15 Test Units DISREGARD PRINTS BEARING EARLIER REVISION DATES REVISION DATES (PRELIMINARY STAGE ONLY) X X SHEET 01 OF

Figure A.2 – Segmental Cover Sheet and Sheet List

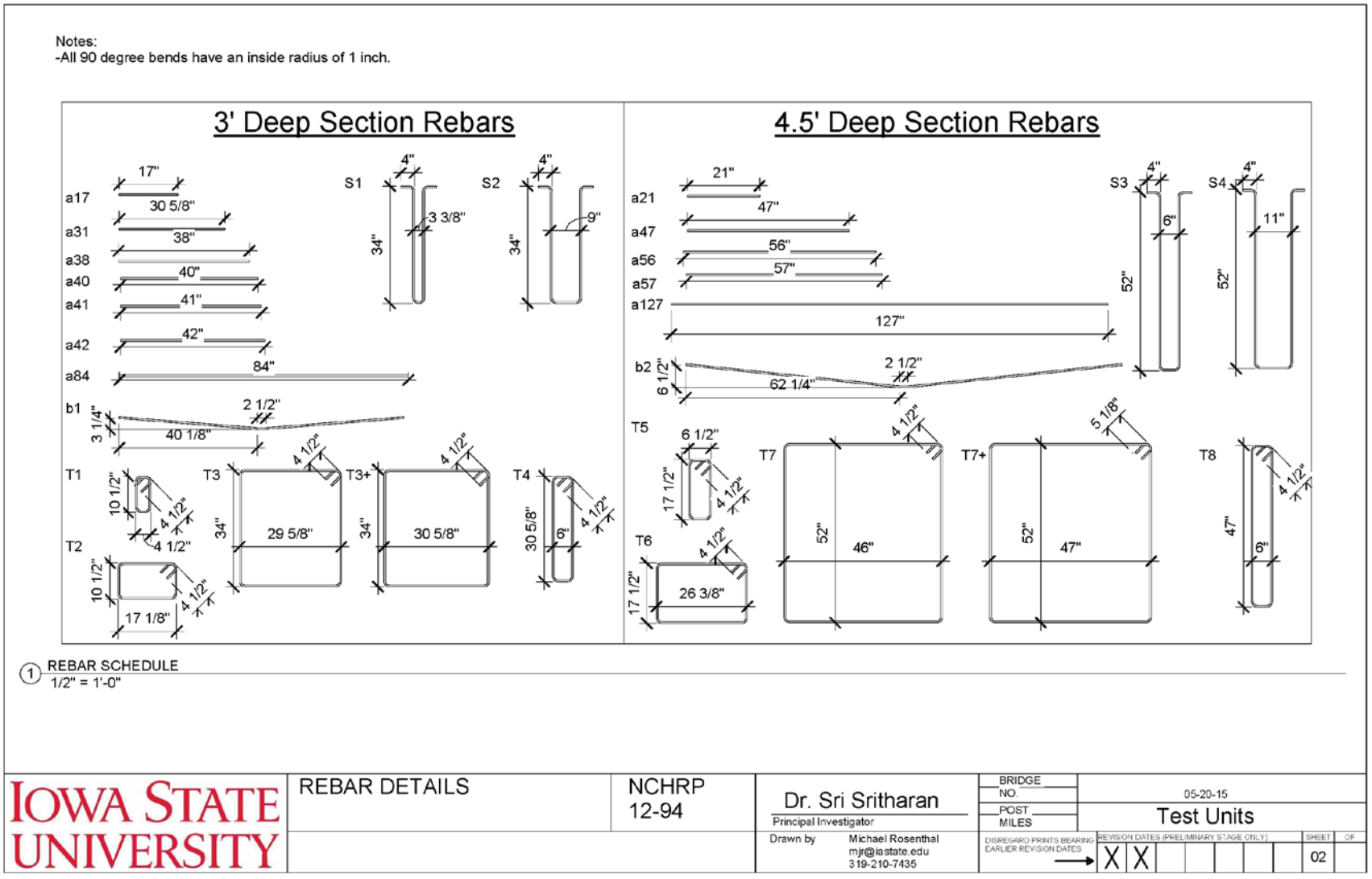

Figure A.3 – Mild Reinforcement Details

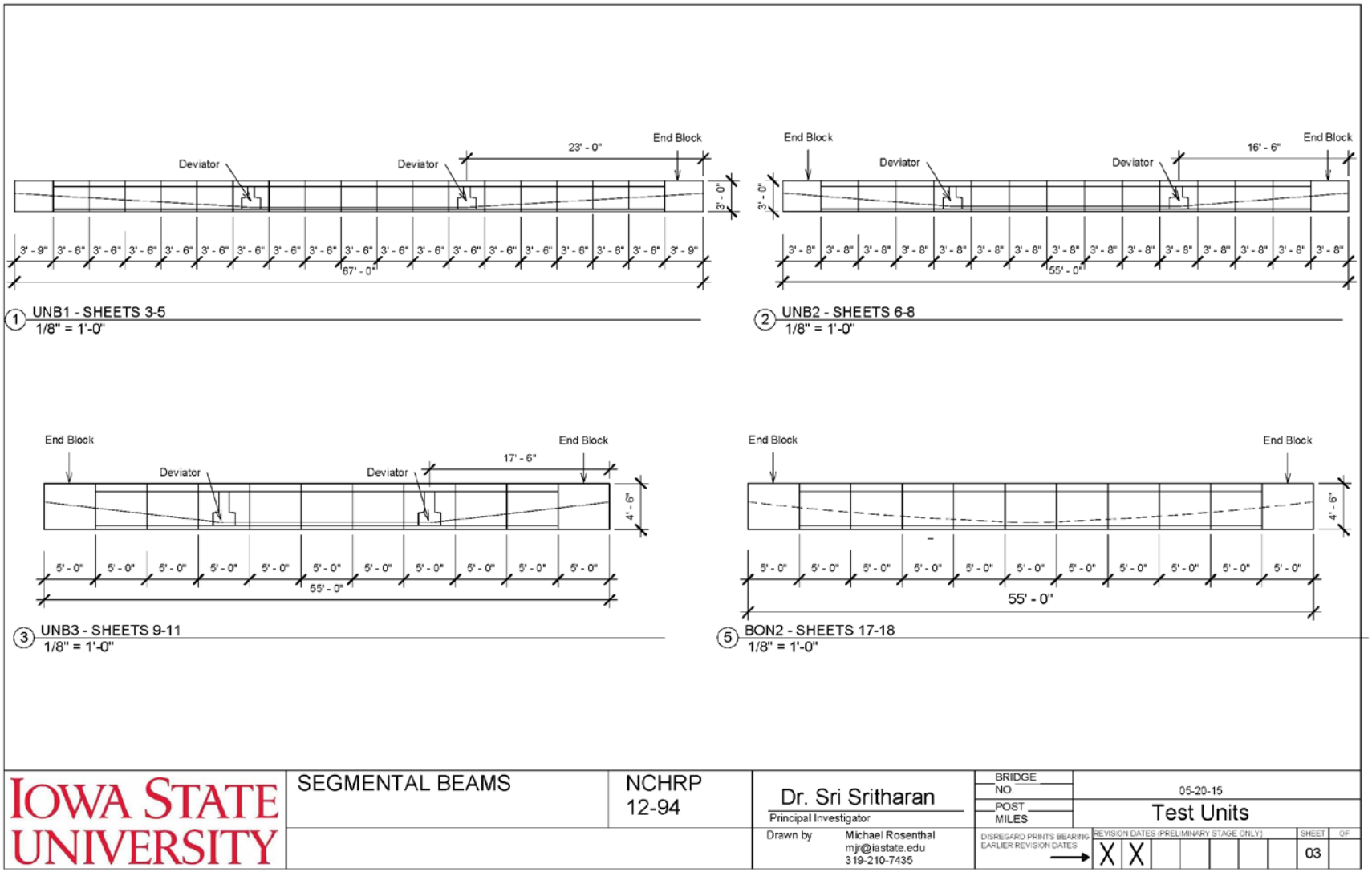

Figure A.4 – Segmental Elevations

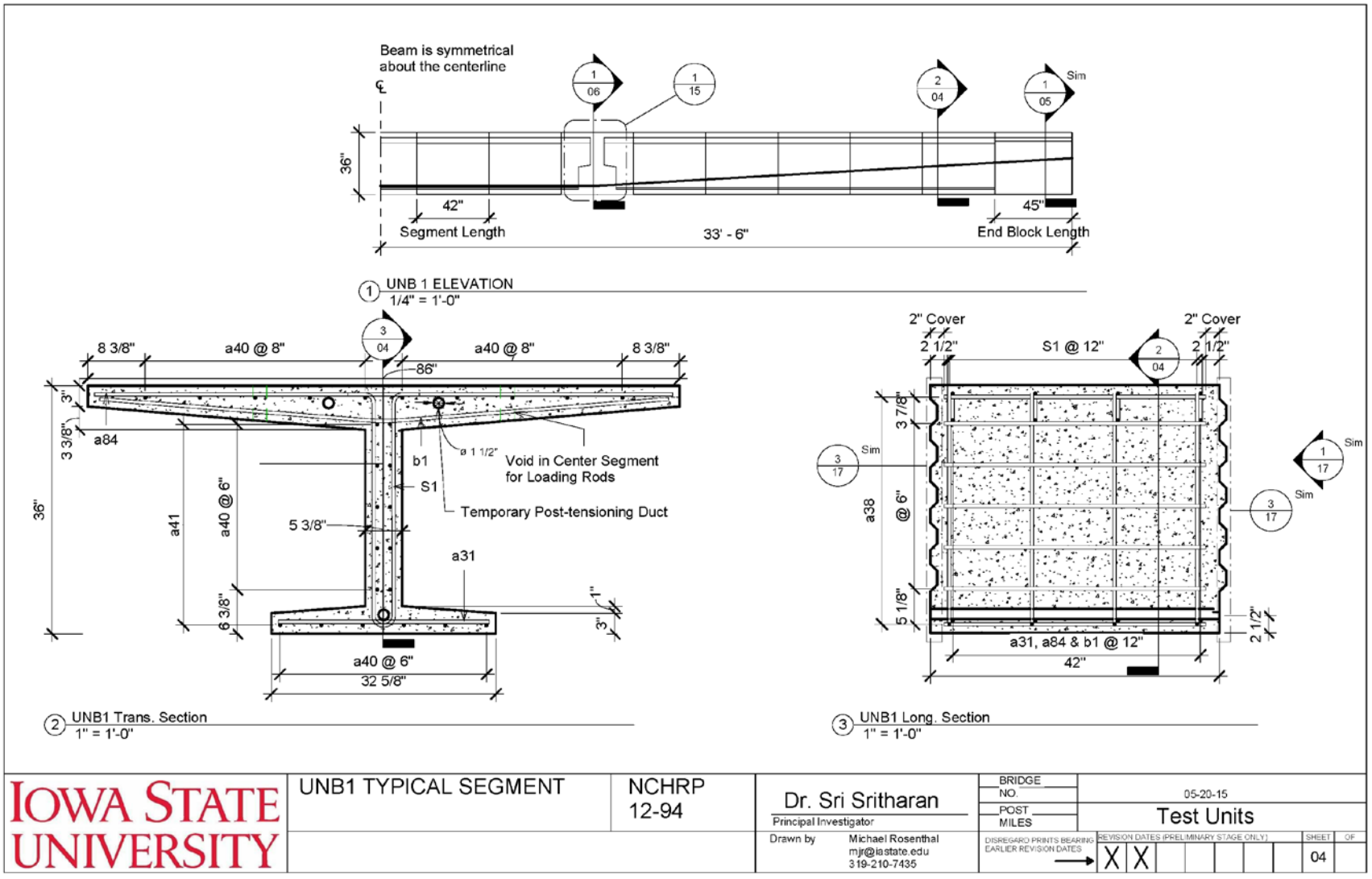

Figure A.5 – UNB1 Typical Longitudinal and Transverse Section

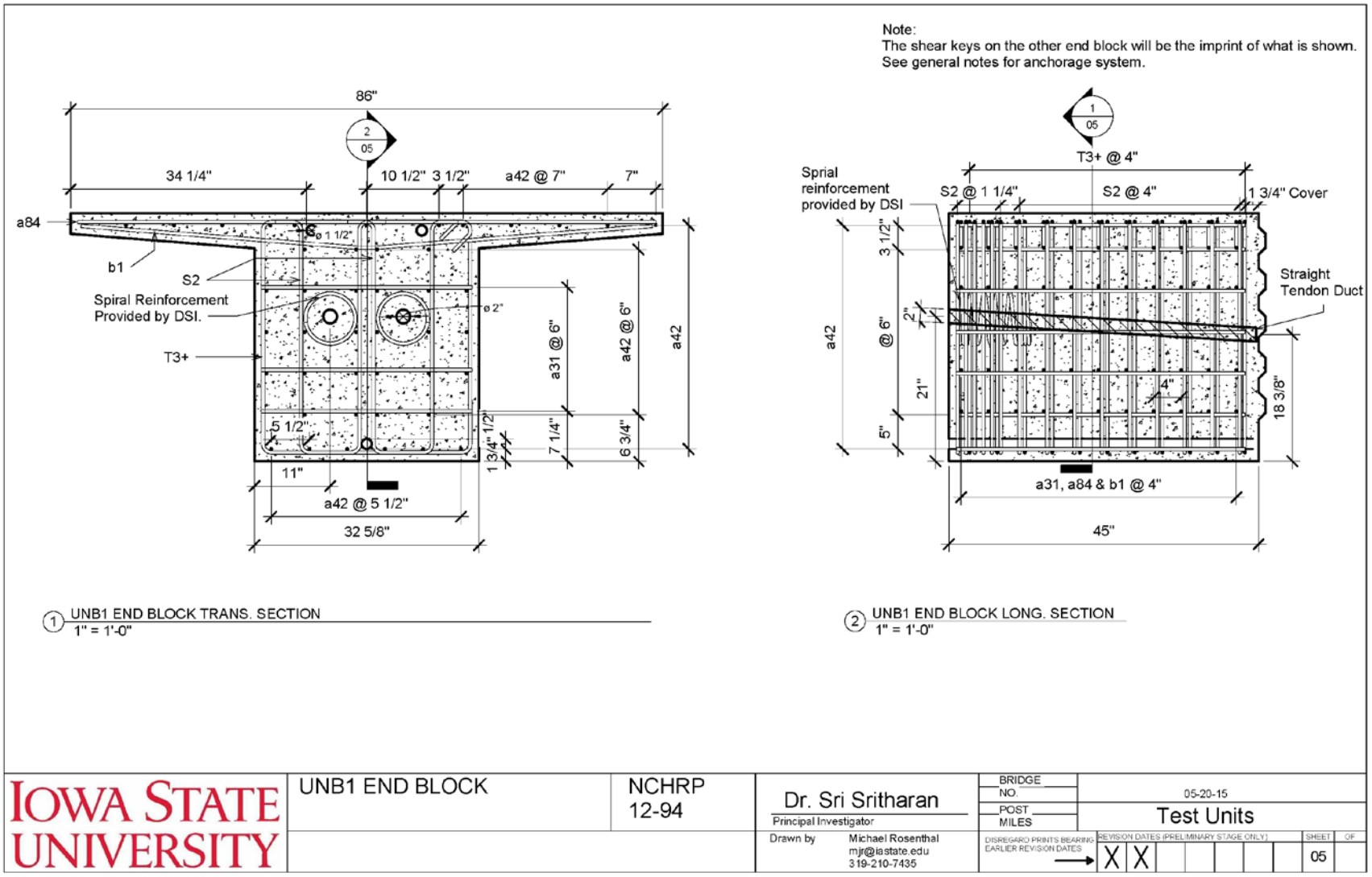

Figure A.6 – UNB1 End Block Longitudinal and Transverse Section

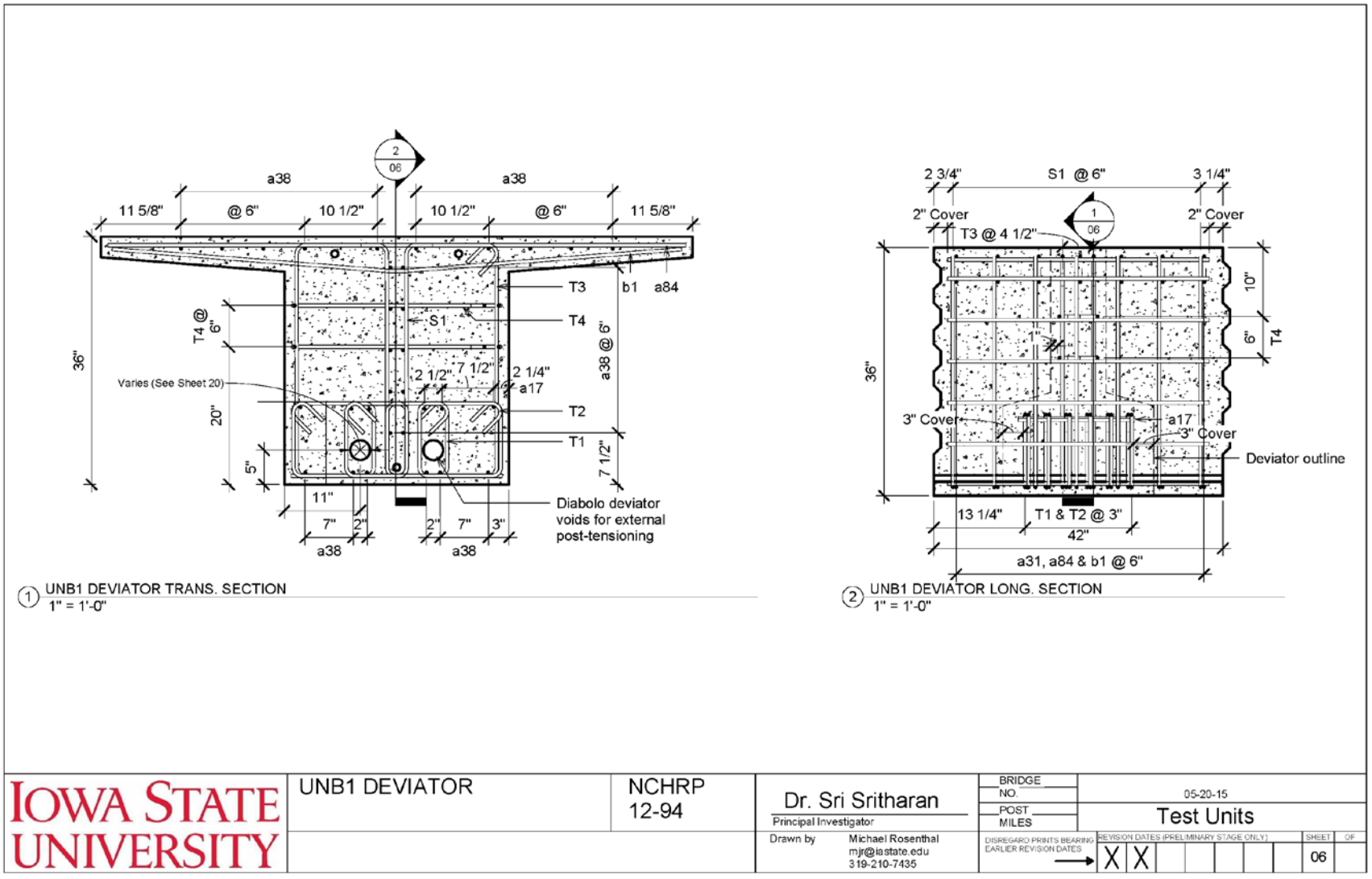

Figure A.7 – UNB1 Deviator Segment Longitudinal and Transverse Section

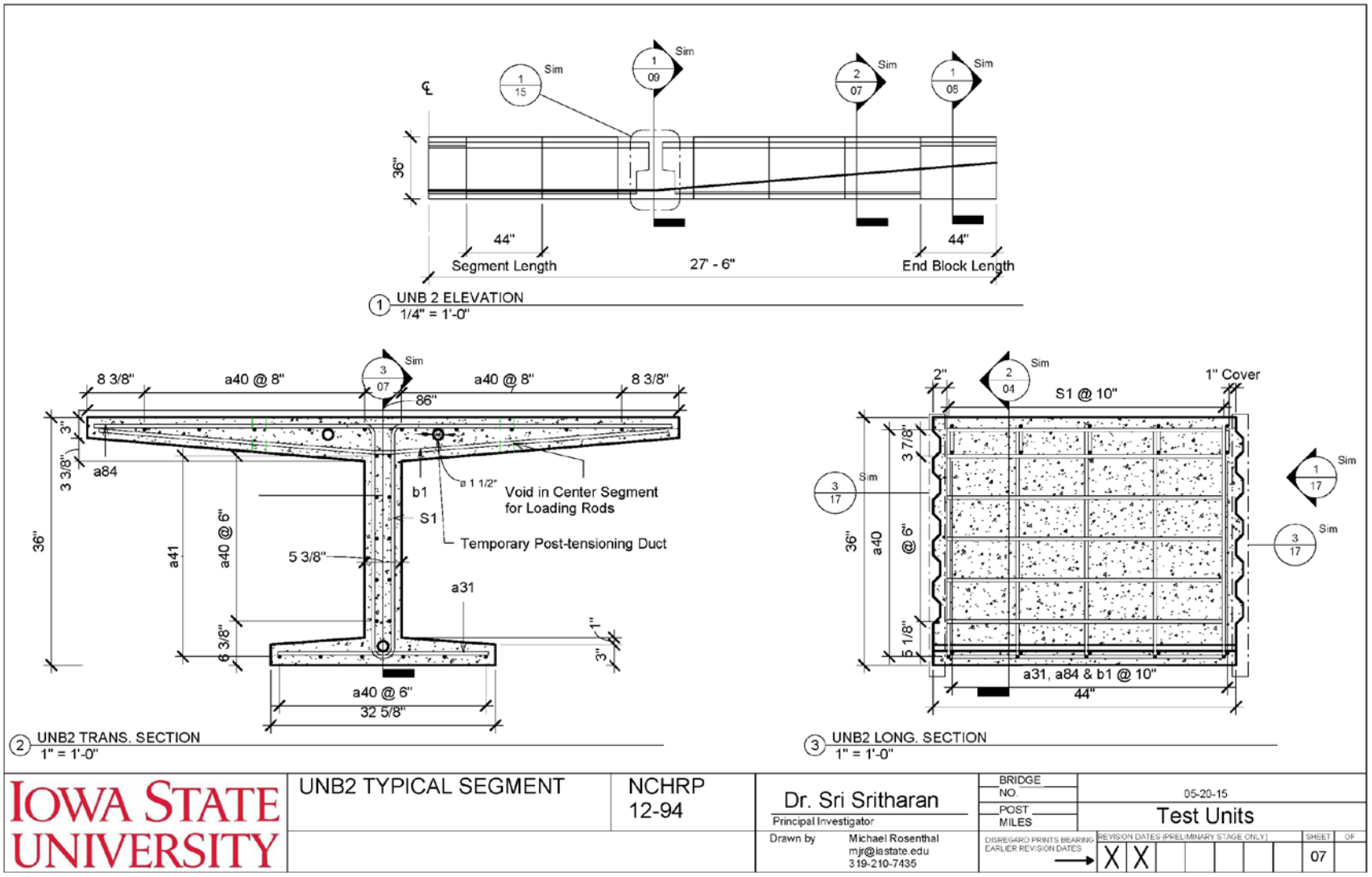

Figure A.8 – UNB2 Typical Longitudinal and Transverse Section

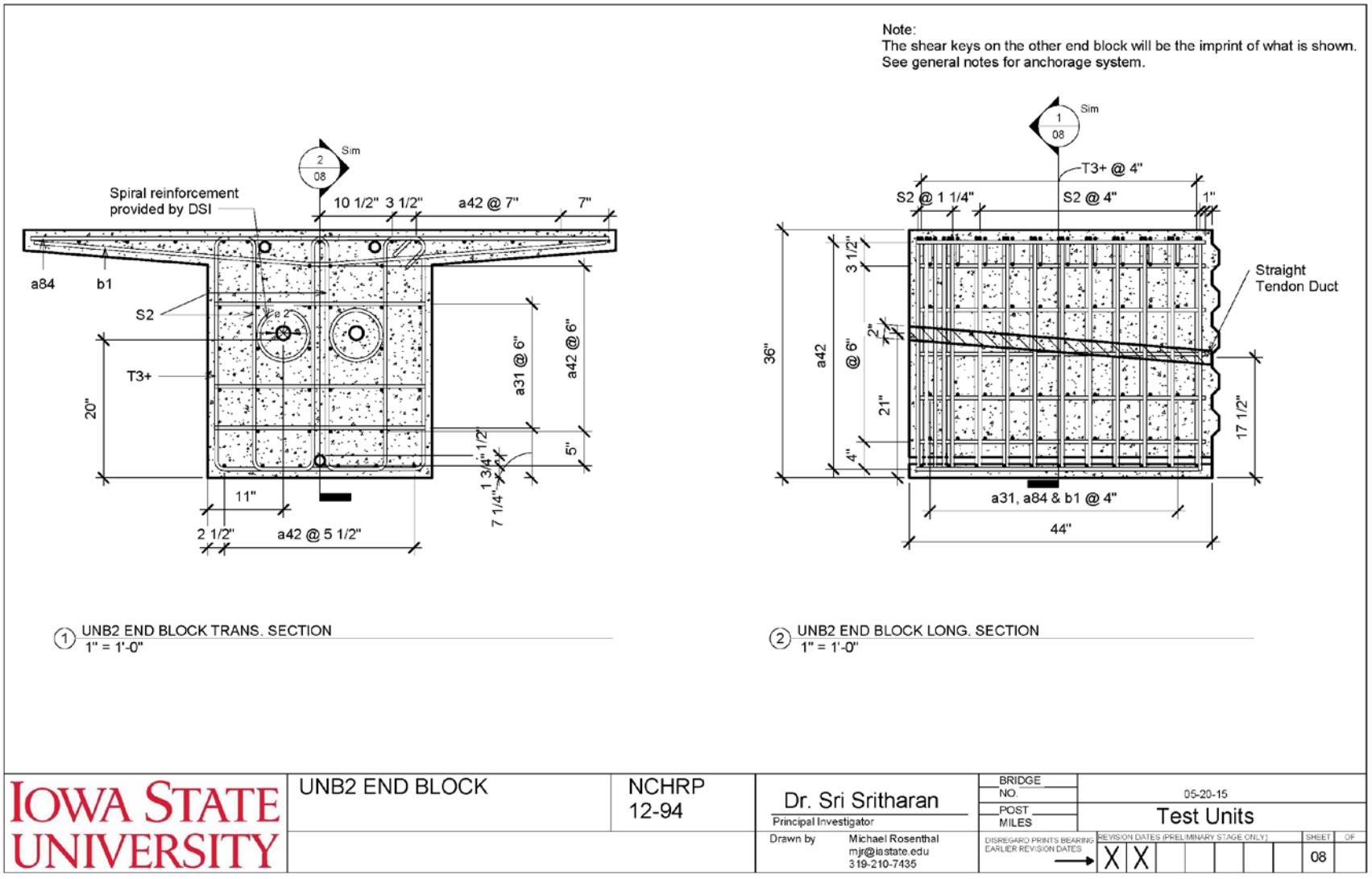

Figure A.9 – UNB2 End Block Longitudinal and Transverse Section

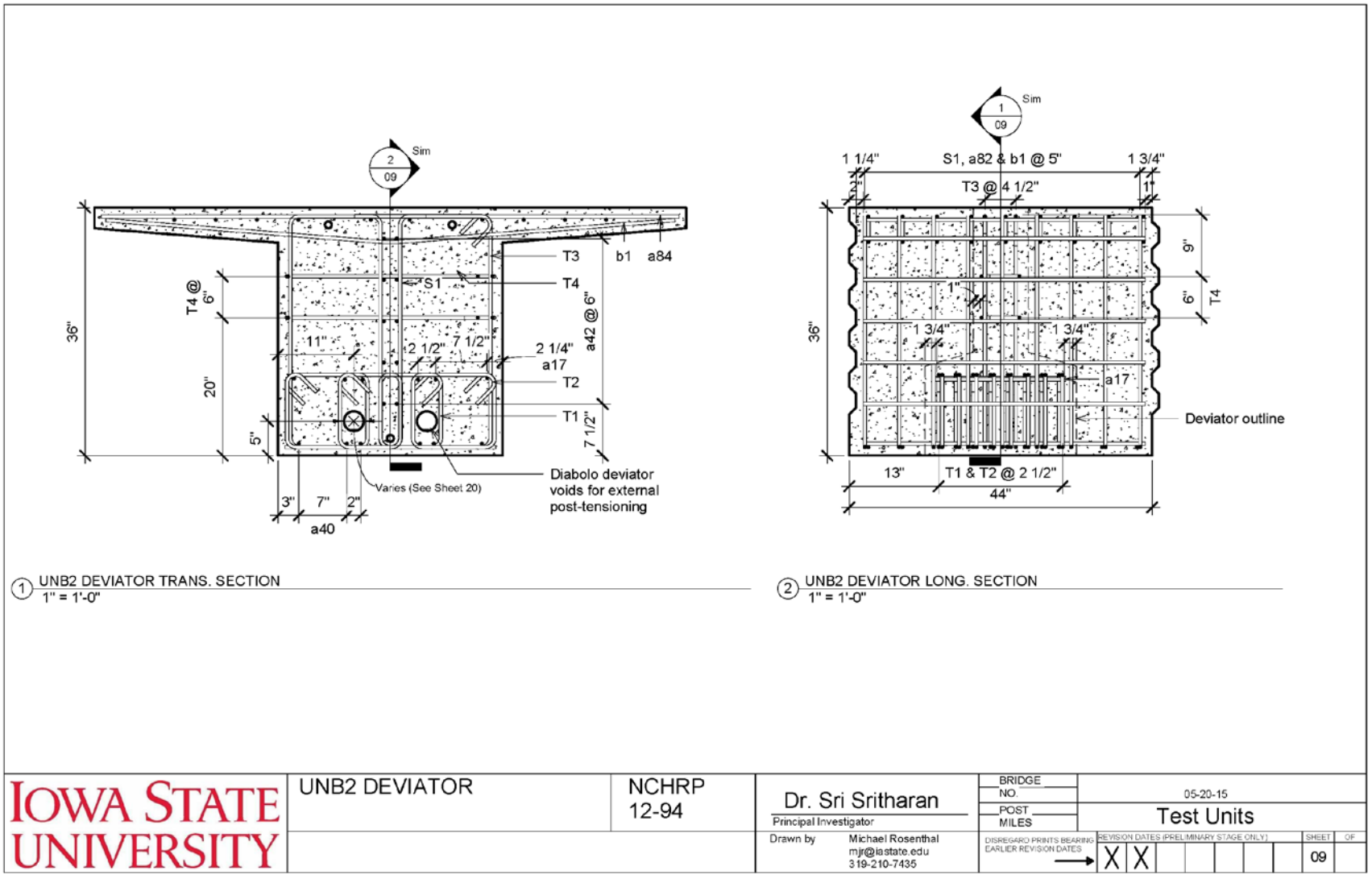

Figure A.10 – UNB2 Deviator Segment Longitudinal and Transverse Section

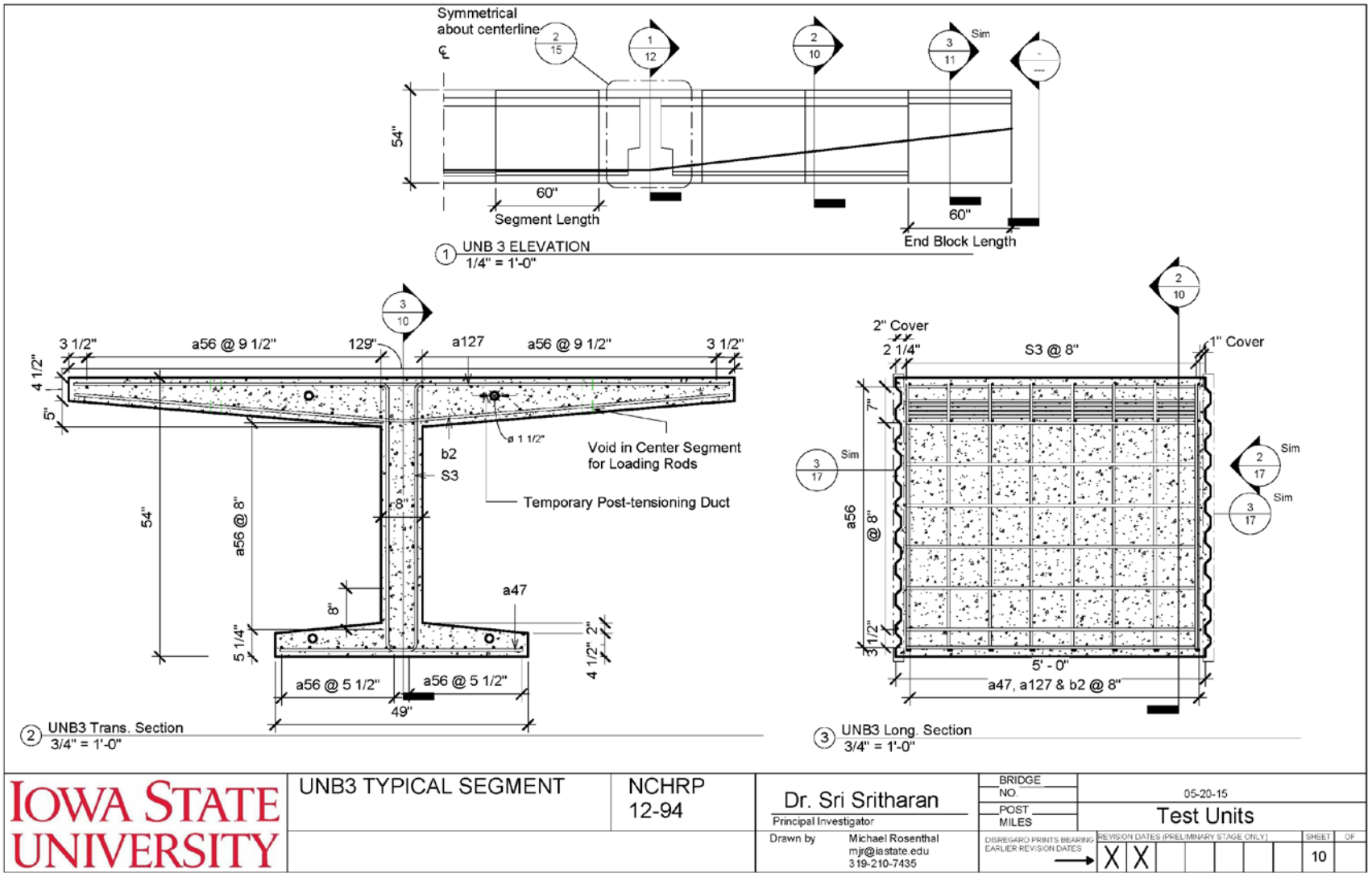

Figure A.11 – UNB3 Typical Longitudinal and Transverse Section

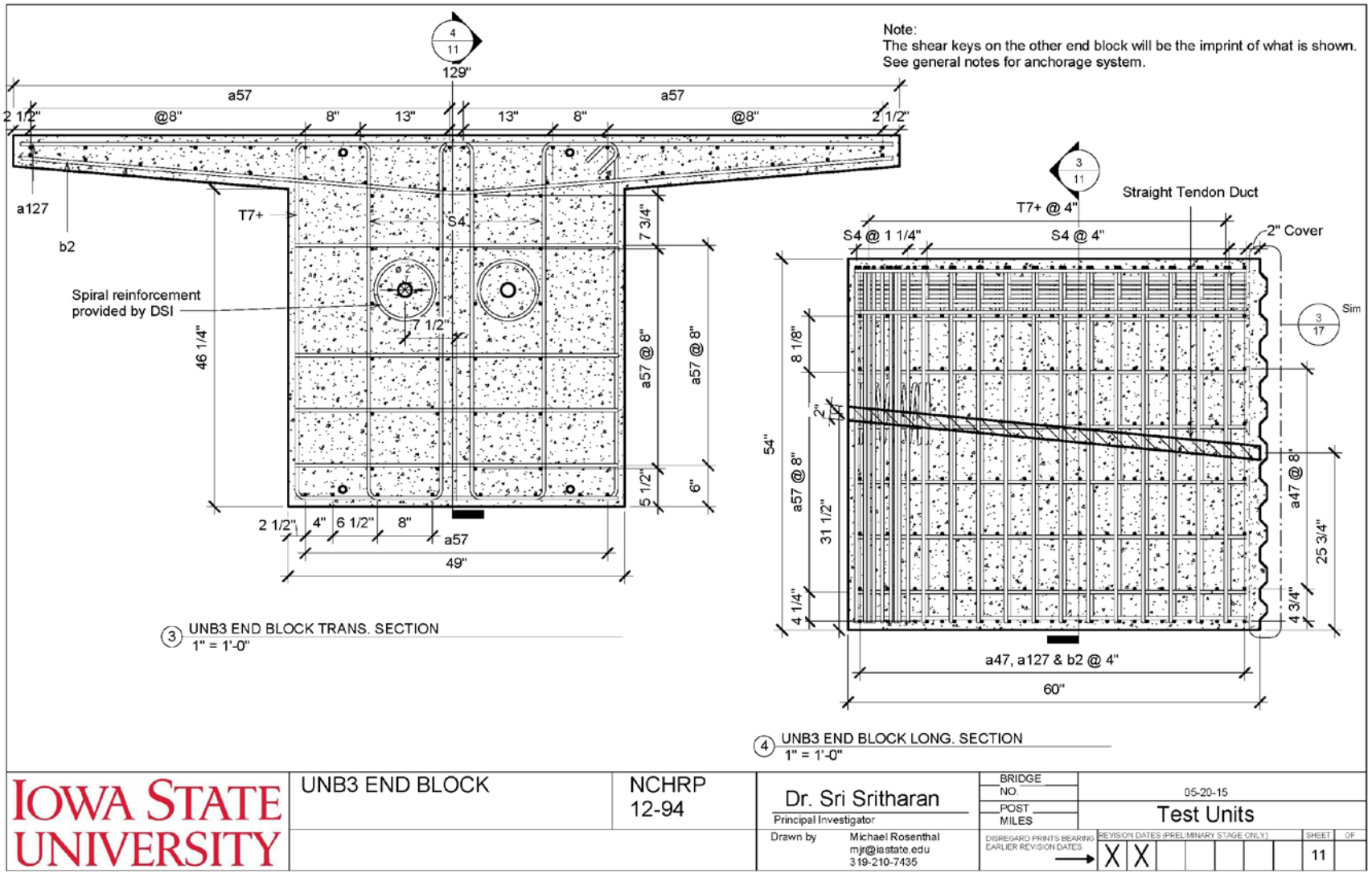

Figure A.12 – UNB3 End Block Longitudinal and Transverse Section

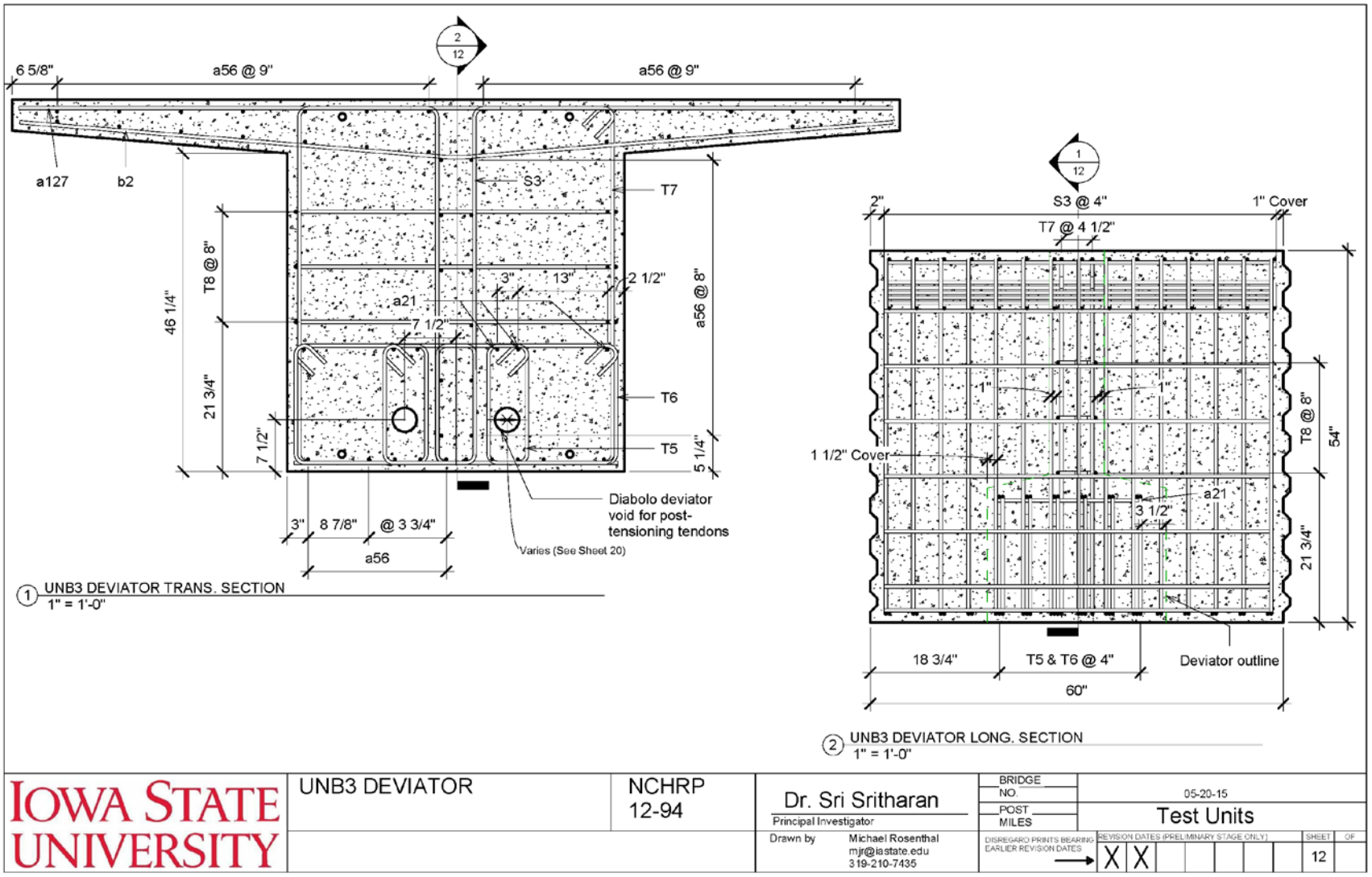

Figure A.13 – UNB3 Deviator Segment Longitudinal and Transverse Section

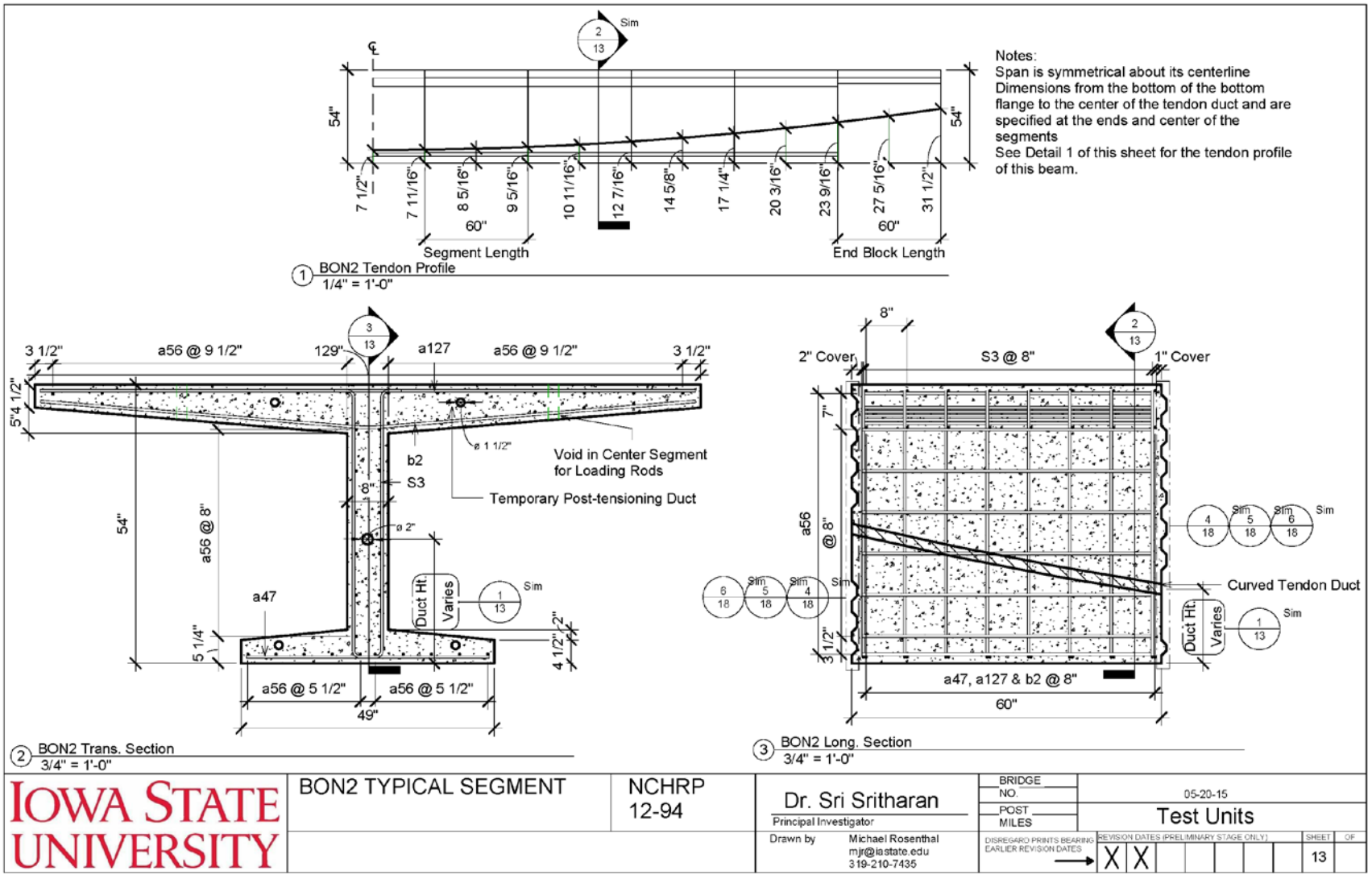

Figure A.14 – BON2 Typical Longitudinal and Transverse Section

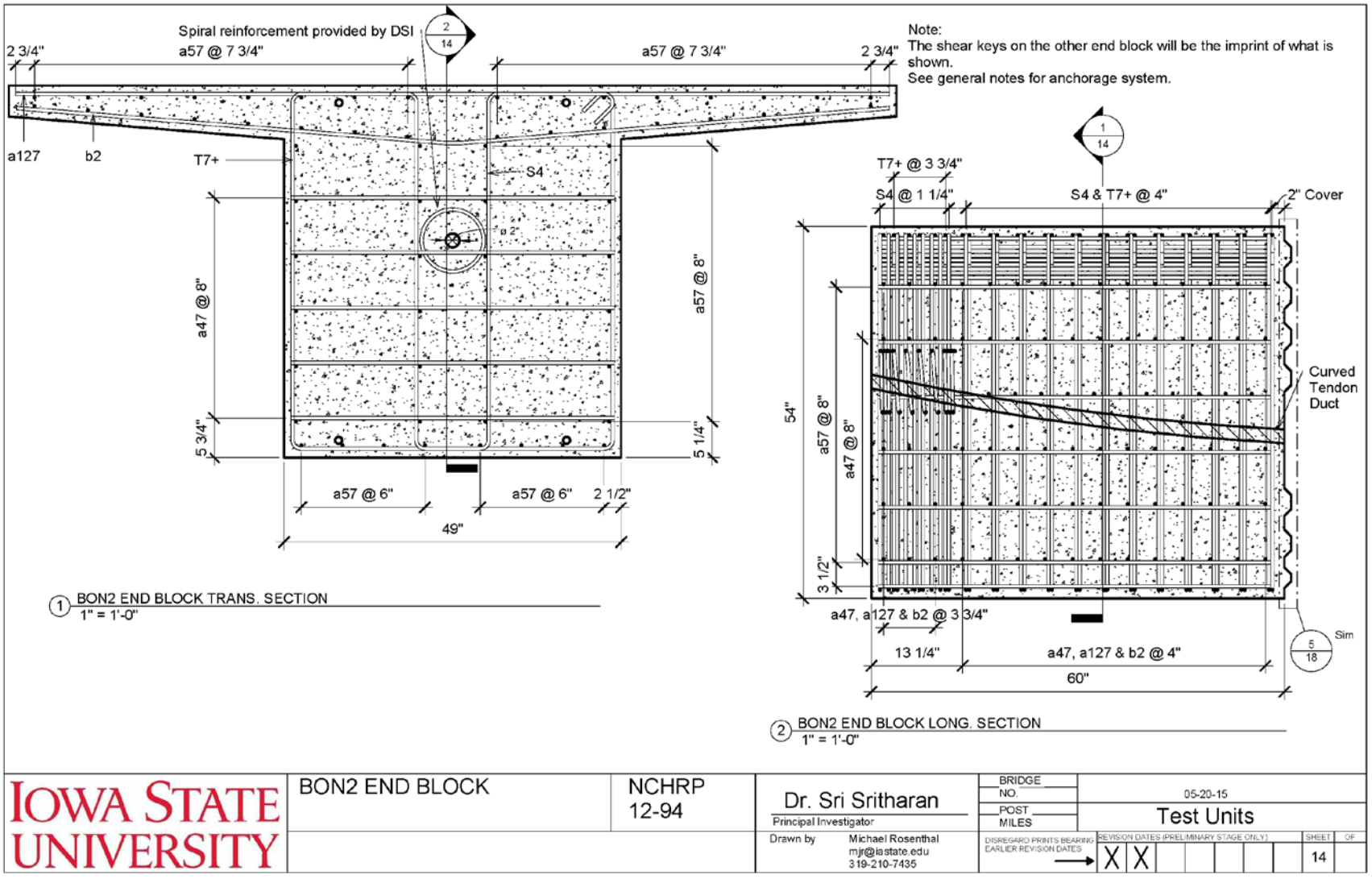

Figure A.15 – Bon2 End Block Longitudinal and Transverse Section

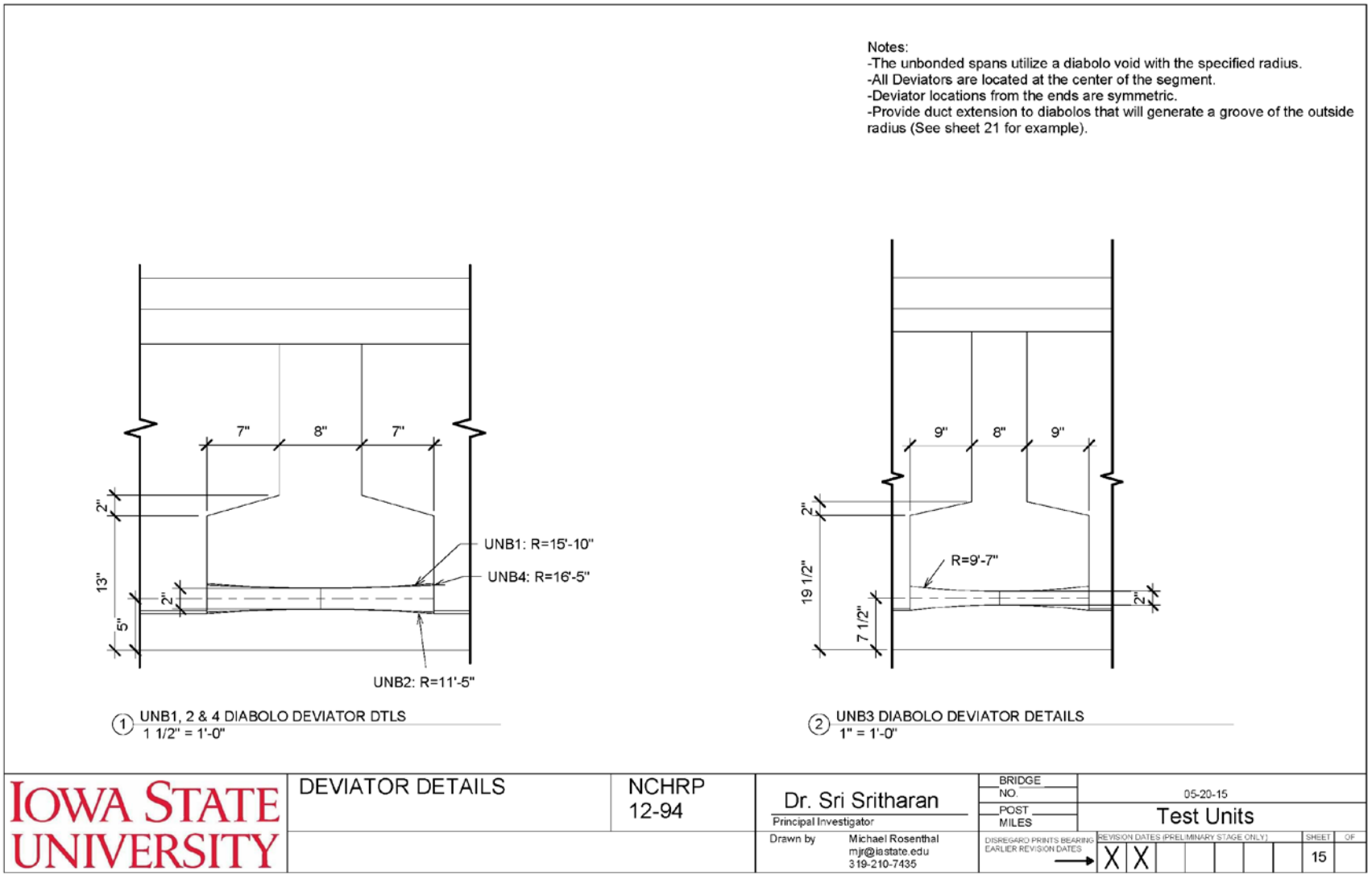

Figure A.16 – Deviator Details

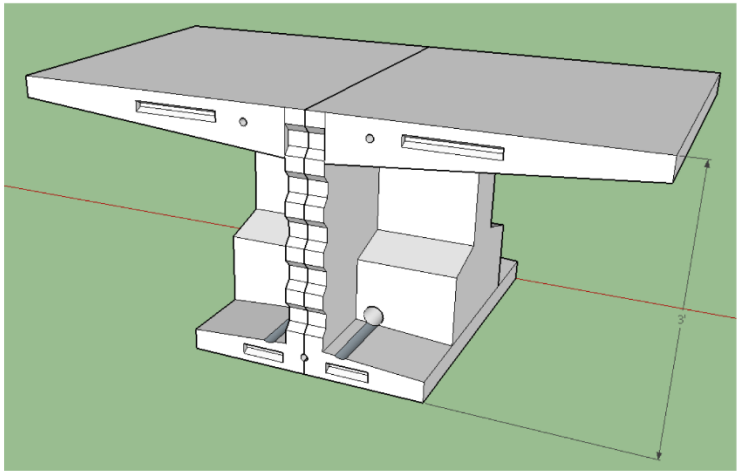

1 UNB2 DEVIATOR SEGMENT ISOMETRIC
1/8" = 1'-0"

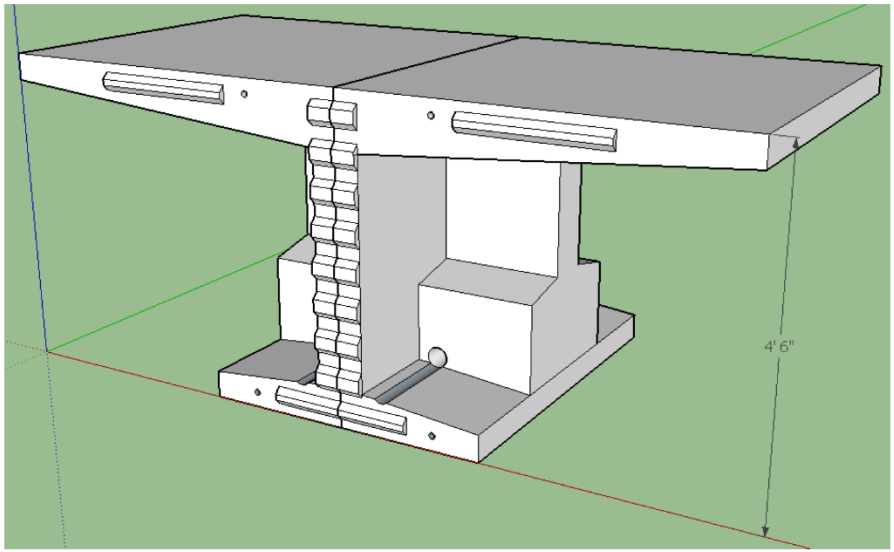

2 UNB3 DEVIATOR SEGMENT ISOMETRIC
1/8" = 1'-0"

IOWA STATE UNIVERSITY	DEVIATOR SEGMENT ISOMETRIC	NCHRP 12-94	Dr. Sri Sritharan Principal Investigator	BRIDGE NO. POST MILES	05-20-15 Test Units
			Drawn by Michael Rosenthal mjr@iastate.edu 319-210-7435	DISREGARD PRINTS BEARING EARLIER REVISION DATES →	REVISION DATES (PRELIMINARY STAGE ONLY) X X; SHEET 16; OF

Figure A.17 – Isometric View of Deviator Section

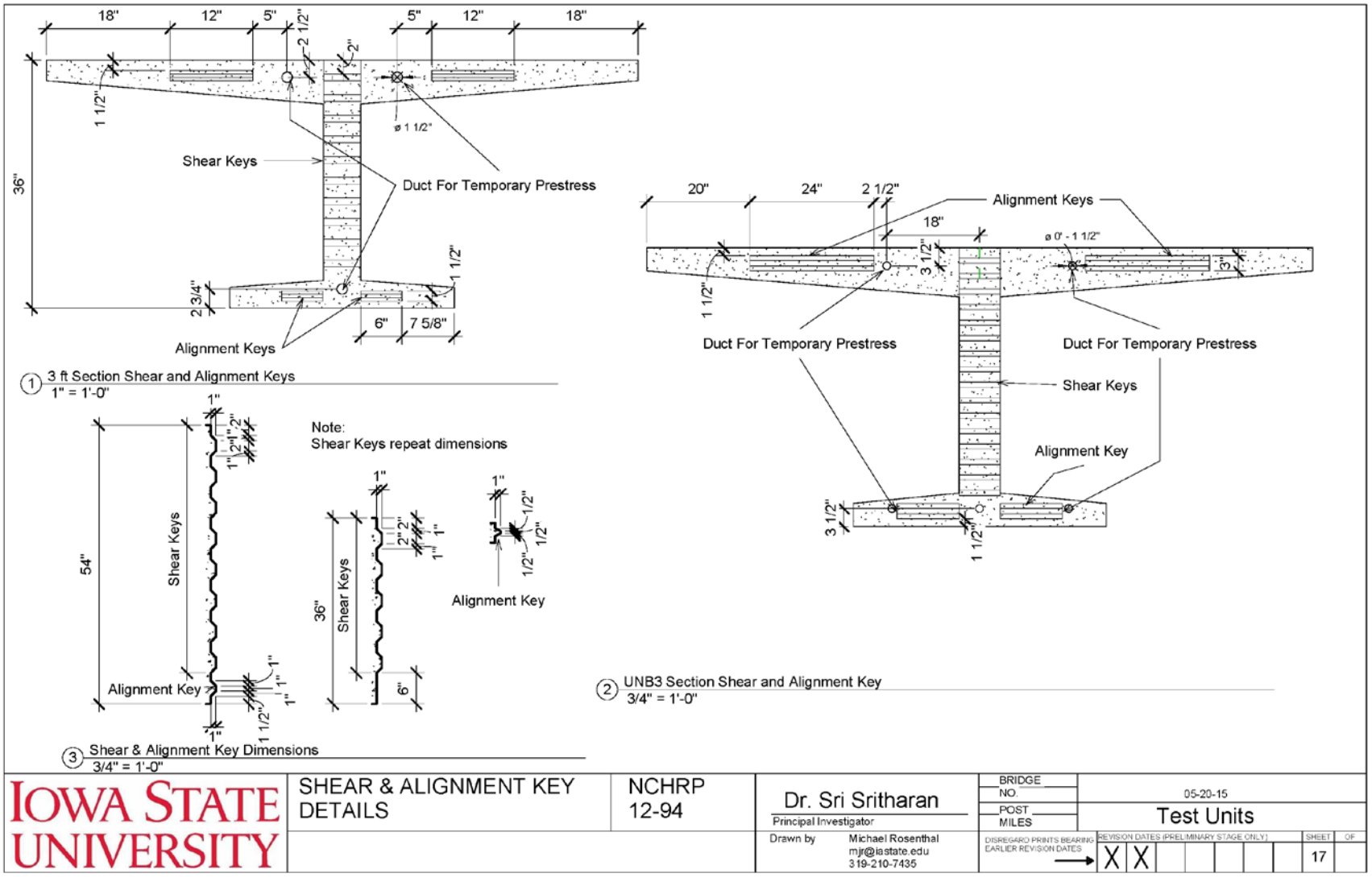

Figure A.18 – Shear and Alignment Key Details

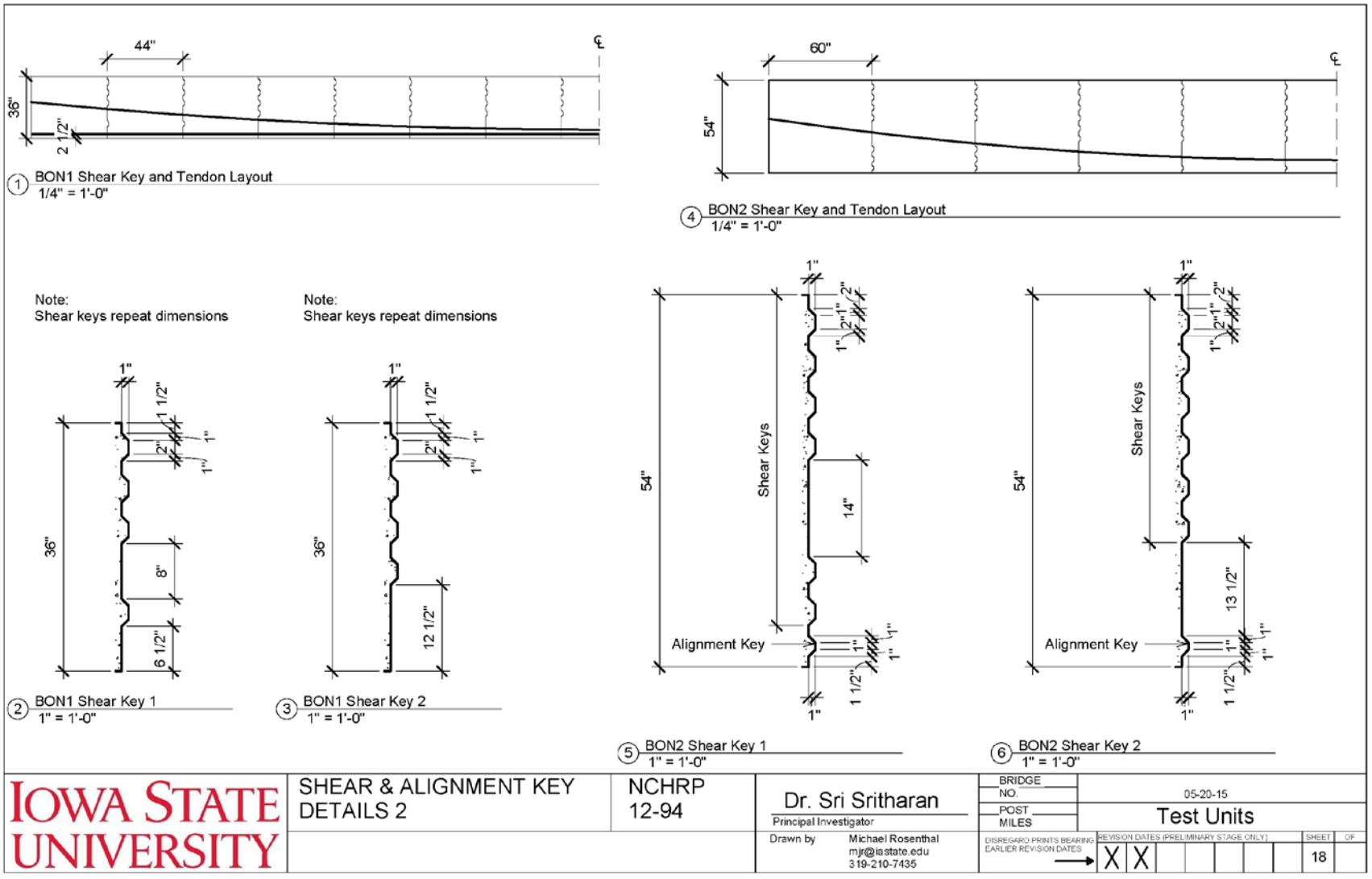

Figure A.19 – Shear and Alignment Key Details for Bonded Segments